A SEARCH FOR DIRECT AND RADIATIVE DECAYS OF THE B^0 MESON TO INVISIBLE FINAL STATES USING A HADRONIC TAGGING METHOD AT THE BABAR DETECTOR

by

NICHOLAS L. BLOUNT

A DISSERTATION

Presented to the Department of Physics
and the Graduate School of the University of Oregon
in partial fulfillment of the requirements
for the degree of
Doctor of Philosophy

December 2008

University of Oregon Graduate School

Confirmation of Approval and Acceptance of Dissertation prepared by:

Nicholas Blount

Title:

"A search for direct and radiative decays of the B0 meson to invisible final states using a hadronic tagging method at the BaBar detector"

This dissertation has been accepted and approved in partial fulfillment of the requirements for the Doctor of Philosophy degree in the Department of Physics by:

Eric Torrence, Chairperson, Physics
David Strom, Advisor, Physics
Nilendra Deshpande, Member, Physics
Dietrich Belitz, Member, Physics
Michael Kellman, Outside Member, Chemistry

and Richard Linton, Vice President for Research and Graduate Studies/Dean of the Graduate School for the University of Oregon.

December 13, 2008

Original approval signatures are on file with the Graduate School and the University of Oregon Libraries.

An Abstract of the Dissertation of

Nicholas L. Blount for the degree of Doctor of Philosophy

in the Department of Physics to be taken December 2008

Title: A SEARCH FOR DIRECT AND RADIATIVE DECAYS OF THE B^0 MESON TO INVISIBLE FINAL STATES USING A HADRONIC TAGGING METHOD AT THE BABAR DETECTOR

Approved: _____

Dr. David Strom

This dissertation describes a search for the decays $B^0 \to$ invisible and $B^0 \to$ invisible+γ, where invisible refers to a final state consisting of long lived particles with a low cross-section for interaction with matter, leading to a low probability of detection in typical particle detectors. While the branching fractions for these decays predicted by the Standard Model are far below what could be feasably measured by current experiments, new physics such as right-handed neutrinos propagating in large extra space-time dimensions or light R-parity violating neutralinos in supersymmetry could greatly enhance the branching fractions. The decays are searched for in data corresponding to $423.5\,\mathrm{fb}^{-1}$ integrated luminosity produced at the $\Upsilon(4S)$ resonance collected with the *BABAR* detector at the PEP-II B factory, corresponding to

2.30×10^8 $B^0\overline{B}^0$ pairs. Using those events that contain a hadronically reconstructed neutral B meson, evidence for the signal decays is sought in the remainder of the event. In $(5.00 \pm 0.02) \times 10^5$ events with a fully reconstructed neutral B meson, a total of 39 events consistent with the $B^0 \rightarrow$ invisible decay mode are seen in data with an expected background of 28.5 ± 7.8(stat.)$\pm$9.2(syst.) events, and 8 events consistent with the $B^0 \rightarrow$ invisible+γ decay mode are seen in data mode with an expected background of 14.1 ± 5.5(stat.)$\pm$8.1(syst.) events, from which upper limits of $\mathcal{B}(B^0 \rightarrow$ invisible$) < 11.7 \times 10^{-5}$ and of $\mathcal{B}(B^0 \rightarrow$ invisible+$\gamma) < 4.3 \times 10^{-5}$ at the 90% confidence level are obtained.

CURRICULUM VITAE

NAME OF AUTHOR: Nicholas L. Blount

PLACE OF BIRTH: El Paso, TX

DATE OF BIRTH: September 28, 1979

GRADUATE AND UNDERGRADUATE SCHOOLS ATTENDED:

University of Oregon, Eugene, Oregon
Reed College, Portland, Oregon

DEGREES AWARDED:

Doctor of Philosophy in Physics, 2008, University of Oregon
Bachelor of Arts in Physics, 2002, Reed College

AREAS OF SPECIAL INTEREST:

Dark matter, Quantum mechanics, Neutrino physics
Teaching

PROFESSIONAL EXPERIENCE:

Graduate Research Assistant,
University of Oregon, 2002 - 2008
Graduate Teaching Fellow,
University of Oregon, 2002 - 2004

TABLE OF CONTENTS

Chapter Page

LIST OF FIGURES

Figure Page

LIST OF TABLES

Table Page

CHAPTER I

THEORY AND PREVIOUS EXPERIMENT

Introduction

This dissertation describes a search for the decays $B^0 \rightarrow$ invisible and $B^0 \rightarrow$ invisible $+\gamma$ with a hadronically tagged $\overline{B}^0$ using a data sample containing 2.35×10^8 $B^0\overline{B}^0$ pairs collected by the *BABAR* detector at the PEP-II B Factory. Invisible is defined as particles with a low probability to decay in or measurably interact with the *BABAR* detector. The charge conjugate modes $B^0 \rightarrow$hadrons, $\bar{B}^0 \rightarrow$ invisible$(+\gamma)$ are also searched for: throughout this dissertation the inclusion of charge conjugate modes is implied. This chapter presents the decays in the context of the Standard Model and considers two theories that could enhance such decays, large extra dimensions and supersymmetry, as well as summarizing the previous search at *BABAR* for the decays. Chapter 2 describes the PEP-II accelerator and *BABAR* detector, as well as the simulation used in the analyses. Chapter 3 presents the $B^0 \rightarrow$ invisible$(+\gamma)$ analyses, including the hadronic tag reconstruction, the cuts applied for background rejection, and determi-nation of systematic errors. Chapter 4 gives the resulting branching fractions and limits, conclusions, and ideas for future research. Appendix

1 details the cut optimi-zation used in Chapter 3, Appendix 2 details the background scaling, and Appendix 3 describes the particle definitions used in the analysis.

Standard Model

The Standard Model of particle physics (SM) is a theoretical framework that describes the fundamental particles so far discovered and their interactions. All matter visible in the universe, and every force that acts on it other than gravity, is composed from 18 quarks, 6 leptons, 12 bosons, and anti-particles corresponding to each of the quarks and leptons. Each of three generations of quark pairs consists of an up type quark with charge $+2/3$ and a down type with charge $-1/3$, while each of three generations of lepton pairs consists of a charged lepton and a neutrino. The three generations of quarks are the up u and down d quarks, the charm c and strange s quarks, and the top t and bottom b quarks. Each quark also comes in three colors, where color is a quantum number affecting how the quark interacts via the strong force. The quarks are never found individually in nature, instead combining to form various charged and neutral hadrons, either as mesons consisting of a quark and an anti-quark, or baryons consisting of three quarks or of three anti-quarks. The three generations of leptons are the electron e^- and electron neutrino ν_e, the muon μ^- and muon neutrino ν_μ, and the tau τ^- and tau neutrino ν_τ.

The bosons mediate the fundamental forces that govern interactions between the particles of the SM. The photon is a massless particle that mediates the electro-

magnetic force and couples to charged particles. Eight types of gluons correspond to the strong nuclear force and couple to quarks and other gluons. They differ by their color composition. Each carries a unit of color and a unit of anti-color. The weak bosons $W^{\pm}$ and Z^0, unlike the photon and gluons, are massive, correspond to the weak nuclear force, and only couple to left-handed particles. Particles with positive chirality are referred to as right-handed, while those with negative chirality are referred to as left-handed, where chirality is a fundamental property of a particle that describes how it behaves under parity transformations. Gravity theoretically also has a boson, the graviton, but as of yet it has not been experimentally verified, and is not included in the SM.

The last SM boson, the Higgs boson, has not been detected experimentally. The Higgs mechanism explains the masses of the massive SM particles, using a scalar field with a non-zero vacuum expectation value. This field corresponds to 4 particles, including the Higgs boson. Experimental searches in e^+e^- data from the LEP experiment constrain the Higgs boson to have a mass greater than 114.4 GeV at the 95% confidence level [1]. Precision electroweak measurements constrain the SM Higgs boson to a mass less than 285 GeV at the 95% confidence level [2].

For the decays $B^0 \to$ invisible$(+\gamma)$, invisible refers to particles that are long lived and have a small cross section, making them unlikely to leave a signature in the *BABAR* detector at a significant rate. In the SM, the only particles that meet the definition of invisibility are neutrinos. Neutrinos are neutral and colorless, and

therefore do not interact via the strong or electromagnetic forces. Since the weak nuclear force has small couplings $G_F/(\hbar c)^3 = 1.166 \times 10^{-5}\,\mathrm{GeV}^{-2}$, they are highly unlikely to measurably interact with the *BABAR* detector. At energies of a few GeV, typical of particles produced in *BABAR*, neutrinos have a cross section of order $\sigma_\nu = 10^{-38}\,\mathrm{cm}^2$ [3]. The average detector density is less than the density of steel, $\rho = 8\,\mathrm{g/\,cm}^3$: given a nucleon mass of $u = 1.66 \times 10^{-24}\,\mathrm{g}$, and a detector radius of $r = 350\,\mathrm{cm}$ this gives a probability for a neutrino produced at the interaction point to interact in the detector of $P < \sigma_\nu \rho r/u \approx 2 \times 10^{-11}$.

$$B^0 \to \nu\overline{\nu} \text{ and } B^0 \to \nu\overline{\nu}\gamma$$

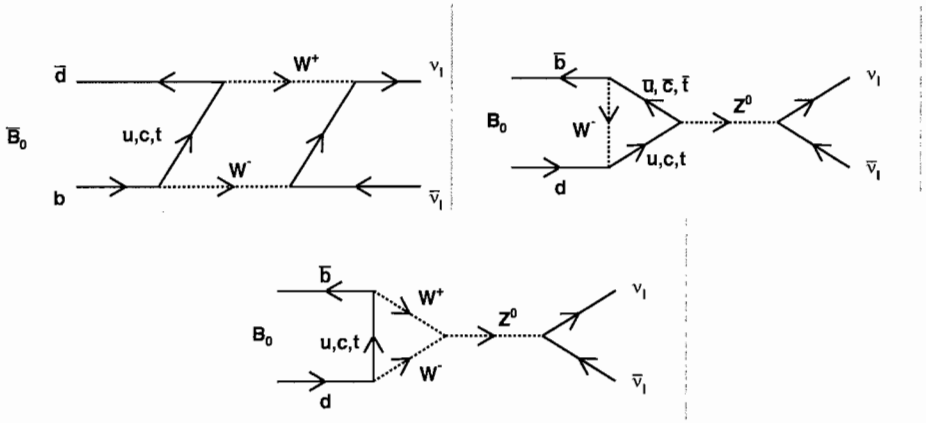

Figure 1.1. Diagrams for $B^0 \to \nu\overline{\nu}$ in the Standard Model.

The B^0 meson is composed of a $\bar{b}$ and a d quark. Since neutrinos do not interact via the strong or electromagnetic forces, in the SM $B^0 \to \nu\overline{\nu}$ must be mediated by $W^\pm$ or Z^0 bosons. The prohibition on flavor changing neutral currents prohibits the $B^0 \to \nu\overline{\nu}(+\gamma)$ decays at the tree level by Z^0 production through the annihilation of

the b quark and $\bar{d}$ quark, so to highest order $B^0 \rightarrow \nu\overline{\nu}$ must occur through a loop or penguin diagram (Figure 1.1). For $B^0 \rightarrow \nu\overline{\nu}\gamma$, the photon can radiate from any charged particle in the decay tree, resulting in decay trees like those in Figure 1.2.

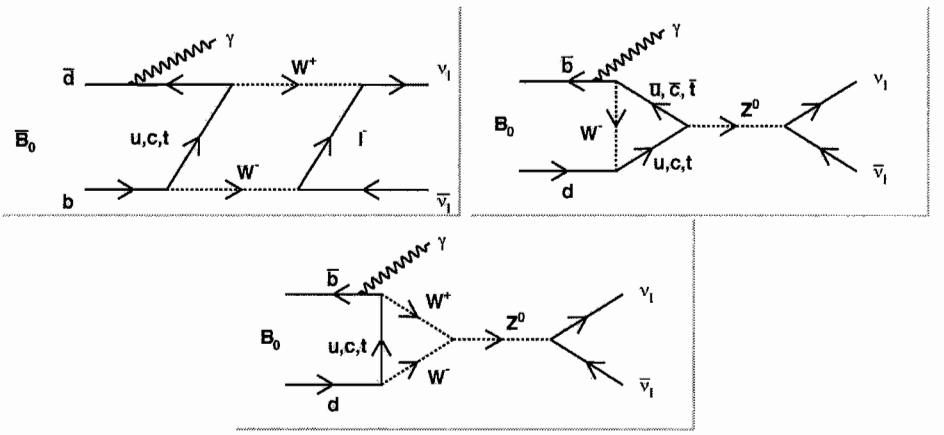

Figure 1.2. Diagrams for $B^0 \rightarrow \nu\overline{\nu}\gamma$ in the Standard Model.

Helicity Suppression and B to Neutrino Anti-neutrino Gamma

The decay $B^0 \rightarrow \nu\overline{\nu}$ is helicity suppressed. The helicity h refers to the component of a particle's spin $\vec{S}$ in its direction of momentum $\hat{p}$, $h = \vec{S} \cdot \hat{p}$. For spin 1/2 particles, the possible values for helicity are $h = \pm\hbar/2$. For massless particles or for massive particles in the relativistic limit, the particle's helicity has the same value as its chirality. For charged leptons, which are left-handed, this leads to the helicity of leptons produced in weak decays to be dominantly negative, with the average helicity proportional to the lepton's velocity v, $h = -v/c \cdot \hbar/2$, for their anti-particles $h = v/c \cdot \hbar/2$. Since B^0 particles are scalar, the daughters in a 2 body decay must have opposite spins and momenta, and therefore identical helicity. As the weak force

only couples to left-handed particles, this leads the decays to be helicity suppressed, with a branching fraction proportional to m^2, where m is the daughter particle mass. Under the SM, with the assumption of massless neutrinos, neutrinos can only be left-handed, and anti neutrinos can only be right-handed, and therefore the decay $B^0 \rightarrow \nu\overline{\nu}$ is forbidden due to helicity conservation.

In 1998, Super-Kamiokande measured neutrino oscillation, showing that neutrinos are not massless [4]. Neutrino oscillation between two types of neutrinos is given by $P_{\alpha\rightarrow\beta} = \sin^2 2\theta \sin^2\left((\Delta m^2 L)/(4E)\right)$, where α and β are two neutrino types, θ is the mixing angle between them, Δm is their difference in mass, L is the distance the neutrino has travelled, and E is the neutrino energy. If neutrinos were massless, Δm^2 and therefore $P_{\alpha\rightarrow\beta}$ would be zero. More recent neutrino oscillation measurements give $\Delta m^2_{21} = 7.58^{+0.14}_{-0.13}(\text{stat.})^{+0.15}_{-0.15}(\text{syst.}) \times 10^{-5}\,\text{eV}^2$ (KamLAND [5]), and $\Delta m^2_{23} = 0.00243 \pm 0.00013\,\text{eV}^2$ (MINOS [6]). The WMAP experiment measured the distribution of light from the early universe, called the cosmic microwave background, and compared the distribution with that predicted under various assumptions about the composition and development of the universe. WMAP put a limit on the total mass of the 3 neutrinos, with a current combined limit of $m_{TOT} < 2\,\text{eV}$ [7]. Therefore, while neutrinos are not massless, their masses are small, and so the decay $B^0 \rightarrow \nu\overline{\nu}$ is allowed but strongly helicity suppressed, with a branching fraction to be proportional to the neutrino mass squared. Assuming the branching fraction for $B^0 \rightarrow \nu\overline{\nu}$ is otherwise the same as for the other dilepton decays, this leads to a branching fraction

of at most 10^{-20}, many orders of magnitude lower than B^0 decays to heavier dileptons such as $B^0 \rightarrow \tau^+ \tau^-$, and far below *BABAR*'s ability to measure.

The addition of an emitted photon from one of the charged particles in $B^0 \rightarrow \nu\overline{\nu}$ breaks the helicity suppression, giving a branching fraction for $B^0 \rightarrow \nu\overline{\nu}\gamma$ of order 10^{-9}, calculated from the partial width given in Equation I.1-Equation I.3 [8]:

$$\Gamma = \frac{C^2 \alpha f_{B_d}^2 m_{B_d}^5}{(144\pi)^2 m_d^2}, \tag{I.1}$$

$$C = \frac{\sqrt{2} G_F \alpha}{\pi \sin^2 \theta_\omega} V_{tb} V_{td}^* \frac{x}{8} \left(\frac{x+2}{x-1} + \frac{3x-6}{(x-1)^2} \ln x \right), \tag{I.2}$$

$$x = m_t^2 / m_W^2, \tag{I.3}$$

where α is the electromagnetic coupling constant, f_{B_d} is the pseudo-scalar decay constant for B decays, m_{B_d} is the mass of the B^0 meson, m_d is the mass of the d quark, G_F is the Fermi coupling constant, θ_ω is the weak-mixing angle, V_{tb} and V_{td} are components of the CKM matrix, m_t is the top quark mass, and m_W is the W boson mass

New Physics

While in the SM $B^0 \rightarrow$ invisible$(+\gamma)$ are not predicted to occur at measurable rates, there are strong reasons to expect particles and processes beyond those of the SM that could greatly enhance the branching fractions. Dark matter, first detected using galaxy rotation measurements, composes much of the matter in the universe and is not explained by the SM. Currently the best estimates of the total dark matter

composition of the universe come from WMAP. The best fitting parameters to the WMAP measurements predict the cold dark matter content of the universe to be $\Omega_c h^2 = 0.1099 \pm 0.0062$, with baryonic matter as $\Omega_b h^2 = 0.02265 \pm 0.00059$ [9]. While most theoretical models that explain dark matter do not predict an enhanced rate of $B^0 \rightarrow$ invisible$(+\gamma)$, the possibility of decays of B^0 to dark matter is not expressly prohibited. New physics might enhance the rate of $B^0 \rightarrow \nu\overline{\nu}(+\gamma)$. One theory that could do so is with large extra dimensions, which neutrinos and gravitons could propagate in, with the other SM particles confined to the standard 4 dimensional spacetime. Supersymmetry is an extension to the SM that proposes a set of additional particles, one partner to each SM particle. It may be possible for invisible supersymmetric particles to be produced in B^0 decays. In this section, large extra dimensions and supersymmetry are examined in more detail.

Large Extra Dimensions

Large Extra Dimensions is one theory that resolves the hierarchy problem. It explains why the Higgs mass, less than 285 GeV at the 95% confidence level, is not of the same scale as the Planck mass $m_P = \sqrt{\frac{\hbar c}{8\pi G}} = 2.43 \times 10^{18}\,\mathrm{GeV}/c^2$, where G is the gravitational constant. In calculating the Higgs mass, fine tuning is needed to avoid quantum corrections leading to terms that are of the order of the Planck mass. One possible alternative is the existence of dimensions beyond the standard 4 spacetime dimensions. If gravitons propagated in these dimensions while most the SM particles were confined to 4 dimensions, the result would be that the observed Planck mass

would follow from a much smaller fundamental Planck mass: $M_{Pl}^2 \approx R^\delta M_*^{\delta+2}$ where M_{Pl} is the 4 dimensional Planck mass, δ is the number of extra dimensions, R is the size of the extra dimensions, and M_* is the fundamental Planck scale. If, further, right handed neutrinos are allowed to propagate in the extra dimensions, left handed neutrino masses would be suppressed to $m \approx \frac{\lambda}{\sqrt{2}}\frac{M_*}{M_{Pl}}\nu$, where λ is a dimensionless 5 dimensional coupling and ν is the Higgs vacuum energy of 246 GeV [10]. In this scenario, the rate for $B^0 \rightarrow$ invisible would be enhanced by additional contributions from Higgs exchange. This effect is large when all the Kaluza Klein modes of the right handed neutrino lighter than the B^0 meson are taken into account, resulting in an enhancement in the $B^0 \rightarrow$ invisible branching fraction up to 10^{-12} [11]. While a large enhancement over the SM, branching ratios of this order are still below what is measureable by *BABAR*.

Supersymmetry

Supersymmetry posits that for every SM particle there is a corresponding super-particle, a fermion for each SM boson and a boson for each SM fermion. In calculating the Higgs mass, fine tuning is needed to avoid quantum corrections leading to terms that are of the order of the Planck mass. With supersymmetry the contributions to these terms by each SM particle are cancelled by the contribution of its super-symmetric partner. While searches for supersymmetric particles have so far been unsuccessful, it is still possible that there are such particles light enough for a B^0 to decay into, but experimentally invisible and therefore undetected (Figure 1.3).

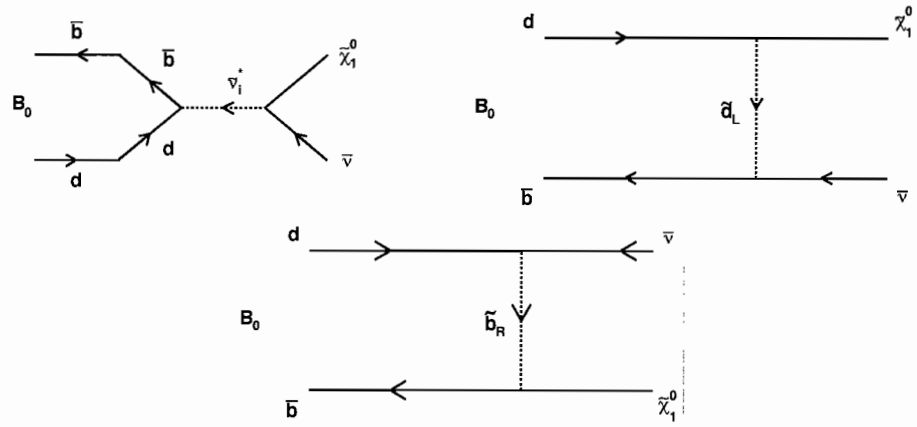

Figure 1.3. $B^0 \rightarrow$ invisible enhancing Feynman diagrams with supersymmetry [12].

As with neutrinos, invisible supersymmetric particles would be long lived neutral fermions. As super-symmetric particles have the same charge as their SM partners, the candidates in supersymmetry that meet these criteria are the neutralinos, the superpartners to the neutral gauge bosons. Searches for supersymmetric particles at LEP and Tevatron found no significant evidence of light supersymmetric particles, and place limits on supersymmetry parameters that heavily restrict light supersymmetric particles [13][14] (Figure 1.4 and Figure 1.5).

NuTeV

Experimentally, neutralinos produced in B^0 decays could have resulted in the excess of dimuon events seen in the NuTeV experiment [12]. NuTeV was the neutrino detector for a neutrino beam produced by fixed target collisions of 800 GeV protons from Fermilab's Tevatron. The detector consisted of a section of alternating layers of iron, scintillators for energy measurements, and drift chambers for position measure-

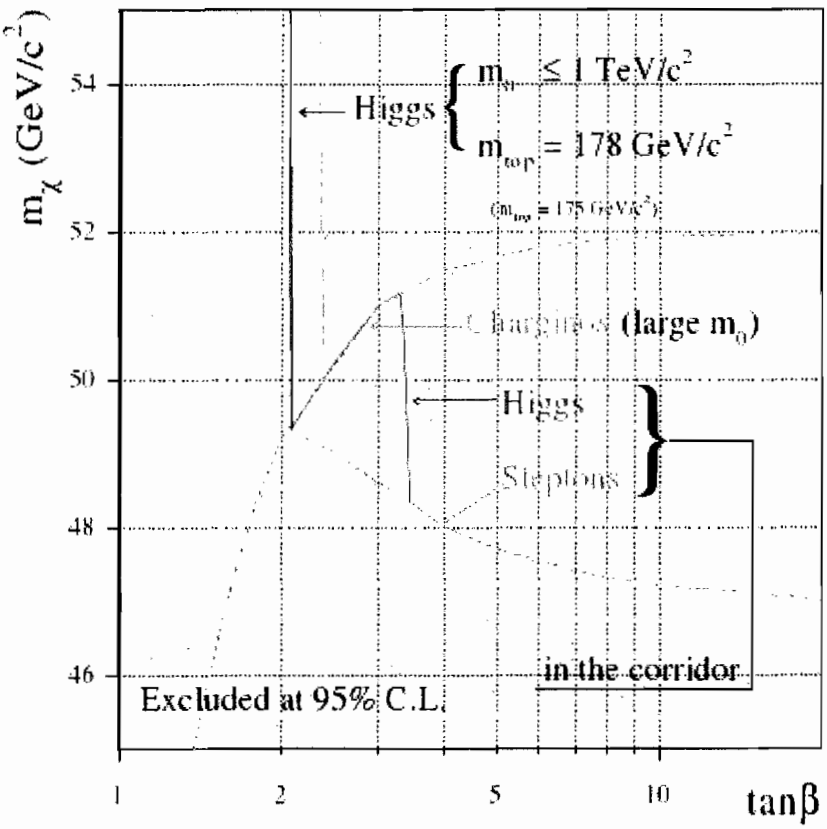

Figure 1.4. Mass limit on the neutralino LSP as function of $\tan\beta$ [13].

ments, followed by a section with alternating toroids and drift chambers, for tracking and measuring the momentum of muons produced in the first section. The NuTeV experiment saw 3 $\mu^+\mu^-$ events, with an expected SM background of 0.069 ± 0.010 events, which when combined with the other dilepton channels corresponds to a 3σ fluctuation. One explanation for the excess events seen is that B mesons produced at NuTeV decayed into R_p violating neutralinos, with the neutralinos subsequently decaying to dimuons $B^0 \rightarrow \chi_1^0\bar{\nu}$, $\chi_1^0 \rightarrow \mu_L^-\mu_R^+\nu_\tau$. LEP constraints prevent pair production of such neutralinos, with subsequent dimuon decays from producing enough

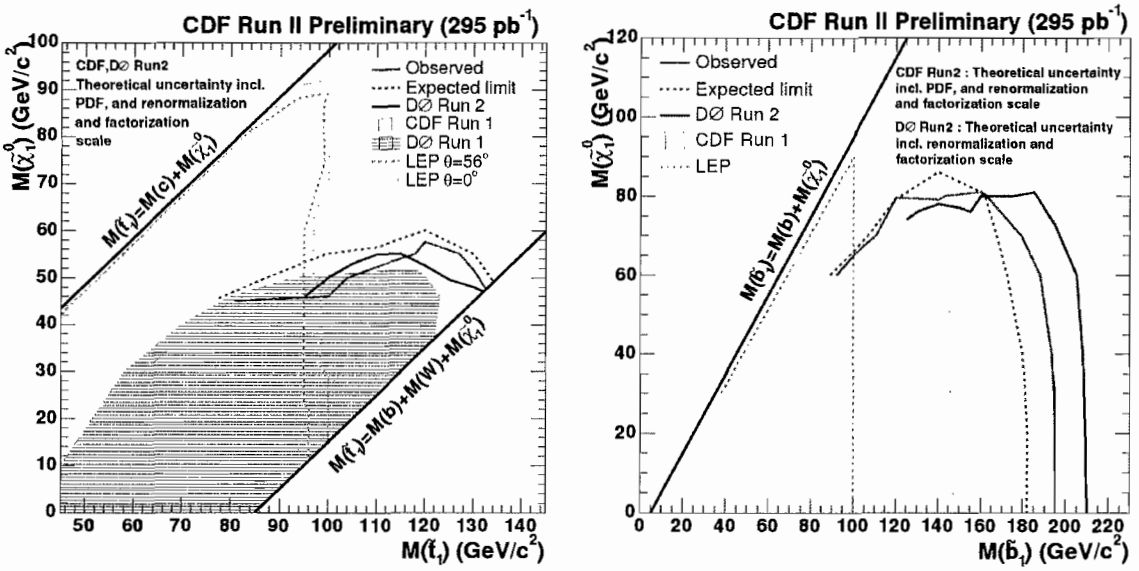

Figure 1.5. Limits on neutralino versus stop (left) and sbottom (right) masses from the CDF search in the heavy flavor + missing transverse energy channel [14].

events to explain the excess of dimuon events in NuTeV. However, if the neutralino is dominantly Bino, the superpartner to the gauge field that forms the 3rd component of weak isospin, it could be produced in B decays while not being pair produced in s channel decays of the Z^0 boson. This would suppress neutralino pair production from Z boson decays and avoid the LEP constraints. The neutralinos would have a lifetime in the range $\tau = 10^{-7}s$ to $10^{-5}s$, corresponding to a decay length of 30m to 3000m, and would thus be invisible to the *BABAR* detector(Figure 1.6). The neutralino mass would be between 4.5 and 5.5 GeV. Such $B^0 \rightarrow$ invisible decays could have branching ratios up to order 10^{-5}, calculated from the width given in Equation I.4

$$\Gamma(B_d^0 \rightarrow \bar{\nu}_i \tilde{\chi}_1^0) = \frac{9\lambda'^2_{i13} g'^2 f_B^2 m^2_{B^0} p_{cm}}{256\pi(m_d + m_b)^2 M^4_{\tilde{f}}}(M^2_{B^0} - M^2_{\tilde{\chi}_1^0}), \qquad \text{(I.4)}$$

where λ'_{i13} are dimensionless R-parity violating coupling constants of supersymmetric

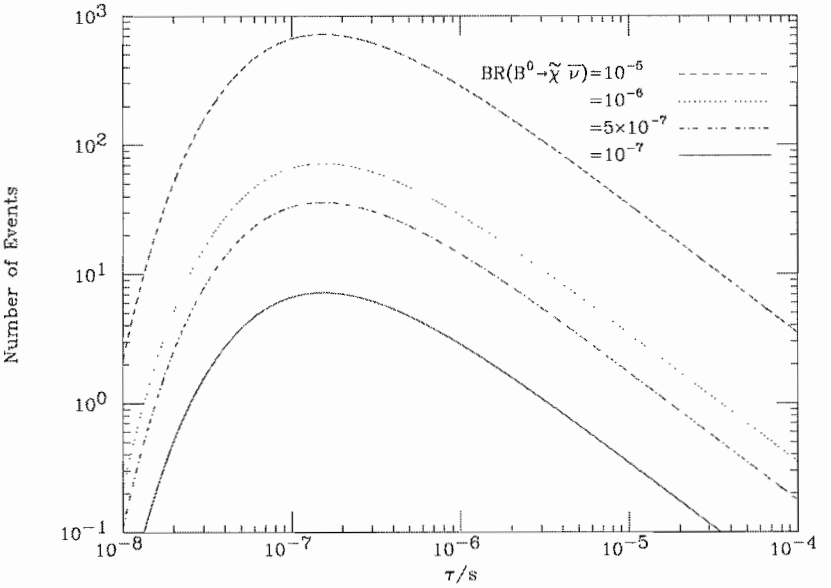

Figure 1.6. Number of events in the NuTeV detector for neutralino production in B-meson decays as a function of the neutralino lifetime and rate of $B^0 \rightarrow$ invisible.

particles, g' is a supersymmetric gauge coupling, f_B is the pseudo-scalar decay constant for B decays, m_{B^0} is the mass of the B^0 meson, p_{cm} is the momentum of the daughter particles, m_d is the mass of the d quark, m_b is the mass of the b quark, $M_{\tilde{f}}$ is the sfermion mass, and $M_{\tilde{\chi}_1^0}$ is the mass of the lightest neutralino.

Previous Experiment

While the SM branching ratio for $B^0 \rightarrow$ invisible is far below what is currently measurable, experimentally the branching ratio is not well constrained. The decay $B^0 \rightarrow$ invisible was searched for in a previous analysis at *BABAR* [15] using 81 fb^{-1} data, and obtained upper limits of $\mathcal{B}(B^0 \rightarrow \text{invisible}) = 22 \times 10^{-5}$ and $\mathcal{B}(B^0 \rightarrow$

invisible + γ) = 4.7×10^{-5}, using a reconstructed $B^0 \rightarrow D^{(*)}l\nu$ decay to tag the other B^0 in the event. It obtained these limits from a fitted signal of $N_{Sig}(B^0 \rightarrow$ invisible) = 17 ± 9 on top of a background of $N_{Bkgrnd}(B^0 \rightarrow$ invisible) = 19^{+10}_{-8}, and a fitted signal of $N_{Sig}(B^0 \rightarrow$ invisible + γ) = $-1.1^{+2.4}_{-1.9}$ on top of a background of $N_{Bkgrnd}(B^0 \rightarrow$ invisible + γ) = 28^{+6}_{-5}. The analysis in this dissertation instead uses an entirely hadronic tagging method, as well as a much larger dataset.

CHAPTER II

DETECTOR AND EXPERIMENT

Experiment Overview

The search for $B^0 \rightarrow$ invisible$(+\gamma)$ with hadronic tag analysis was run on data produced at the PEP-II asymmetric $e^+ e^-$ collider and B factory at the Stanford Linear Accelerator Center. The PEP-II experiment was designed for precision measurements of B meson decays at high luminosities. The PEP-II collider consists of a 3.2 km long particle accelerator, which leads to two storage rings of 2.2 km in circumference [16]. The storage rings share a tunnel, with the Low Energy Ring (LER), which contains the positron bunches, mounted 0.89 m above High Energy Ring (HER) carrying the electron bunches. Permanent bending magnets bring the LER beam to collide head on with the HER beam at the IP. The *BABAR* detector is located where the two beams intersect (Figure 2.1).

Luminosity

The performance of the PEP-II collider is characterized by the luminosity delivered to the *BABAR* detector. The rate dN/dt of interaction is determined by the physical process that produces the interaction, given by the cross section σ, and by the

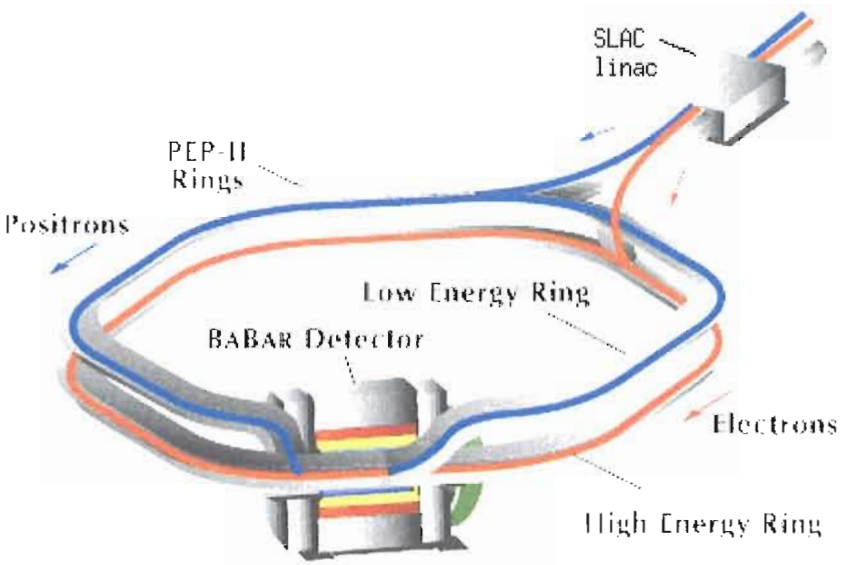

Figure 2.1. PEP-II rings

Table 2.1. PEP-II beam parameters. Values are given for the design, for typical colliding beam operation in the first year, and the best values obtained as of April 2008. HER and LER refer to the high energy e^- and low energy e^+ ring, respectively. σ_{Lx}, σ_{Ly}, and σ_{Lz} refer to the horizontal, vertical, and longitudinal rms size of the luminous region [17][18].

Parameters	Design	Typical	Best
Energy HER/LER (GeV)	9.0/3.1	9.0/3.1	9.0/3.1
Current HER/LER (A)	0.75/2.15	0.7/1.3	2.07/3.21
# of bunches	1658	553-829	1732
Bunch spacing (ns)	4.2	6.3-10.5	
σ_{Lx} (μm)	110	120	
σ_{Ly} (μm)	3.3	5.6	
σ_{Lz} (mm)	9	9	
Luminosity ($10^{33}\,\mathrm{cm}^{-2}\mathrm{s}^{-1}$)	3	2.5	12
Luminosity (pb^{-1}/d)	135	120	911

Table 2.2. Production cross sections at $\sqrt{s} = M(\Upsilon(4S))$. The e^+e^- cross section is the effective cross section, expected within the experimental acceptance [19].

$e^+e^- \rightarrow$	Cross section (nb)
$b\bar{b}$	1.05
$c\bar{c}$	1.30
$s\bar{s}$	0.35
$u\bar{u}$	1.39
$d\bar{d}$	0.35
$\tau^+\tau^-$	0.94
$\mu^+\mu^-$	1.16
e^+e^-	40

mechanics producing the interaction, given by the luminosity $\mathcal{L}$: $dN/dt = \mathcal{L} \cdot \sigma$. The cross sections are determined by what particles are involved in the interaction and the center of mass (CMS) energy of the interaction. Cross sections of some processes for e^+e^- at 10.58 GeV are given in table (Table 2.2).

Luminosity is given by the equation $\mathcal{L} = fn\frac{N_1 N_2}{A}$ where L is the luminosity, f is the revolution frequency, n is the number of bunches in one beam of the storage ring, N_i is the number of particles in each bunch from beam i, and A is the cross section of each beam. Parameters for the PEP-II beams are given in Table 2.1. Over the lifetime of the *BABAR* experiment, the detector collected an integrated luminosity of 531.43 fb^{-1}, with a peak luminosity of $12.069 \times 10^{33} cm^{-2} sec^{-1}$ (Figure 2.2). This corresponds to 227.3 million $B^0\overline{B}^0$ pairs, assuming $\mathcal{B}(\Upsilon(4S) \rightarrow B^0\overline{B}^0) = 0.5$.

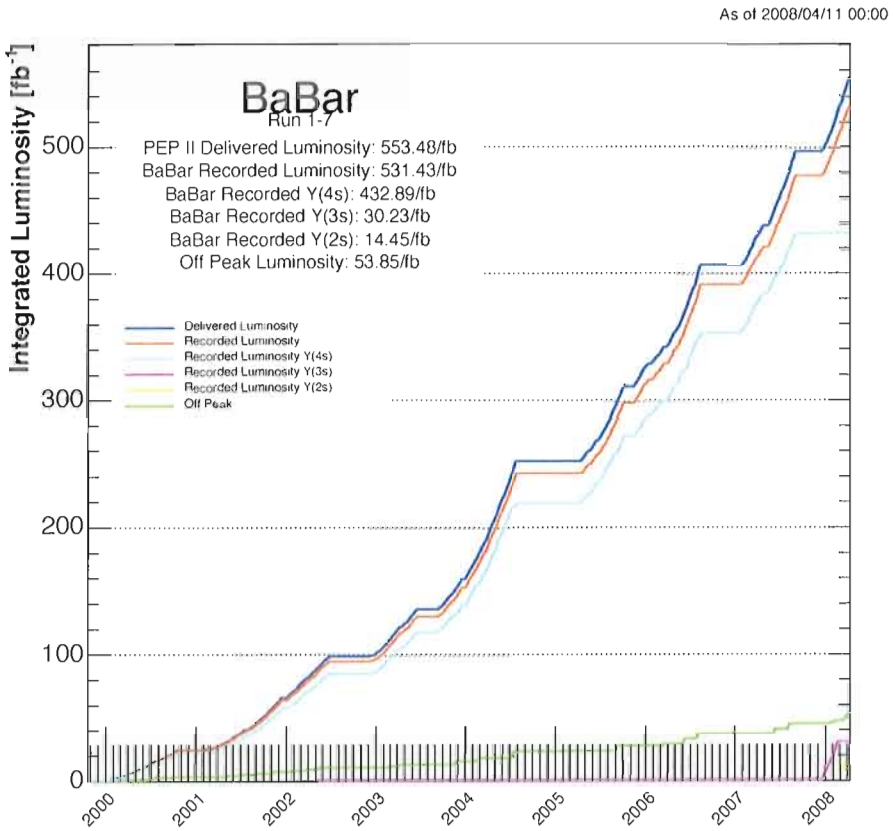

Figure 2.2. Integrated luminosity at the *BABAR* detector.

The Detector

The *BABAR* detector consists of a series of subsystems designed to detect and characterize particles produced at the interaction point (IP). From innermost to outermost, it consists of the silicon vertex tracker (SVT), drift chamber (DCH), detector of internally reflected Cherenkov light (DRC), and electromagnetic calorimeter (EMC) contained in a superconducting solenoid producing a 1.5T magnetic field, surrounded by the instrumented flux return (IFR) (Figure 2.3). The SVT and DCH measure the trajectories of charged particles as they emerge from the interaction point (IP). Combined with curvature of the trajectories due to the solenoid field, the momenta and energy loss of the tracks can also be measured. The DRC uses Cherenkov radiation to measure charged track velocities, enabling improved differentiation between types of charged particles. The EMC uses electromagnetic showers to detect and measure the energy of photons and electrons produced at the IP. The IFR detects showers produced in the steel surrounding the solenoid, detecting neutral hadrons undetected by the other subsystems and allowing improved differentiation between muons and charged kaons. This section describes the subsystems in greater detail [17]. In describing these subsytems, I will use the following coordinate system: with $+z$ along beampipe in direction of electron travel, $+x$ in direction away from the center of the ring, and y in the upward direction. For angles, θ is the angle from $+z$ axis and ϕ is the angle around the z axis from $+x$. The center of the detector is

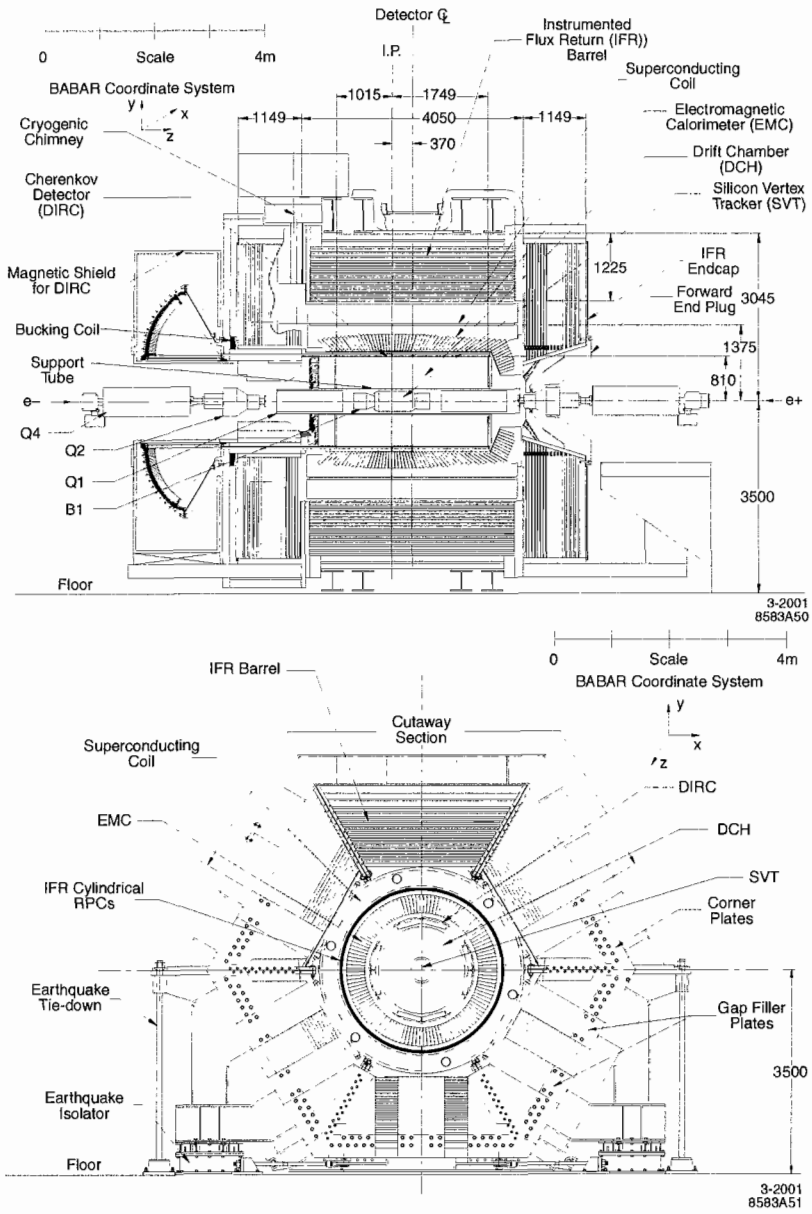

Figure 2.3. The *BABAR* detector side view and end view [17].

offset from the IP by 37cm in the +z direction. The detector coverage extends from 350 mrad from the $+z$ axis in the forward direction to 400 mrad from the $-z$ axis in the backward direction.

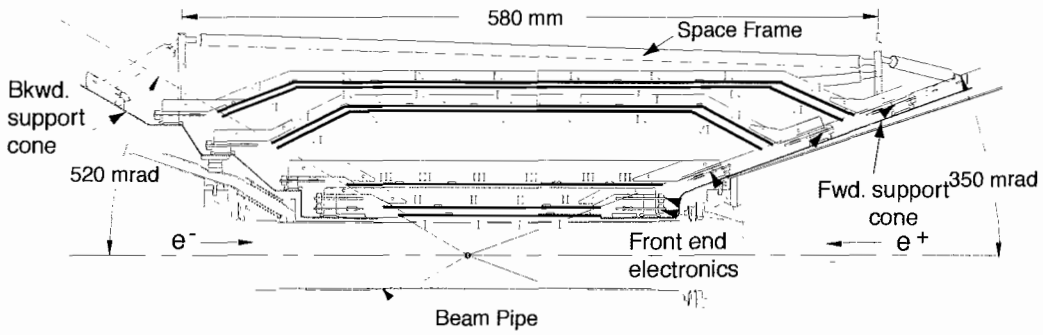

Figure 2.4. Silicon Vertex Tracker [17].

SVT

The innermost subdetector of *BABAR* is the SVT. The purpose of the SVT is to detect the locations of charged particles as they leave the IP region with enough precision to trace the tracks (series of hits left by a charged particle as it travels through the detector) back to common vertices with vertex location precision of 80 μm in z. (Figure 2.4). To this end, the SVT was designed to be compact and located close to the IP.

The SVT consists of 5 layers of double-sided silicon strips. The inner 3 layers are located just outside the beampipe (3.2 to 5.4 cm), with the outer two farther out (9.1-14.4 cm). Tracks create charge-hole pairs in the strips, which are read out to give the locations where charged tracks intersected the strips. Strip overlap ensures complete coverage in ϕ. The SVT has a 97% hit efficiency with a resolution that varies with track angle but is at most 40 microns for both z and ϕ.

DCH

The DCH is designed for tracking with millimeter resolution and provides momentum measurements of the charged tracks (Figure 2.5) in the 1.5T magnetic field. Combined with dE/dx measurements from the DCH, particle masses can also be obtained, allowing particle identification.

The drift chamber consists of 40 layers of hexagonal cells formed by 6 grounded aluminum field wires, strung in the z direction. Each cell has a tungsten-rhenium sense wire $20\,\mu$m in diameter at $+1969\,V$ strung down the middle, and the DCH is filled with a gas of 80% helium 20% isobutane. Properties of this gas mixture are given in Table 2.3 [17]. Longitudinal positioning of the tracks is obtained by angling 24 of the layers at small angles (45-76 mrad) from the z axis. As charged particles pass through the gas, they produce electron/positron pairs in the gas. The electrons are attracted to the sense wires, ionizing the gas and forming avalanches as they near the sense wires. The isobutane quenches electrons in the avalanches, keeping the avalanches localized. From the amount and time of charge collected by the sense wires, the paths of charged particles traversing the DCH can be determined. The curvature of a track due the 1.5T magnetic field allows the momentum of the track to be determined.

The drift chamber is able to measure dE/dx for bhabha events with a resolution of 7.5%. It is able to detect tracks with energy greater than 200 MeV and $\theta > 500$ mrad with an efficiency of $98 \pm 1\%$. Lower energy charged tracks rely on the SVT for

Table 2.3. Properties of helium-isobutane gas mixture at atmospheric pressure and 20°C. The drift velocity is given for operation without magnetic field, while the Lorentz angle is stated for a 1.5T magnetic field.

Parameter	Values
Mixture He : C_4H_{10}	80:20
Radiation Length	807 m
Primary Ions	21.2/cm
Drift Velocity	22 μm/ ns
Lorentz Angle	32°
dE/dx Resolution	6.9%

detection: the SVT can detect tracks with a transverse momentum greater than 50 MeV with greater than 80% efficiency. Combined, the track resolution for the DCH and SVT is $\sigma_{d_0} = 23\mu$m, $\sigma_{z_0} = 29\mu$m, $\sigma_{\phi_0} = 0.43$ mrad, and $\sigma_{\tan\lambda} = 0.53 \cdot 10^{-3}$, where d_0 and z_0 are the distance of closest approach of the trajectory of the charged track to the IP in the $x - y$ plane and along the z axis, respectively, and λ is the dip angle of the charged track relative to the transverse plane. In transverse momentum, the resolution is $\sigma_{p_t}/p_t = (0.13 \pm 0.01)\% \cdot p_t + (0.45 \pm 0.03)\%$ (Figure 2.5).

DRC

The DRC, located outside the DCH, is designed to measure the velocity of high energy charged particles. Combined with the momentum information from the DCH, this allows for a calculation of the mass of the particle producing the track. A primary motivation for this is for pion/kaon separation.

The DRC consists of synthetic fused silica, which causes high energy charged particles passing through to emit a cone of Cherenkov radiation. The cone is produced

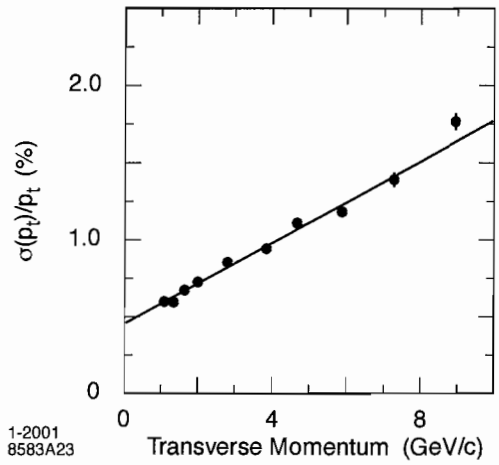

Figure 2.5. Resolution in the transverse momentum p_T determined from cosmic ray muons traversing the DCH and SVT [17].

with an opening angle of $\cos\theta = 1/(n\beta)$, where n is the refractive index of the medium. The Cherenkov is transmitted by total internal reflection and is subsequently detected by photomultiplier tubes. From the location and time of arrival of photons to the photomultiplier tubes, the angle of emission of the light cone is reconstructed. The DRC measures the Cherenkov angle with a resolution of 2.5 mrad, which leads to a π/K separation of greater than 4σ for tracks between 700 MeV and 4.2 GeV.

EMC

The EMC serves to cause photons, electrons, and positrons to produce electromagnetic showers, depositing their energy into the material of the EMC, allowing the energy of the particle to be measured (Figure 2.6).

The EMC consists of thallium doped cesium-iodide (Cs-I(Tl)) crystals that collect electromagnetic showers. The energy deposited and location of a shower are read out

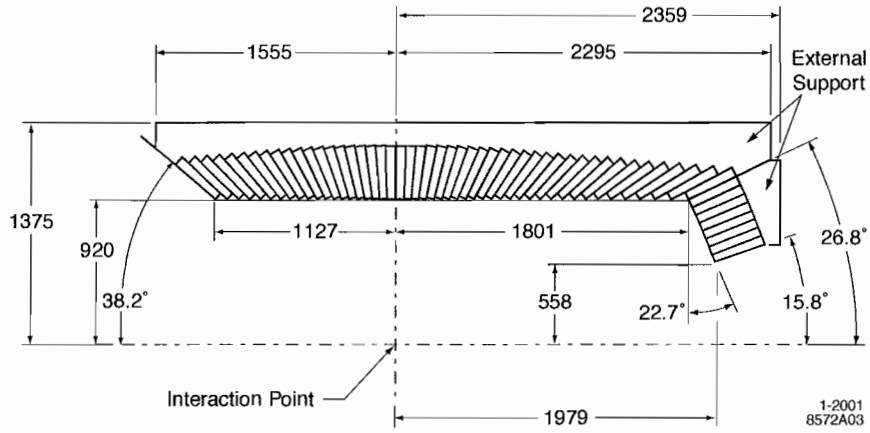

Figure 2.6. Electromagnetic Calorimeter [17].

by silicon PIN diodes glued to the outside of each crystal. The EMC consists of 16-17.5 radiation lengths of material. The EMC is able to obtain an energy resolution of $\sigma_E/E = (1.9 \pm 0.07)\%$ at 7.5 GeV, and $(5.0 \pm 0.8)\%$ at 6.13 MeV. The angular resolution ranges from 12 mrad for low energy photons to 30 mrad at high energies.

IFR

Because of their similar masses, muons (105.7 MeV) and charged pions (139.6 MeV) are difficult to distinguish by mass, and both pass through the SVT, DCH, DRC, and EMC with little momentum loss or chance of interaction. The steel of the IFR increases the chance of interactions, allowing for improved muon ID. By the time they hit the IFR, muons and hadrons have traveled through 0.3-2.0 radiation lengths of material. Neutral hadrons rarely interact before the IFR, so the IFR also serves as a detector of K_L mesons and other neutral hadrons.

The IFR consists of resistive plate capacitors (RPCs) and limited streamer tubes

(LSTs) in between layers of flux return steel, which is used as a muon filter and hadron absorber. The RPCs consist of an argon, freon, and isobutane gas mixture sandwitched between layers of bakelite. Layers of graphite on the backelite are held at 0V and 8kV. External layers of aluminum serve as capacitive conductors to measure streamers produced in the gas mixture (Figure 2.7). In 2006-2007, the barrel RPCs were replaced with LSTs, which consist of groups of PVC tubes oriented in the z direction [20]. Each has a gold plated anode signal wire running down the middle. The inside wall of each tube is painted with graphite, which is grounded. Streamers in the CO_2, argon, and isobutane gas mixture that fill the LSTs are collected by the sense wires. A layer of copper strips runs perpendicular to the LST tubes to provide z coordinates for hits in the LSTs. Showers in the iron ionize gas in the detector. The electrons from the ionization are collected on the wire or plate.

The RPCs achieved a muon identification rate of 90% with a charged pion fake rate of $6 - 8\%$ for tracks in the range $1.5 - 3\,\text{GeV}$, and a neutral hadron detection efficiency of $20 - 40\%$ over the range $1 - 4\,\text{GeV}$.

MC Simulation

The *BABAR* experiment uses detailed Monte Carlo (MC) simulation to simulate the production of particles in an underlying physics event, transport the particles through the material of the detector, calculate the idealized energy deposits in the detector, overlay backgrounds and digitize the energy deposits, and reconstruct the event.

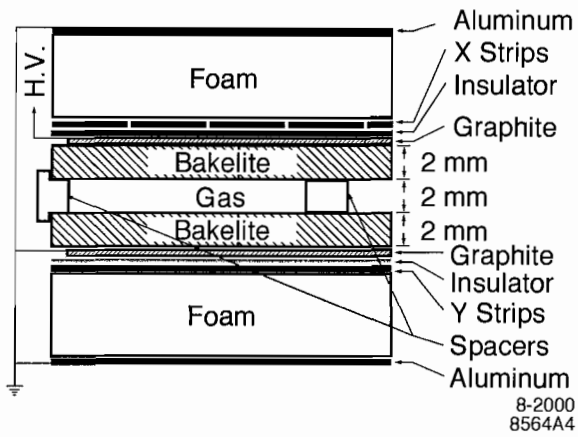

Figure 2.7. Resistive plate capacitor cross section [17].

The program Bogus, consisting of a detailed simulation model of the material and electromagnetic fields of the detector used with Geant4 [21], combined with various event generators depending on the physics of the event performs the generation, transport, and energy deposit calculations. The event generators model initial decay at or near the IP, using predicted branching ratios, angles, and momentum distributions to give the daughter particles propagated by Geant4. Geant4 is a toolkit produced by CERN to simulate the passage of particles through matter, to model the behavior of the particles as they traverse the detector. The detector simulation defines non-overlapping regions, each giving the space occupied by a section of uniform material in the detector. Particles are transported in steps of the smaller of 1 cm and the distance to a region boundary, for each step calculating energy deposited and any changes to the particle's location and momentum due to interactions and electromagnetic fields. The program SimApp converts the idealized energy deposits

into simulated detector signals, using measured responses of the *BABAR* detector to events in data, and uses background mixing to add effects of cosmic radiation and detector noise, using cosmic ray data measured in the *BABAR* detector. The program Bear performs the MC reconstruction, using the same methods as are used in data.

CHAPTER III

ANALYSIS

Overview

For a given event registered in the *BABAR* detector, particles are reconstructed into charged tracks and neutral clusters. Momentum, energy, charge, and velocity measurements from the various detectors are used to identify possible particle identification (PID) for each track and cluster. Combinations of tracks and neutrals are then combined to form reconstructed particle candidates.

This analysis searches for signal events of the topology $e^+e^- \rightarrow \Upsilon(4S) \rightarrow B^0\overline{B}^0$ ($B^0 \rightarrow$hadrons,$\overline{B}^0 \rightarrow$Invisible($+\gamma$)). The analysis strategy follows. First, events are found that contain a hadronically decaying B^0. Cuts are applied to reduce the number of background events in the tagged sample. MC simulation is used to determine the efficiency of signal events to pass these cuts, as well as predict the number of background events remaining. The number of events in the tagged sample, signal efficiency, background estimate, and data events remaining after applying cuts are used to obtain a branching fraction calculation and upper limit.

Dataset

The events used in this analysis are divided into data and MC collections. A collection is a file containing the reconstructed events in a data or MC sample, along with any composite particle information and calculated variables associated with the events.

The data used in this analysis are summed up in Table 3.1. The luminosity and number of events in the table were determined from the BbkLumi script, which uses bhabha events in the data to calculate the luminosity. Off-peak data is used to study continuum backgrounds (See Table 3.2). Off-peak data is data taken 40 MeV below the $\Upsilon(4S)$ resonance.

Table 3.1. Data samples used in this analysis.

Run	$\mathcal{L}(\text{fb}^{-1})$	$B^0\overline{B}^0$ Events ($\times 10^6$)
Run 1	20.403	11.173
Run 2	61.076	33.697
Run 3	32.278	17.784
Run 4	100.28	55.255
Run 5	133.26	73.595
Run 6	76.156	41.018
Total or Average	$423.5\,\text{fb}^{-1}$	2.325×10^8

To help understand the behavior of signal and background in the data while keeping the analysis unbiassed, Monte Carlo(MC) simulated events were used. The MC events used in this analysis are given in Table 3.3 for background MC, and Table 3.4 for signal MC. The MC events are normalized to the data luminosity using

Table 3.2. Off-peak data samples used in this analysis

Run	$\mathcal{L}(\text{fb}^{-1})$
Run 1	2.165
Run 2	6.923
Run 3	2.486
Run 4	10.121
Run 5	14.485
Run 6	7.275
Total	43.437

the luminosities in Table 3.1 with the luminosity determined by the number of events produced and the known cross sections at the $\Upsilon(4S)$ resonance. The $B^0 \rightarrow$ invisible+γ MC uses phase space to model the photon energy distribution. The $B^0\overline{B}^0$ Cocktail MC sample consists of events where one B^0 decays into one of a set of modes ($B^0 \rightarrow D^{(*)-}X, X = \pi^+, \rho^+$, or $a1^+$) that are easily reconstructed using the hadronic method used in this analysis with the other neutral B in the event decaying freely, and is used when greater statistics of peaking $B^0\overline{B}^0$ background is needed. Peaking events refers to events with a correctly reconstructed B meson. When used, the $B^0\overline{B}^0$ Cocktail MC sample is compared to the $B^0\overline{B}^0$ generic sample to ensure the two are in agreement.

Event Reconstruction

Recorded signals in SVT and DCH are reconstructed into charged tracks. Tracks are found using hits in the DCH using a Kalman filter algorithm. They are further refined by performing a helix fit to the hits found by the Kalman filter algorithm,

Table 3.3. Background Monte Carlo samples used in this analysis

Background Simulation Sample	σ(nb)	$\mathcal{L}$(fb^{-1})	Events ($\times 10^6$)
$B^0\overline{B}^0$ generic	0.549	1274	699.68
$B^0\overline{B}^0$ Cocktail	0.0209	3758	78.537
B^+B^- generic	0.549	1303	715.3
$c\bar{c}$ generic	1.30	841	1093.288
udsgeneric	2.09	435	906.386
$\tau^+\tau^-$ generic	0.94	413	387.884

Table 3.4. Signal Monte Carlo samples used in this analysis. Cocktail samples have one B^0 decay to a $B^0 \rightarrow D^{(*)-}X$ with $X = \pi^+$,ρ^+, or $a1^+$, representing 3.99% of B^0 decays.

Signal Simulation Sample	Events ($\times 10^6$)
$B^0 \rightarrow \nu\overline{\nu}$	5.828
$B^0 \rightarrow \nu\overline{\nu}\gamma$	5.828

and searching for hits in the DCH that may be associated with the track but were not identified by the Kalman filter fit, followed by refitting using the Kalman filter algorithm. The tracks are then extrapolated to the SVT, and hits in the SVT consistent with the tracks are identified. The tracks are then refit using the combined DCH and SVT hits. Hits in the SVT that are not associated to tracks are then passed to another track finding algorithm, to look for tracks that only register in the SVT. The tracks are then extrapolated to the EMC, and clusters (energy deposits in single EMC crystals) consistent with the tracks are merged with them. Clusters not merged with tracks are used to fill the EMC neutrals list: CalorNeutral. The extrapolation is then continued to the IFR, and hits not associated with the tracks or neutral EMC lists are then used to create a neutral hadron list: NeutralHad. These track and

neutral candidates are then used to create sublists for track quality, based on number of hits in the detectors, distance from the IP. Those that fit certain mass/momentum requirements are used to fill particle identification (PID) lists. Combinations of track and neutral particles are used to fill composite particle lists. The track, neutral, PID, and composite particle lists used this analysis are described in Appendix C.

Composite particles are defined using desired daughter particle lists, vertexing, and mass requirements. For each event, particles and composites are checked for consistency with these composite particle definitions, and used to fill composite particle lists. The composite particles used in this analysis are detailed in Appendix C.

Event Tagging

Since the daughter particles of $B^0 \rightarrow$ invisible are invisible to the detector, the first step in the analysis is to fully reconstruct the other neutral B meson in the event, referred to as the "tag B^0". The particles in the event not associated with the tag B^0 are the "signal side," which is checked for consistency with the expected noise, lost particles, and background of $B^0 \rightarrow$ invisible events. This section details the reconstruction of the tag B^0.

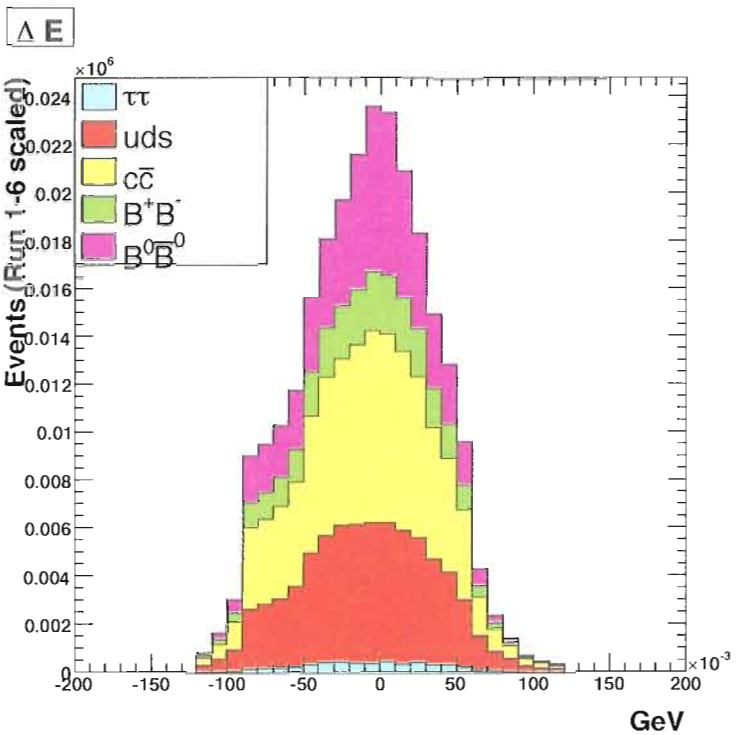

Figure 3.1. ΔE plot after preselection. The uneven cutoffs are due to the mode dependent ΔE cuts.

Tag Side Variables

A reconstructed B^0 candidate is considered a good B^0 candidate if it has $5.2\,\mathrm{GeV} < m_{\mathrm{ES}} < 5.3\,\mathrm{GeV}$, and $|\Delta E| < 0.04\,\mathrm{GeV}$. The variables m_{ES} and ΔE are defined in equations Equation III.1 and Equation III.2:

$$m_{\mathrm{ES}} = \sqrt{E_{beam}^2 - p_B^2} \tag{III.1}$$

$$\Delta E = E_B - E_{beam}, \tag{III.2}$$

where E_{beam} is half the beam energy in the center of momentum system (CMS), the inertial reference frame where the average electron momentum of an electron in the

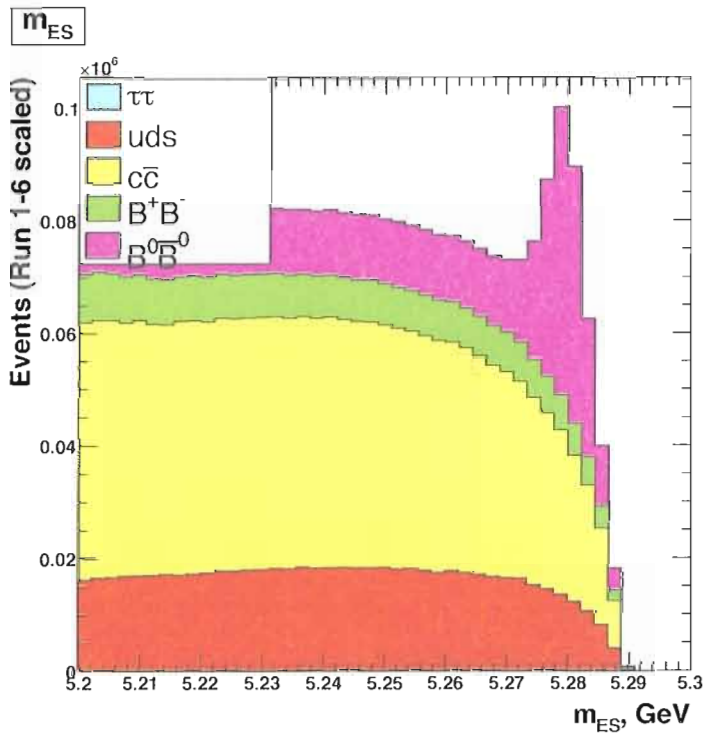

Figure 3.2. Plot of $m_{\rm ES}$ after preselection.

electron beam is opposite the average momentum of a positron in the positron beam, E_B and p_B are the reconstructed energy and momentum of the tag B^0 in the CMS frame, and the purity is defined as the fraction of the events in the peak of a $m_{\rm ES}$ plot for a given mode. The value $m_{\rm ES}$ is the reconstructed B^0 mass, using the beam energy for better resolution, and for a correctly reconstructed B^0 meson peaks at the true B^0 mass of 5.28 GeV, and ΔE is the difference of the reconstructed B^0 energy with half the CMS beam energy, which for correctly reconstructed B^0 mesons peaks at zero, as each daughter B^0 particle in the two body decay $e^+e^- \rightarrow \Upsilon(4S) \rightarrow B^0\overline{B}^0$ has half the CMS energy. Combinatoric backgrounds, where combinatoric events are

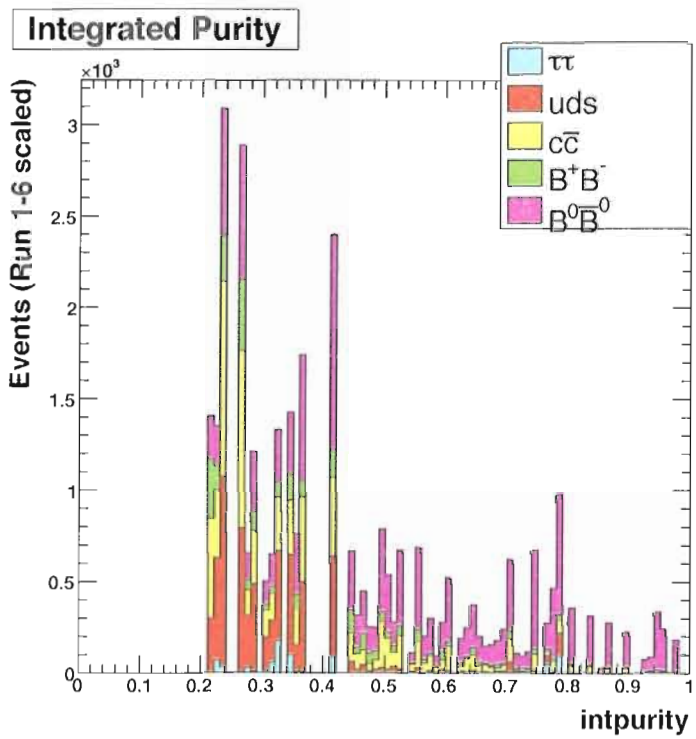

Figure 3.3. Integrated Purity plot after preselection. The cutoff at 0.2 in integrated purity is due to the 0.1 purity cut in preselection.

events where a tag B^0 is found but the particles composing the tag B^0 do not come from a single B meson, are Argus in shape in $m_{\rm ES}$ and peak more broadly in ΔE than correctly reconstructed B^0 mesons, where the Argus distribution is defined in Equation III.3,

$$f(x) = x \cdot \sqrt{1-(x/c)^2}\exp\{-\chi\cdot(1-(x/c)^2)\} \text{ for } x > 0 \qquad \text{(III.3)}$$

where c is the cutoff and χ the curvature of the distribution [22]. The variables $m_{\rm ES}$ and ΔE function as mass and momentum constraints on the B^0 candidates, using the precisely known beam parameters to improve resolution, and integrated purity serves to eliminate reconstruction modes dominated by combinatoric backgrounds.

Semi-Exclusive Skim

The tag B^0 is reconstructed using the Semi-Exclusive hadronic method [23], which works as follows. Hadrons (π^+, π^0, K^+, and K_s candidates) are added to an initial $D^{(*)+}$ candidate to form a B^0 candidate. Charged tracks are required to pass the requirements of the GoodTracksVeryLoose list and fail eMicroTight and muMicroTight (see Appendix C for particle ID information). The D^{*+} is reconstructed in the modes given in Table C.1. The masses of the charm particles used in making the seed are in Table C.2. The B^0 candidate is considered a tag B^0 if it is a neutral composite with loose m_{ES} and ΔE requirements (III.1 and III.2), and has a purity greater than 0.1. The BSemiExcl skim consists of events passing the BGFMultiHadron tagbit and containing one or more such candidates, where skim refers to a subset of a data or MC sample that pass a given set of tag bits, and a tag bit is a binary value associated with an event that indicates whether the event passes desired particle composition and event shape criteria. BGFMultiHadron is a tag bit requiring $N_{CT} > 2$ and R2 < 0.98, where N_{CT} is the number of ChargedTracks in the event and R2 is the ratio of the second to zeroth Fox-Wolfram moments. Fox-Wolfram moments are defined as $H_l = \sum_{i,j} \frac{|p_i||p_j|}{E_{vis}^2} P_l(\cos\theta_{ij})$, where E_{vis} is the total visible energy in the event, θ_{ij} is the opening angle between hadrons i and j, and P_l are Legendre polynomials. For two-jet events, common for $c\bar{c}$ and uds events, R2 peaks near R2 $= 1.0$, while events with particles more evenly distributed in the detector, typical of $B^0\overline{B}^0$ events, peak closer to zero.

The best B^0 for an event is defined as the tag B^0 candidate in the event with the highest integrated purity (and ΔE closest to 0 if there is a tie for highest integrated purity). For events with multiple tag B^0 candidates, the best B^0 is used as the tag B^0. Plots of $m_{\rm ES}$, ΔE, and integrated purity for background MC are shown in Figure 3.1, Figure 3.2, and Figure 3.3.

Data are blinded in the region $m_{\rm ES} > 5.26\,{\rm GeV}$, $E_{neu} < 0.6\,{\rm GeV}$ where E_{neu} is the total energy in the CMS of neutral candidates not associated with tag side particles or the radiated photon of $B^0 \rightarrow$ invisible $+ \gamma$. Data in the blinded region, after the signal selection cuts are applied, is hidden to avoid any possibility of bias by the experimenter towards a particular final result, until the signal side cuts and systematic errors on background events are finalized. MC is not blinded, so this only affects plots and tables that include data. The $m_{\rm ES}$ sideband ($5.22 < m_{\rm ES} < 5.25\,{\rm GeV}, 0 < E_{neu} < 0.6\,{\rm GeV}$) is a sample of incorrectly reconstructed tag B^0s that can be used to compare combinatoric events in data and MC without unblinding the data.

Yield

The yield is defined as the number of correctly reconstructed Semi-Exclusive B^0 mesons in data after the hadronic tag B^0 selection described above, and is determined from $m_{\rm ES}$ in data and MC. The yield is calculated for use in the final branching fraction calculations. The combinatoric background shapes are obtained from $c\bar{c}$, B^+B^- , uds, and combinatoric $B^0\overline{B}^0$ MC. The peaking component of $B^0\overline{B}^0$ MC is

removed from the $B^0\overline{B}^0$ MC sample to get the combinatoric $B^0\overline{B}^0$ sample using the cut $\theta^{P*} > 0.4$ or $N_{trk}^{diff} > 0$, where θ^{P*} is the angle between the reconstructed B^0 momentum vector and the momentum vector of the B^0 generated for the MC event, and N_{trk}^{diff} is the number of tracks used in reconstructing the tag B^0 that aren't associated with the corresponding B^0 generated for the MC event (Figure 3.4). They are used as a straightforward method to determine whether the tag B^0 was properly reconstructed from one of the two B^0s generated in the MC. The combinatoric MC samples are luminosity scaled and added together. The combined sample is then scaled to data in the region $5.22\,\text{GeV} < m_{\text{ES}} < 5.26\,\text{GeV}$, with data a factor of 1.08564 ± 0.00058 greater than combinatoric MC. The yield of true Semi Exclusive B^0 mesons is taken as the difference of the number of events in data and in combinatoric MC in the range $5.27\,\text{GeV} < m_{\text{ES}} < 5.29\,\text{GeV}$. The yield is $(500.8 \pm 2.0)\times 10^3$ events (Figure 3.5). The process is repeated, fitting combinatoric MC to the full luminosity scaled background MC to obtain the correctly reconstructed B^0 mesons after tagging in the MC, giving a MC yield of $(546.6 \pm 1.5)\times 10^3$ (Figure 3.6). The ratio of the yield to the MC yield is $C_{MC} = 0.9163 \pm 0.004439$ which is used as a correction to peaking background MC for the cut optimization.

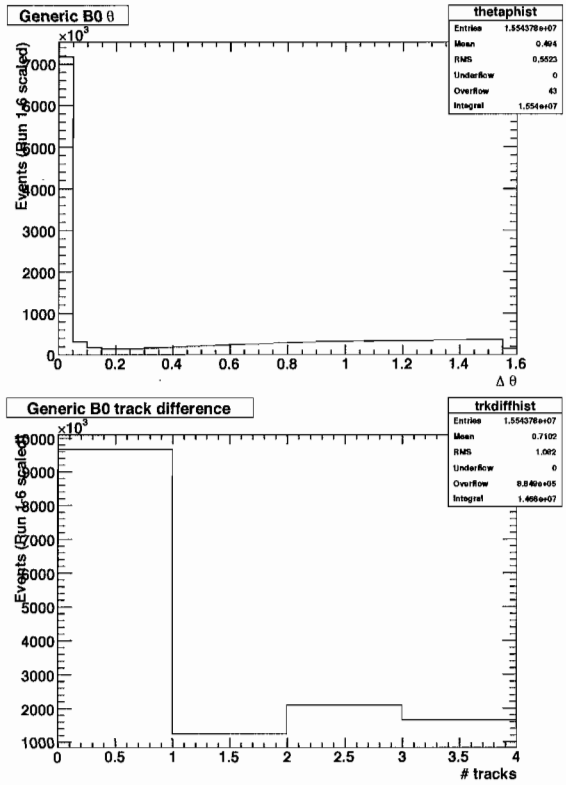

Figure 3.4. θ^{P*} and N_{trk}^{diff} for generic $B^0\overline{B}^0$ events.

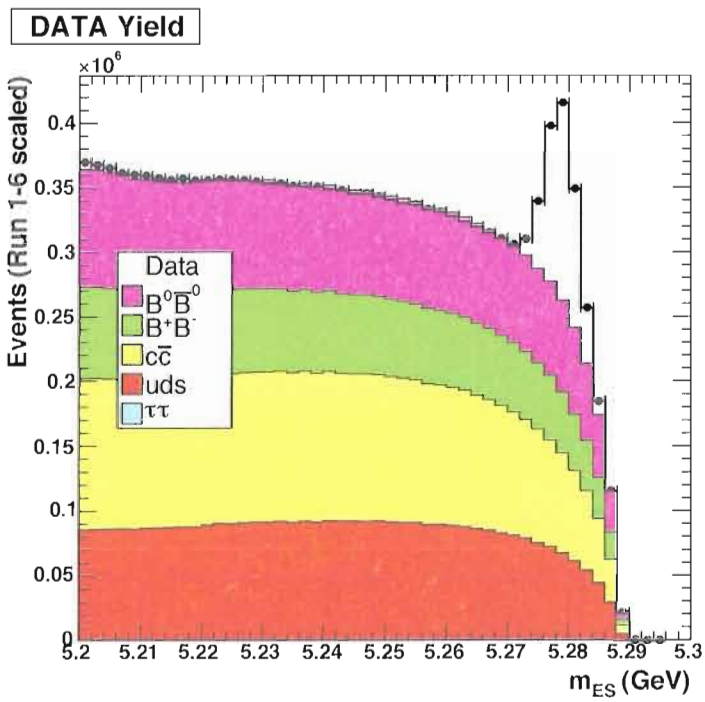

Figure 3.5. m_{ES} plot for data (points) and combinatoric MC simulation.

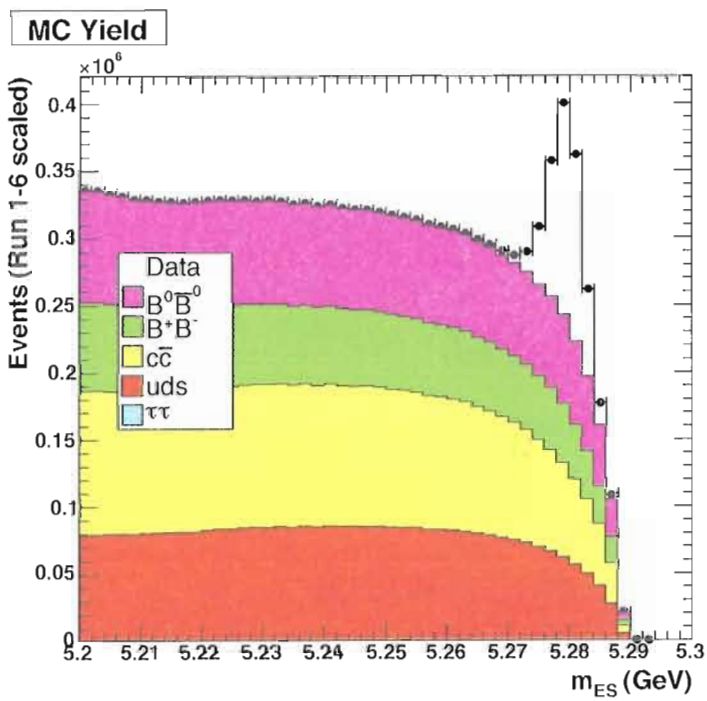

Figure 3.6. m_{ES} plot for MC (points) and combinatoric MC simulation.

Table 3.5. Signal Event Tag Efficiency Corrections

	raw $B^0\overline{B}^0$ events	tags	e ciency (%)
generic $B^0\overline{B}^0$	6.997×10^8	$(1.840 \pm 0.001) \times 10^6$	0.1315 ± 0.0001
$B^0 \rightarrow$ invisible MC	$(5.828 \pm 0.002) \times 10^6$	$(10.30 \pm 0.10) \times 10^3$	0.1767 ± 0.0017
$B^0 \rightarrow$ invisible $+ \gamma$ MC	$(5.828 \pm 0.002) \times 10^6$	$(10.45 \pm 0.10) \times 10^3$	0.1793 ± 0.0018

$B^0 \rightarrow$ invisible Correction:	$C_{B^0 \rightarrow \nu\overline{\nu}} = 1.344 \pm 0.013$
$B^0 \rightarrow$ invisible $+ \gamma$ Correction:	$C_{B^0 \rightarrow \nu\overline{\nu}\gamma} = 1.363 \pm 0.014$

Signal Yield Correction

The efficiency to tag signal events differs from the efficiency to tag generic $B^0\overline{B}^0$ events. To correct for this in the branching fraction calculations, the ratios of the tag efficiency in signal MC and in generic $B^0\overline{B}^0$ MC are calculated, for both $B^0 \rightarrow$ invisible and $B^0 \rightarrow$ invisible $+ \gamma$, and use them as a correction factor when calculating the final branching ratio (Table 3.5). The yields include $m_{\mathsf{ES}} > 5.27$, $\theta^{P*} < 0.40\,\mathrm{GeV}$, $N_{trk}^{diff} = 0$, and $|\Delta E < 0.04|$ cuts.

Signal Cuts

Signal Side Definition and Preselection

The signal side of an event is defined to be all ChargedTracks and CalorNeutral objects not used to reconstruct the tag B^0, where ChargedTracks and CalorNeutral are the loosest collection of reconstructed charged particles and of reconstructed clusters in the EMC not associated with a charged track respectively. Two preselection cuts are applied: $N_{GTL} < 3$ and $E_{neu} < 1.5\,\mathrm{GeV}$. The value E_{neu} is the total energy contained in electromagnetic calorimeter clusters on the signal side not associated

with a charged track not including the highest energy cluster for $B^0 \rightarrow$ invisible $+ \gamma$. The value N_{GTL} is the number of GoodTracksLoose, charged tracks on the signal side of the event originating from near the interaction point, 1.5 cm in x-y and 10 cm in z, with at least 12 hits in the drift chamber. For $B^0 \rightarrow$ invisible$+\gamma$, the cut $E_{hi} > 1.0$ GeV is applied, where E_{hi} is the CMS energy of the highest energy CalorNeutral cluster on the signal side of the event.

Signal Box

The signal box is defined as the region $m_{\mathsf{ES}} > 5.27$ GeV and $E_{neu} < 0.6$ GeV. Most of the signal MC events lie in this region, as the lack of signal side particles suppresses combinatoric B^0 tags, causing signal B^0 tags to peak strongly in m_{ES}, and the lack of signal side particles leaves little extra energy in the EMC, causing signal events to peak at small E_{neu}. The variable E_{neu} will also be used as a signal side cut variable, allowing for tighter requirements for E_{neu}. The E_{neu} sideband is defined as the region $m_{\mathsf{ES}} > 5.27$ GeV and $E_{neu} > 0.6$ GeV, and the double sideband as $5.22 < m_{\mathsf{ES}} < 5.26$ GeV and $E_{neu} > 0.6$ GeV. These sidebands, along with the m_{ES} sideband, do not have significant signal even if $\mathcal{B}(B^0 \rightarrow$ invisible) is measurably large, and so can be used to test the ability of background MC to model backgrounds in data. The E_{neu} sideband is rich in peaking events, and being sparse in signal can be used to compare peaking events in MC to data without unblinding the analysis. The double sideband is used to study combinatoric backgrounds for events with large E_{neu} to better understand the combinatoric backgrounds in the E_{neu} sideband.

$B^0 \rightarrow$ invisible Cuts

After the reconstruction of the tag B^0 the next step is to apply further cuts to reduce the number of expected background events in the Signal Box. Cuts are chosen which maximize the figure of merit FOM (see Equation III.4)

$$FOM = \frac{N_{Sig}}{3/2 + \sqrt{N_{Bkgrnd}}} \text{ [24]}, \tag{III.4}$$

where N_{Sig} is the number of luminosity weighted events in $B^0 \rightarrow$ invisible MC using the scaling of peaking and combinatoric MC, and N_{Bkgrnd} is the total number of events in the luminosity weighted high statistics sample.

To increase background Monte Carlo statistics during cut optimization and to provide an independent sample for checking the robustness of the cuts during optimization, I create a high statistics sample as follows. Samples of uds, $c\bar{c}$, B^+B^- , and $\tau^+\tau^-$ events are taken from the m_{ES} sidebands of the respective generic MC samples, weighted by the ratio of the number of events in the signal region to the number of events in the m_{ES} sideband region, after precuts. For $B^0\overline{B}^0$, a Crystal Ball plus Argus are fit to the $B^0\overline{B}^0$ generic MC sample after precuts. The Crystal Ball distribution is a piecewise defined function combining a Gaussian with a power law tail, and is given in Equation III.5-Equation III.7:

$$f(x;\alpha,\sigma,n,\bar{x}) = N \cdot \begin{cases} \exp(-(x-\bar{x})^2/(2\sigma^2)), & \text{for}(x-\bar{x})/\sigma > -\alpha \\ A \cdot (B-(x-\bar{x})/\sigma)^{-n}, & \text{for}(x-\bar{x})/\sigma \geq -\alpha \end{cases} \tag{III.5}$$

$$A = (n/|\alpha|)^n \cdot \exp(-|\alpha|^2/2) \tag{III.6}$$

$$B = n/|\alpha| - |\alpha| \tag{III.7}$$

where α determines at what point of the Gaussian the tail begins, σ is the width of the Gaussian, n determines the size of the tail, and $\bar{x}$ is the mean of the Gaussian [25]. The high statistics $B^0\overline{B}^0$ sample consists of events from the $m_{\rm ES}$ sideband of the $B^0\overline{B}^0$ generic sample weighted by the ratio of the area of the Argus in the signal region to the area in the sideband region to model the combinatoric component, plus all the events from the $B^0\overline{B}^0$ Cocktail MC sample weighted by the ratio of the number of events in the $B^0\overline{B}^0$ Cocktail sample to the area of the Crystal Ball to model the peaking component, after preselection. The $B^0\overline{B}^0$ Cocktail sample appears to lack a significant combinatoric component to $m_{\rm ES}$. A comparison of the high statistics sample with generic MC can be found in Appendix A.

The figure of merit is chosen over the significance, $N_{Sig}/\sqrt{N_{Sig}+N_{Bkgrnd}}$, and $N_{Sig}/\sqrt{N_{Bkgrnd}}$ because the former is dependent on the choice of the signal branching ratio, and the latter is not well behaved as N_{Bkgrnd} goes to zero, which is possible if tight enough cuts are chosen. The 3/2 in the equation optimizes the cuts for a signal present at the 3σ level. This is chosen as a compromise between setting a good upper limit if no signal is found and maximizing the sensitivity of the search for $B^0\rightarrow$ invisible.

Variables used in the cut optimization are

- N_{CT}— the number of reconstructed charged tracks on the signal side of the event,

- N_{GTL}— the number of good quality charged tracks originating from the IP on the signal side of the event,
- E_{neu}— the total energy in the CMS frame of neutral clusters on the signal side of the event, not including the radiated photon from $B^0 \rightarrow$ invisible $+ \gamma$,
- N_{π^0}— the number of reconstructed neutral pions in the signal side of the event, and
- R2— the ratio of the second to zeroth Fox-Wolfram moments.

Both N_{CT} and N_{GTL} are considered to allow for the possibility of accepting events with a track not originating at the IP, such as those produced by a tag side particle looping in the detector's magnetic field or with a sharp change in direction due to scattering, resulting in the particle registering as more than a single track, or tracks from beam backgrounds or cosmic rays.

The FOM is optimized for each variable, in order, holding cuts on the other variables fixed. This is iterated until no cuts are changed by an iteration of the optimization. The cuts that optimize the significance for $B^0 \rightarrow$ invisible in this manner are $N_{GTL} = 0$, $E_{neu} < 0.16\,\text{GeV}$, $N_{CT} = 0$, R2 < 0.62, and $N_{\pi^0} < 2$ (Figure 3.7-Figure 3.10). N_{GTL} is not shown, as GoodTracksLoose is a subset of ChargedTracks, so after the $N_{CT} = 0$ cut is applied, the remaining events do not have any signal side GoodTracksLoose. The following plots show signal MC, generic background MC, and the figure of merit for these cuts, after all the cuts for the other variables have been

applied. The optimization is done in MC, to keep the data blinded. The upper left plot shows signal MC scaled to a branching fraction of 10^{-4}; the lower left plot shows background MC. The right plot shows the figure of merit, FOM, for events in the acceptance region for the variable vs. cut value on that variable. The efficiency of signal and number of background events is given in Table 3.7.

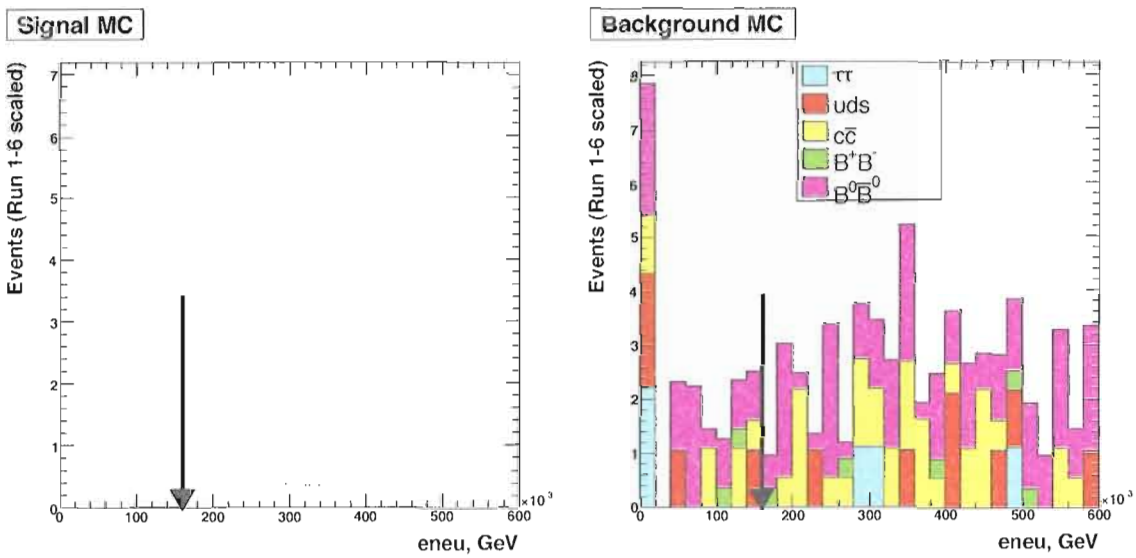

a) b)

Figure 3.7. E_{neu} in a) $B^0 \rightarrow$ invisible and b) background

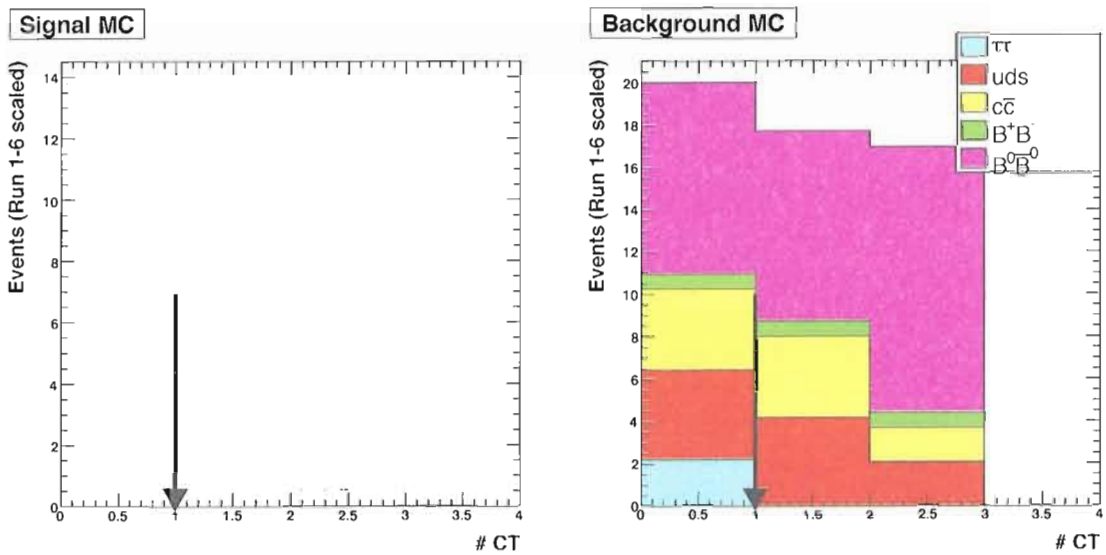

a) b)

Figure 3.8. N_{CT} in a) $B^0 \rightarrow$ invisible and b) background

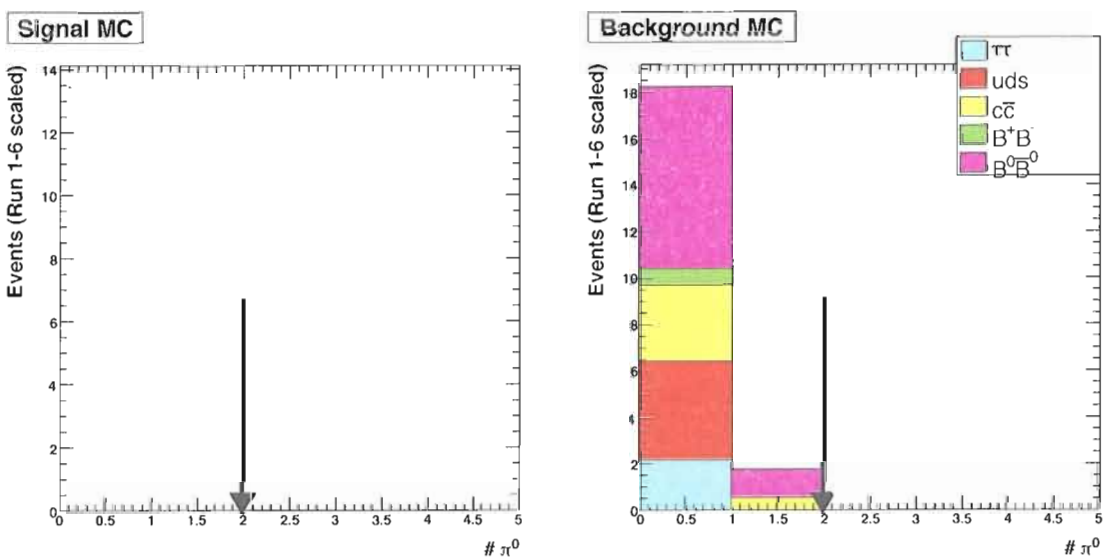

a) b)

Figure 3.9. N_{π^0} in a) $B^0 \rightarrow$ invisible and b) background

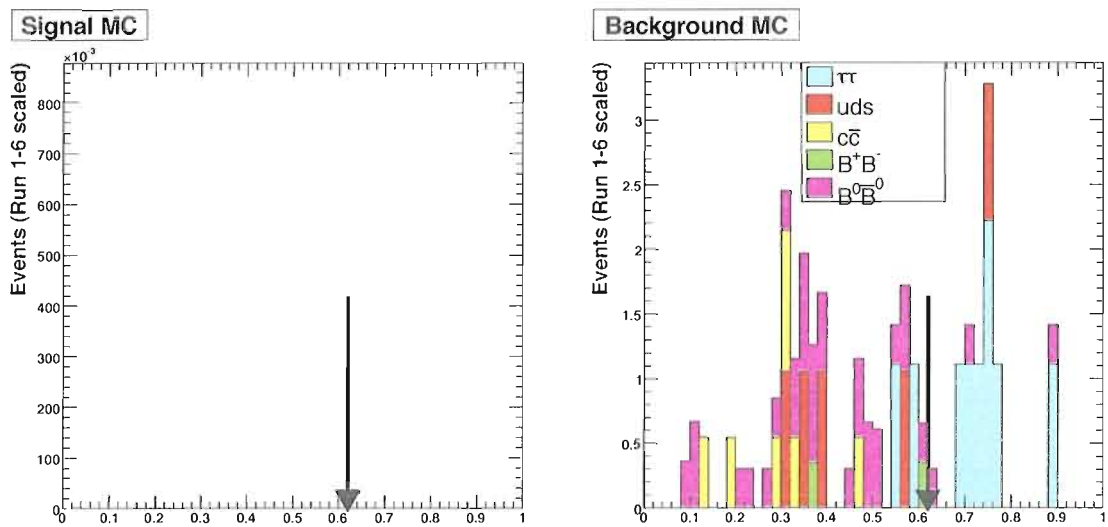

a) b)

Figure 3.10. R2 in a) $B^0 \rightarrow$ invisible and b) background

$B^0 \rightarrow$ invisible $+ \gamma$ Cuts

For $B^0 \rightarrow$ invisible $+ \gamma$ the energy of the highest energy photon E_{hi} is separated from the energy of the rest of the signal side neutral energy, E_{neu}. The cuts that optimize the figure of merit for $B^0 \rightarrow$ invisible $+ \gamma$ are $N_{GTL} = 0$, $E_{neu} < 0.28\,\text{GeV}$, $N_{CT} = 0$, R2 < 0.62, and $N_{\pi^0} = 0$.

Plots Figure 3.11-Figure 3.14 show the cut variables for events in the signal box passing all other cuts but the one being plotted for $B^0 \rightarrow$ invisible $+ \gamma$. Again, there is a $N_{CT} = 0$ cut, eliminating events with $N_{GTL} > 0$, so the N_{GTL} plot is not shown. The upper left plot shows signal MC scaled to a branching fraction of 10^{-4}; the lower left plot shows background MC. The right plot shows the figure of merit, FOM, for events in the acceptance region for the variable vs. cut value on that variable. The efficiency of signal events and number of background events is given in Table 3.9.

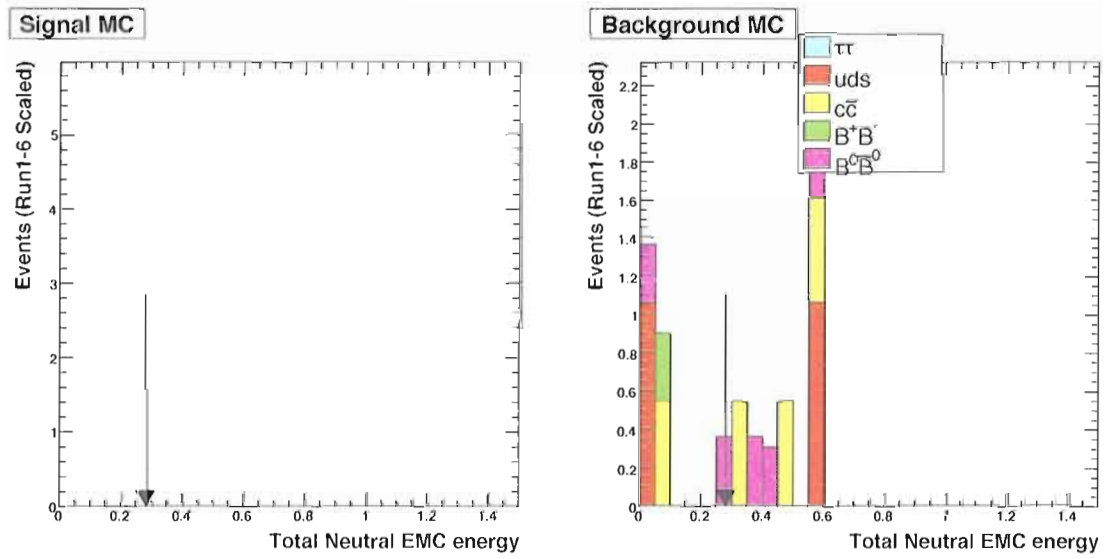

a) b)

Figure 3.11. E_{neu} in a) $B^0 \rightarrow$ invisible + γ and b) background

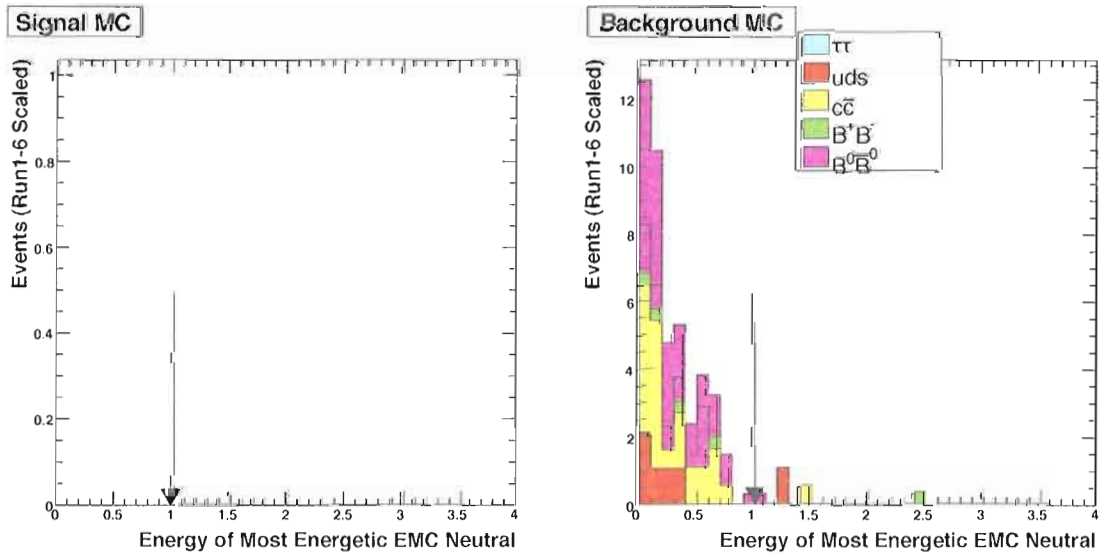

a) b)

Figure 3.12. Energy of E_{hi} in a) $B^0 \rightarrow$ invisible + γ and b) background

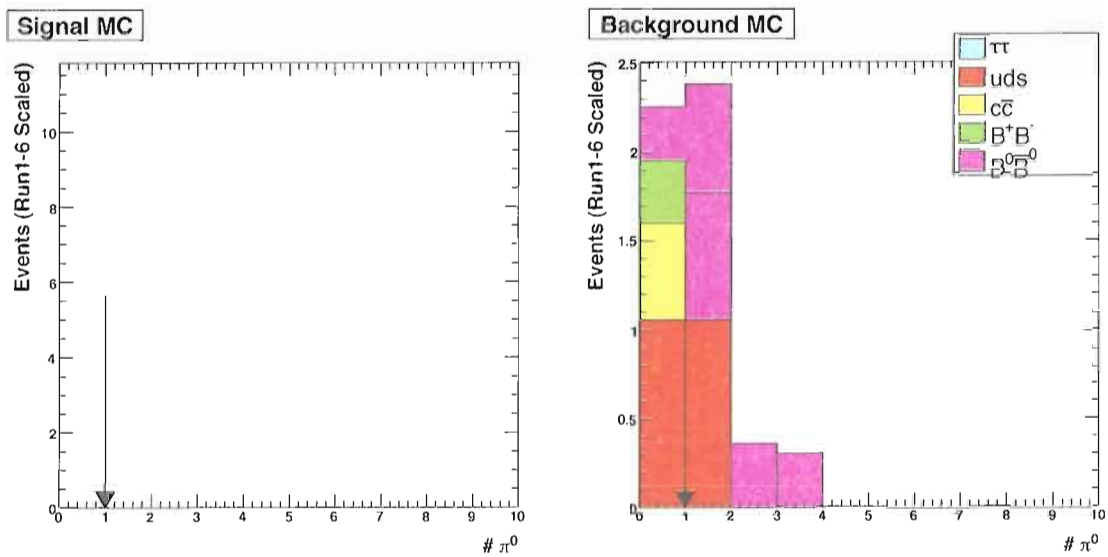

a) b)

Figure 3.13. N_{π^0} in a) $B^0 \rightarrow$ invisible + γ and b) background

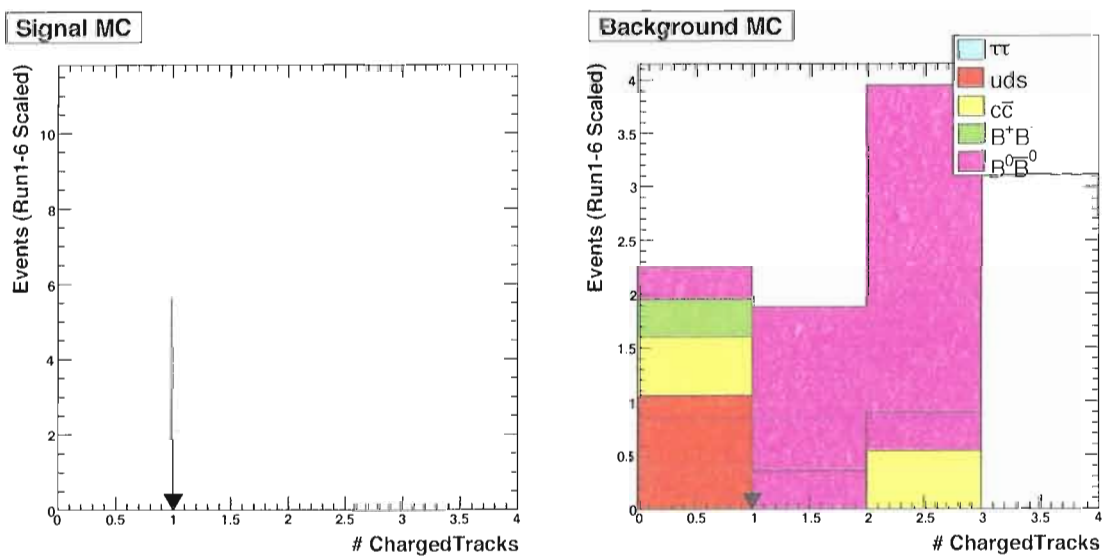

a) b)

Figure 3.14. N_{CT} in a) $B^0 \rightarrow$ invisible + γ and b) background

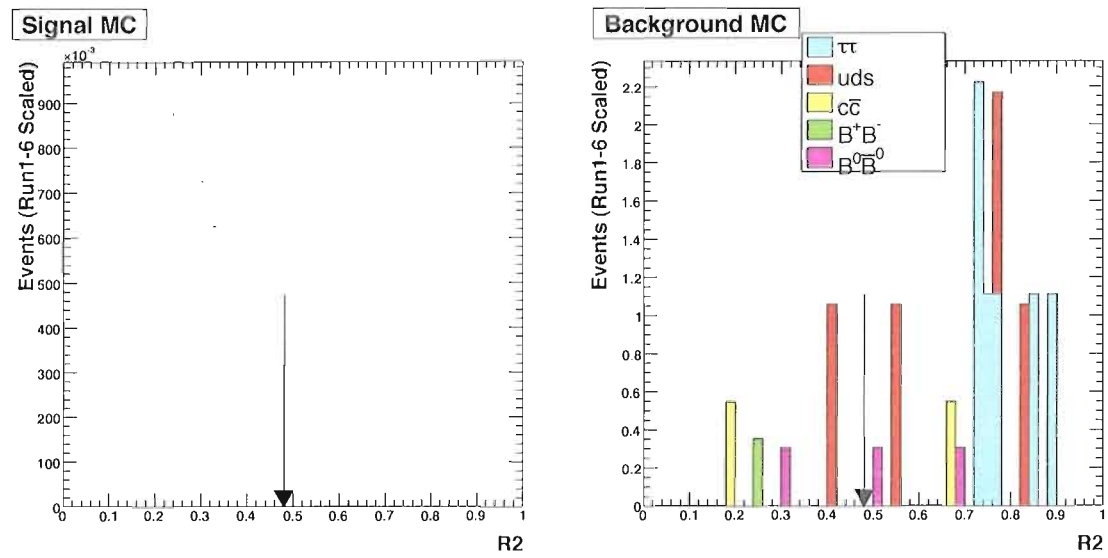

a) b)

Figure 3.15. R2 in a) $B^0 \rightarrow$ invisible + γ and b) background

Efficiencies

After optimization, the number of combinatoric background events for $B^0 \rightarrow$ invisible is given in Table 3.6. The combinatoric events are scaled to data using the m_{ES} sideband.

Table 3.7 gives the cumulative efficiency of signal to pass the $B^0 \rightarrow$ invisible signal side cuts, with the tag B^0 selection and preselection included in the efficiencies. It also gives the number of peaking background and combinatoric background events, the total number of background events, and number of events in data for $B^0 \rightarrow$ invisible. The peaking background in Table 3.7 is scaled to the peaking data in the E_{neu} sideband, where the peaking data in the E_{neu} sideband is calculated by scaling combinatoric background to data in the double sideband, and subtracting combinatoric background from data in the E_{neu} sideband using this scaling. Cocktail MC is used for the peaking events, to enhance statistics. The scaling factors and a comparison of generic MC versus cocktail MC can be found in Appendix B.

$B^0 \rightarrow$ invisible $+ \gamma$ Efficiencies

After optimization, the number of combinatoric background events for $B^0 \rightarrow$ invisible is given in Table 3.8. The combinatoric events are scaled to data using the m_{ES} sideband.

Table 3.9 gives the efficiency of signal to pass the $B^0 \rightarrow$ invisible signal side cuts, with the tag B^0 selection and preselection included in the efficiencies. It also gives the number of peaking background and combinatoric background events, the total

number of background events, and number of events in data for $B^0 \rightarrow$ invisible. The peaking background in Table 3.9 is scaled to the peaking data in the E_{neu} sideband, where the peaking data in the E_{neu} sideband is calculated by scaling combinatoric background to data in the double sideband, and subtracting combinatoric background from data in the E_{neu} sideband using this scaling. Cocktail MC is used for the peaking events, to enhance statistics. The scaling factors and a comparison of generic MC versus cocktail MC can be found in Appendix B.

Table 3.6. $B^0 \rightarrow$ invisible combinatoric background cutflow table. Combinatoric $B^0\overline{B}^0$ events are those that have $\theta^{P*} > 0.4$ or $N_{trk}^{diff} \neq 0$. Combinatoric background is given as a number of events. Combinatoric is scaled to the $m_{\rm ES}$ sideband.

Cut	$\tau^+\tau^-$	uds	$c\bar{c}$	B^+B^-	Comb $B^0\overline{B}^0$	Comb tot.
Signal Box	82±20.	439±24	441±18	179±8.9	515±17	1655±46
R2< 0.62	20.6±5.0	387.3±22.3	422±18	177.7±8.9	517±17	1525±42
$N_{\pi^0} < 2$	15.3±4.3	312±20.	330.±15	122.0±7.1	399±14	1178±35
$N_{GTL} = 0$	9.1±3.5	74±10.	84.2±8.5	14.4±2.5	47.2±5.1	229±18
$N_{CT} = 0$	7.7±3.5	17.5±5.3	32.4±5.7	5.3±1.7	15.9±3.1	79±11
$E_{neu} < 0.16$	3.9±2.9	7.4±4.0	6.6±2.9	1.23±0.91	2.5±1.4	21.6±7.2

Table 3.7. $B^0 \rightarrow$ invisible cutflow table. Peaking $B^0\overline{B}^0$ events are those that have $\theta^{P*} < 0.4$ and $N_{trk}^{diff} = 0$; combinatoric events do not. Signal is given as an efficiency for tagged events, background and data as a number of events. Combinatoric is scaled to the $m_{\rm ES}$ sideband, peaking to the E_{neu} sideband.

Cut	$B^0 \rightarrow$ invisible efficiency (10^{-4})	Peaking $B^0\overline{B}^0$	Comb tot.	Bkg tot	Data
Signal Box	14.8±1.6	2011±80.	1655±46	3666±92	3633±60.
R2< 0.62	13.2±1.5	1955±52	1525±42	3480±67	3393±58
$N_{\pi^0} < 2$	12.9±1.5	1755±6	1178±35	2933±75	2803±53
$N_{GTL} = 0$	12.7±1.5	127±25	229±18	356±31	376±19
$N_{CT} = 0$	10.0±1.3	33±14	79±11	112±18	BLINDED
$E_{neu} < 0.16$	6.5±1.1	6.9±3.1	21.6±7.2	28.5±7.8	BLINDED

Table 3.8. $B^0 \rightarrow$ invisible $+ \gamma$ combinatoric background cutflow table. Combinatoric $B^0\overline{B}^0$ events are those that have $\theta^{P*} > 0.4$ or $N_{trk}^{diff} \neq 0$. Combinatoric is scaled to the $m_{\rm ES}$ sideband.

Cut	$\tau^+\tau^-$	uds	$c\bar{c}$	B^+B^-	Comb $B^0\overline{B}^0$	Comb tot.
Signal Box	176±14	1559±43	1573±33	591±16	1415±27	5314±79
R2 < 0.48	8.9±3.1	933±33	1132±27	542±15	1335±26	3951±62
$E_{hi} > 1.0$	0±0	98±11	83.9±7.4	34.2±3.6	73.5±5.9	290.±18
$N_{\pi^0} = 0$	0±0	27.6±5.6	22.1±3.7	6.7±1.5	17.2±2.7	73.5±8.8
$N_{GTL} = 0$	0±0	3.6±2.2	4.9±1.9	1.19±0.72	2.03±0.97	11.7±3.5
$N_{CT} = 0$	0±0	3.7±2.8	3.8±2.1	0.62±0.64	1.26±0.95	9.4±4.2
$E_{neu} < 0.28$	0±0	2.6±2.7	1.3±1.4	0.86±0.91	0±0	4.8±3.5

Table 3.9. $B^0 \rightarrow$ invisible $+ \gamma$ cutflow table. Peaking $B^0\overline{B}^0$ events are those that have $\theta^{P*} < 0.4$ and $N_{trk}^{diff} = 0$. Signal is given as an efficiency for tagged events, background and data as a number of events. Combinatoric is scaled to the $m_{\rm ES}$ sideband, peaking to the E_{neu} sideband.

Cut	$B^0 \rightarrow$ invisible $+ \gamma$ efficiency (10^{-4})	Peaking $B^0\overline{B}^0$	Comb tot.	Bkg tot	Data
Signal Box	14.99±0.16	4784±185	5314±79	10098±201	9975±100.
R2 < 0.48	12.06±0.14	4257±165	3951±62	8208±176	8097±90.
$E_{hi} > 1.0$	8.77±0.12	295±27	290.±18	584±33	664±26
$N_{\pi^0} = 0$	7.08±0.11	129±31	73.5±8.8	203±32	177±13
$N_{GTL} = 0$	6.96±0.11	24.3±9.4	11.7±3.5	36±10.	29±5.4
$N_{CT} = 0$	5.561±0.098	20.5±8.5	9.4±4.2	29.9±9.5	BLINDED
$E_{neu} < 0.28$	4.85±0.091	9.3±4.3	4.8±3.5	14.1±5.5	BLINDED

Systematic Errors

Some of the systematic errors only apply to events that are peaking in m_{ES}, or to combinatoric events. Because of this, I calculate the systematic errors on N_{Bkgrnd} in terms of number of events, using the numbers of background events predicted in Table 3.7 and Table 3.9.

Tag B^0 Yield Systematics

To check the dependence of the yield on the relative amounts of $B^0\overline{B}^0$, $c\bar{c}$, uds, and B^+B^- , the yield is recalculated with the relative amounts allowed to float when fitting the combinatoric MC to the data. This results with a fit yield of $(505.9 \pm 2.0)\times10^3$ in data, 1.01% more than the tag yield, $(500.8 \pm 2.0)\times10^3$ (Figure 3.16).

To determine the dependence of the yield on the combinatoric $B^0\overline{B}^0$ shape, the θ^{P*} cut on $B^0\overline{B}^0$ is varied and the yield is recalculated. For a θ^{P*} of 0.35 GeV a low-θ^{P*} yield of $(493.8 \pm 2.0)\times10^3$ is obtained in data, 1.4% smaller than the tag yield with $\theta^{P*} > 0.10\,\mathrm{GeV}$ For a θ^{P*} of 0.45 GeV, a high-θ^{P*} yield of $(507.1 \pm 2.0)\times10^3$ is obtained, 1.2% bigger than the tag yield. Letting $N_{trk}^{diff} < 2$, a loose-N_{trk}^{diff} yield of $(517.2 \pm 2.0)\times10^3$ is obtained in data, 3.3% larger than the tag yield. Taking the largest discrepancy as a systematic error on peaking events, this gives a systematic error for signal efficiency of 3.3%.

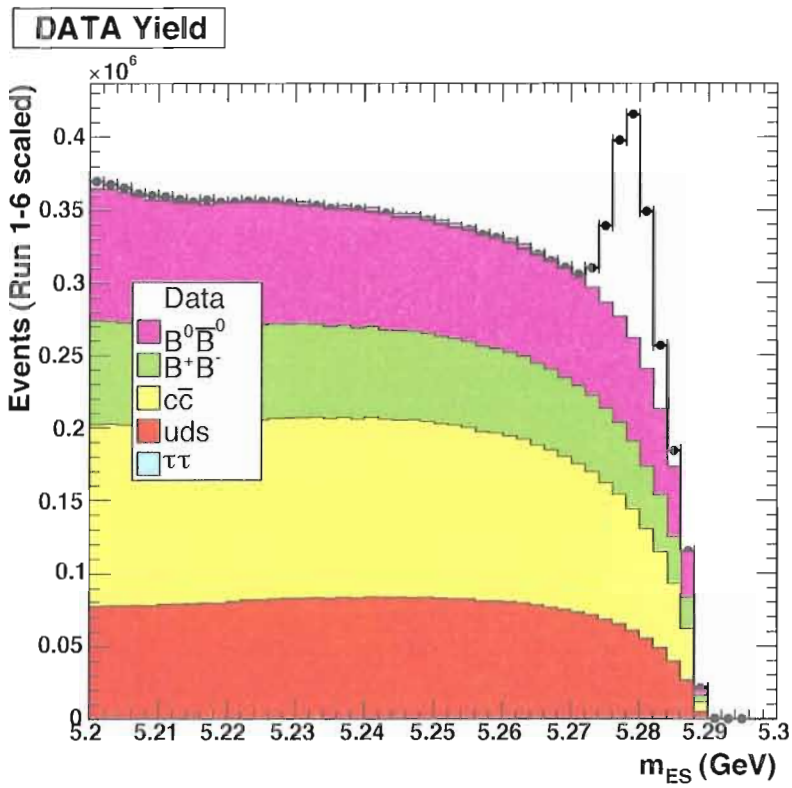

Figure 3.16. Tag B^0 yield with combinatoric contributions floated.

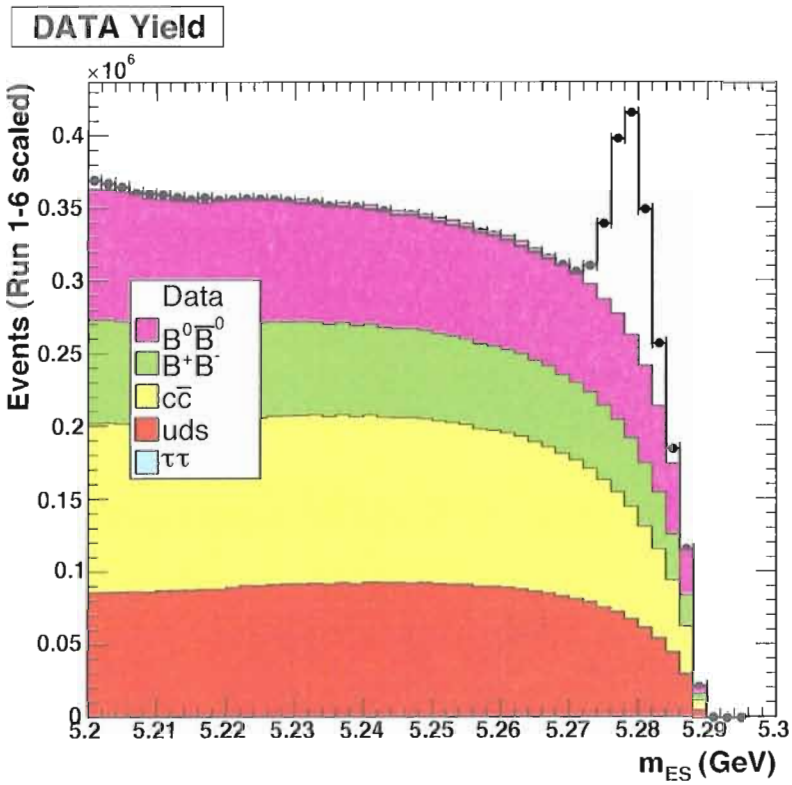

Figure 3.17. Tag B^0 yield with $c\bar{c}$, uds, and $\tau^+\tau^-$ scaled to offpeak data.

Control Sample Systematics

After finding the tag B^0 and applying a loose set of signal side cuts to generic MC in order to select events like the ones that would pass the final selection, the simulated B^0 decays used to produce the events were examined, for $B^0 \rightarrow$ invisible and $B^0 \rightarrow$ invisible $+ \gamma$, and many of the events were found to contain neutrinos or K_L^0 mesons. To check the ability of MC to model events with neutrinos and kaons, I use low multiplicity e^-, μ^-, and K_S^0 control samples. The e^- control sample is required to contain a single $e^{\pm}$, the μ^- control sample a single $\mu^{\pm}$, and the K_S^0 control sample a single K_S^0 reconstructed in the mode $K_S^0 \rightarrow \pi^+ \pi^-$ plus a single charged pion. The signal side of each control sample is then redefined to be the tracks and neutral clusters that are not associated with the tag B^0 or with the particle or particles that identify the event as an e^-, μ^-, or K_S^0 control sample event. E_{neu} for the samples are shown in figures Figure 3.18, Figure 3.19, and Figure 3.20.

Using the $B^0 \rightarrow$ invisible cuts, the number of events in the e^- control sample is 70±8.4 in data and 61.8±6.3 in MC, for a ratio of 0.883±0.139. The number of events in the μ^- control sample is 62±7.9 in data and 65.1±6.8 in MC, for a ratio of 1.050±0.172. Combined, the two control samples give a MC/data ratio of 0.961 ± 0.163. The error of this ratio is taken as a systematic on the total number of background events, giving a total error of 16.3%, or 4.65 events in $B^0 \rightarrow$ invisible. As a check, the number of events in the K_S^0 control sample is 56±7.48 in data and 45.5±7.01 in MC, for a ratio of 0.813±0.166.

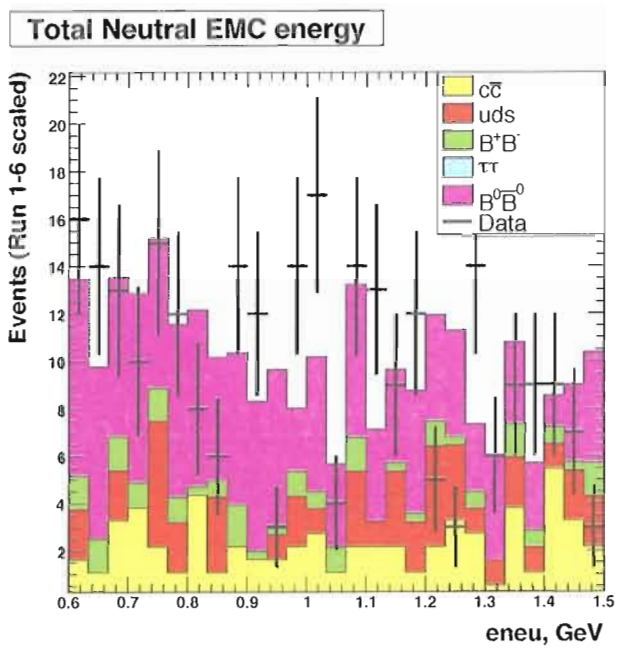

a)

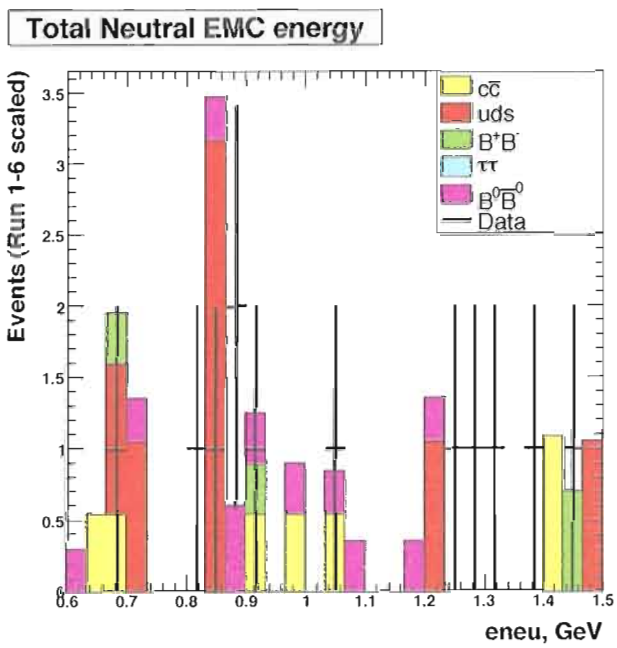

b)

Figure 3.18. E_{neu} for the K_s^0 sample in data and MC for a)$B^0 \rightarrow$ invisible and b)$B^0 \rightarrow$ invisible $+ \gamma$

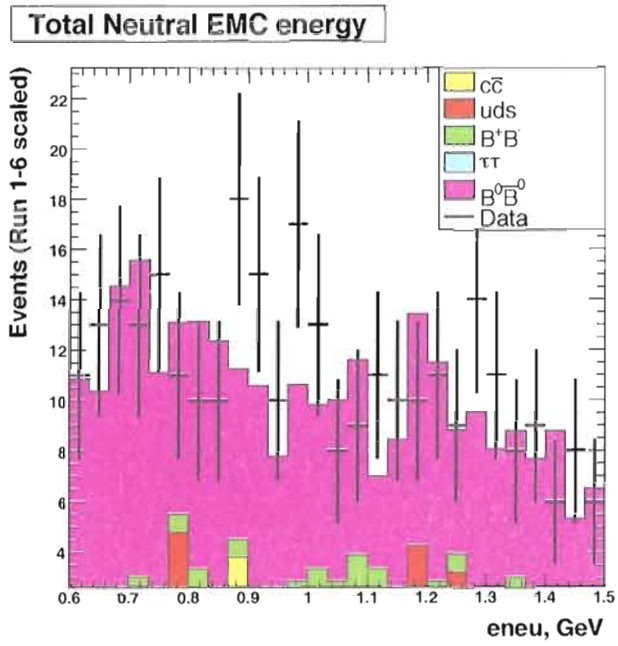

a)

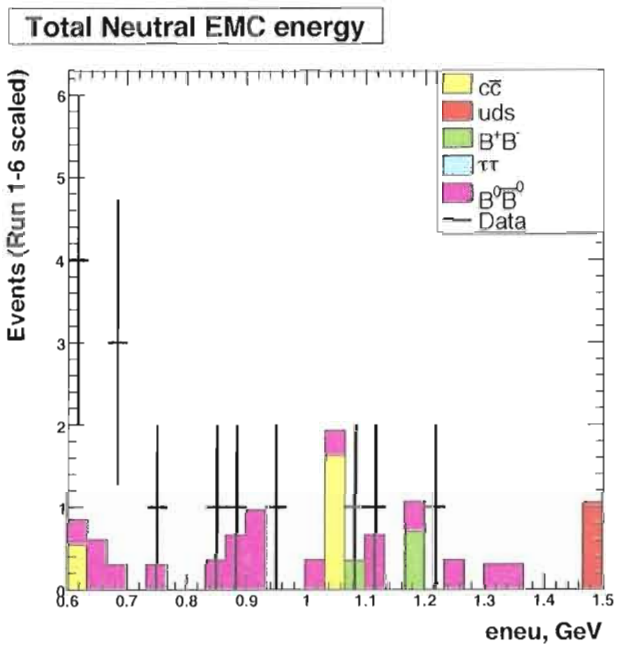

b)

Figure 3.19. E_{neu} for the μ^- in data and MC for a)$B^0 \rightarrow$ invisible and b)$B^0 \rightarrow$ invisible + γ

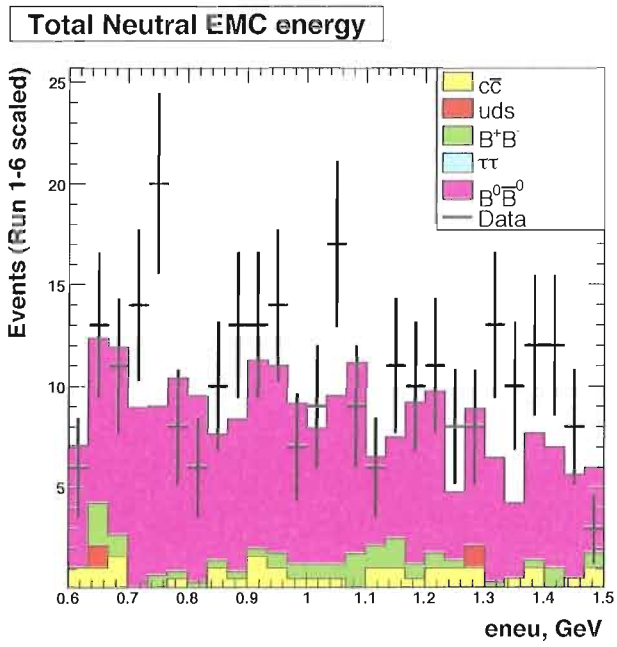

a)

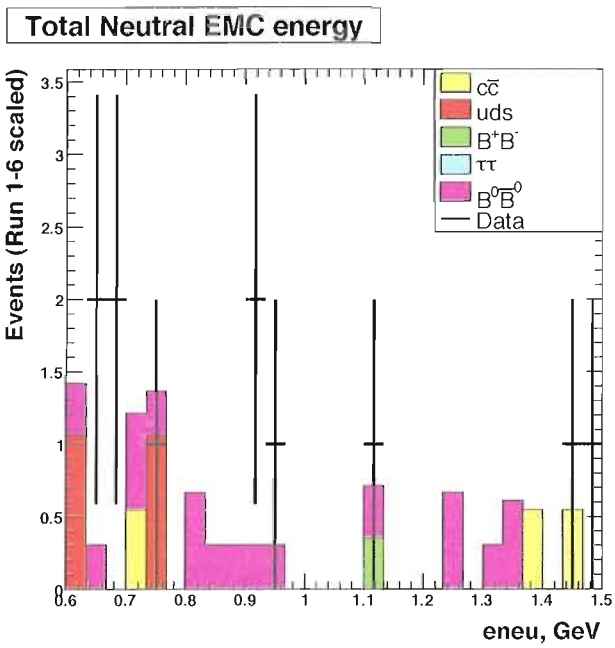

b)

Figure 3.20. E_{neu} for the e^- in data and MC for a)$B^0 \rightarrow$ invisible and b)$B^0 \rightarrow$ invisible $+ \gamma$

Using the $B^0 \rightarrow$ invisible $+ \gamma$ cuts, the number of events with one e^- is 11±3.3 in data and 8.0±4.8 in MC, for a ratio of 0.725±0.486. The number of events with one μ^- is 8±2.83 in data and 16.0±6.72 in MC, for a ratio of 2.00±1.098. Combined, the two control samples give a MC/data ratio of 1.26 ± 0.521. The error is taken as a systematic on the number of background events, giving a systematic error of 52.1%, or 7.34 events in $B^0 \rightarrow$ invisible $+ \gamma$. As a check, the number of events in the K^0_S control sample is 7±2.65 in data and 10.4±5.87 in MC, for a ratio of 1.486±1.01.

Combinatoric Scaling

I apply a systematic error on the number of combinatoric events equal to half the combinatoric correction applied by scaling the combinatoric MC to data in the m_{ES} sideband. For $B^0 \rightarrow$ invisible the correction is 1.74±0.38, for a systematic of 37% or 7.99 events. For $B^0 \rightarrow$ invisible $+ \gamma$ the correction is 2.43, for a systematic of 72% or 3.40 events.

Table 3.10. $B^0 \rightarrow$ invisible e^- control cutflow table. Peaking $B^0\overline{B}^0$ events are those that have $\theta^{P*} < 0.4$ and $N_{trk}^{diff} = 0$; combinatoric events do not. Signal is given as efficiency for tagged events, background and data as number of events. Combinatoric is scaled to the $m_{\rm ES}$ sideband, peaking to the E_{neu} sideband.

Cut	$\tau^+\tau^-$	uds	$c\overline{c}$	B^+B^-	Comb $B^0\overline{B}^0$	Comb tot
Signal Box	17.4±7.1	276±28	929±39	1071±35	2994±70.	5285±112
R2< 0.62	2.9±2.9	245±26	845±37	1074±36	2998±70.	5165±109
$N_{\pi^0} < 2$	0±0	203±24	672±33	773±29	2426±61	4074±92
$N_{GTL} = 0$	0±0	20.9±4.9	46.5±5.6	41.7±4.4	130.6±9.4	240.±16
$N_{CT} = 0$	0±0	1.2±1.2	6.7±2.1	9.8±2.2	39±5.5	56.7±7.5
$E_{neu} < 0.16$	0±0	1.4±1.4	1.4±1.1	1.38±0.87	7.1±2.6	11.3±3.9

Cut	Peaking $B^0\overline{B}^0$	Comb tot	Bkg tot	Data
Signal Box	5286±123	5285±112	10571±166	15962±126
R2< 0.62	5220±122	5165±109	10385±163	15778±126
$N_{\pi^0} < 2$	4546±106	4074±92	8620±140.	13279±115
$N_{GTL} = 0$	677±40.	240.±16	917±43	810±28
$N_{CT} = 0$	228±20.	56.7±7.5	285±22	258±16
$E_{neu} < 0.16$	50.5±5.0	11.3±3.9	61.8±6.3	70±8.4

Table 3.11. $B^0 \rightarrow$ invisible μ^- control cutflow table. Peaking $B^0\overline{B}^0$ events are those that have $\theta^{P*} < 0.4$ and $N_{trk}^{diff} = 0$; combinatoric events do not. Signal is given as efficiency for tagged events, background and data as number of events. Combinatoric is scaled to the $m_{\rm ES}$ sideband, peaking to the E_{neu} sideband.

Cut	$\tau^+\tau^-$	uds	$c\bar{c}$	B^+B^-	Comb $B^0\overline{B}^0$	Comb tot
Signal Box	55±12	954±49	1437±46	1093±33	2922±62	6461±122
R2< 0.62	5.1±3.6	816±46	1364±45	1097±33	2945±63	6229±117
$N_{\pi^0} < 2$	2.5±2.5	692±42	1099±40.	789±27	2326±53	4910±99
$N_{GTL} = 0$	1.0±1.0	51.0±7.4	82.9±7.4	50.0±4.6	142.8±9.3	328±19
$N_{CT} = 0$	0±0	8.5±3.1	15.3±3.2	12.7±2.4	37.1±4.9	73.5±8.9
$E_{neu} < 0.16$	0±0	2.2±1.6	3.9±1.7	1.08±0.67	5.9±2.0	13.0±4.0

Cut Peaking $B^0\overline{B}^0$	Comb tot	Bkg tot	Data	
Signal Box	5364±135	6461±122	11825±182	17706±133
R2< 0.62	5293±133	6229±117	11522±177	17382±132
$N_{\pi^0} < 2$	4573±116	4910±99	9483±152	14560±121
$N_{GTL} = 0$	677±41	328±19	1004±45	957±31
$N_{CT} = 0$	213±21	73.5±8.9	286±23	268±16
$E_{neu} < 0.16$	52.1±5.5	13.0±4.0	65.1±6.8	62±7.9

Table 3.12. $B^0 \rightarrow$ invisible K^0_S control cutflow table. Peaking $B^0\overline{B}^0$ events are those that have $\theta^{P*} < 0.4$ and $N^{diff}_{trk} = 0$; combinatoric events do not. Signal is given as efficiency for tagged events, background and data as number of events. Combinatoric is scaled to the $m_{\rm ES}$ sideband, peaking to the E_{neu} sideband.

Cut	$\tau^+\tau^-$	uds	$c\bar{c}$	B^+B^-	Comb $B^0\overline{B}^0$	Comb tot
Signal Box	7.5±4.3	3312±94	3708±75	1508±37	3859±66	12395±170
R2< 0.62	0±0	2974±88	3535±73	1501±37	3852±66	11860±164
$N_{\pi^0} < 2$	0±0	2400±78	2774±63	1053±30	2972±56	9198±138
$N_{GTL} = 0$	0±0	303±18	379±16	129.4±7.0	412±15	1222±37
$N_{CT} = 0$	0±0	25.9±5.6	27.3±4.3	12.6±2.3	40.0±4.7	106±11
$E_{neu} < 0.16$	0±0	1.3±1.4	4.2±1.9	0.45±0.46	4.6±1.7	10.5±3.4

Cut	Peaking $B^0\overline{B}^0$	Comb tot	Bkg tot	Data
Signal Box	5880±246	12395±170	18275±299	23358±153
R2< 0.62	5846±245	11860±164	17706±294	22804±151
$N_{\pi^0} < 2$	4740±250	9198±138	13938±286	18412±136
$N_{GTL} = 0$	2097±116	1222±37	3319±122	3417±58
$N_{CT} = 0$	148±25	106±11	253±28	281±17
$E_{neu} < 0.16$	34.9±6.2	10.5±3.4	45.5±7.1	56±7.5

Table 3.13. $B^0 \to$ invisible $+ \gamma$ e^- control cutflow table. Peaking $B^0\overline{B}^0$ events are those that have $\theta^{P*} < 0.4$ and $N_{trk}^{diff} = 0$; combinatoric events do not. Signal is given as efficiency for tagged events, background and data as number of events. Combinatoric is scaled to the $m_{\rm ES}$ sideband, peaking to the E_{neu} sideband.

Cut	$\tau^+\tau^-$	uds	$c\bar{c}$	B^+B^-	Comb $B^0\overline{B}^0$	Comb tot
Signal Box	42.4±8.7	760.±36	1906±42	1949±35	4506±58	9165±100.
R2 < 0.48	0±0	440.±28	1378±39	1882±40.	4398±75	8098±126
$E_{hi} > 1.0$	0±0	106±16	144±14	99.8±9.3	231±16	580.±34
$N_{\pi^0} = 0$	0±0	41±11	45.2±8.4	19.4±4.3	60.4±8.7	166±20.
$N_{GTL} = 0$	0±0	6.6±3.2	6.1±2.4	1.75±0.94	4.0±1.6	18.4±5.4
$N_{CT} = 0$	0±0	1.3±1.4	2.1±1.6	0.45±0.48	0.46±0.49	4.3±2.6
$E_{neu} < 0.28$	0±0	1.8±2.0	0.9±1.0	0.59±0.67	0±0	3.3±2.7

Cut	Peaking $B^0\overline{B}^0$	Comb tot	Bkg tot	Data
Signal Box	10169±246	9165±100.	19334±266	25630±160.
R2 < 0.48	9521±229	8098±126	17619±261	23817±154
$E_{hi} > 1.0$	408±32	580.±34	988±47	1266±36
$N_{\pi^0} = 0$	88±30.	166±20.	254±36	374±19
$N_{GTL} = 0$	0±0	18.4±5.4	18.4±5.4	55±7.4
$N_{CT} = 0$	8.9±7.7	4.3±2.6	13.2±8.1	16±4.0
$E_{neu} < 0.28$	4.7±3.9	3.3±2.7	8.0±4.8	11±3.3

Table 3.14. $B^0 \to$ invisible + γ μ^- control cutflow table. Peaking $B^0\overline{B}^0$ events are those that have $\theta^{P*} < 0.4$ and $N_{trk}^{diff} = 0$; combinatoric events do not. Signal is given as efficiency for tagged events, background and data as number of events. Combinatoric is scaled to the $m_{\rm ES}$ sideband, peaking to the E_{neu} sideband.

Cut	$\tau^+\tau^-$	uds	$c\bar{c}$	B^+B^-	Comb $B^0\overline{B}^0$	Comb tot
Signal Box	68±10.	1978±55	2939±51	1970±34	4447±57	11399±124
R2 < 0.48	0±0	1204±43	2160±43	1914±33	4374±56	9652±107
$E_{hi} > 1.0$	0±0	195±19	219±16	109.2±8.6	255±15	779±36
$N_{\pi^0} = 0$	0±0	69±12	63.5±8.8	25.6±4.3	68.8±7.9	227±21
$N_{GTL} = 0$	0±0	6.8±2.6	7.9±2.2	2.53±0.94	4.3±1.3	21.5±4.8
$N_{CT} = 0$	0±0	1.0±1.0	1.49±0.97	0.64±0.49	1.31±0.77	4.4±2.0
$E_{neu} < 0.28$	0±0	0.9±1.0	0±0	0.62±0.52	0.32±0.35	1.9±1.4

Cut	Peaking $B^0\overline{B}^0$	Comb tot	Bkg tot	Data
Signal Box	10246±269	11399±124	21645±296	28516±169
R2 < 0.48	9763±250.	9652±107	19415±272	25910±161
$E_{hi} > 1.0$	549±33	779±36	1328±49	1545±39
$N_{\pi^0} = 0$	154±34	227±21	381.±40.	434±21
$N_{GTL} = 0$	35±17	21.5±4.8	57±17	47±6.9
$N_{CT} = 0$	22.±10.	4.4±2.0	27±10.	11±3.3
$E_{neu} < 0.28$	14.1±6.6	1.9±1.4	16.0±6.7	8±2.8

Table 3.15. $B^0 \to$ invisible $+ \gamma$ K^0_S control cutflow table. Peaking $B^0\overline{B}^0$ events are those that have $\theta^{P*} < 0.4$ and $N^{diff}_{trk} = 0$; combinatoric events do not. Signal is given as efficiency for tagged events, background and data as number of events. Combinatoric is scaled to the $m_{\rm ES}$ sideband, peaking to the E_{neu} sideband.

Cut	$\tau^+\tau^-$	uds	$c\bar{c}$	B^+B^-	Comb $B^0\overline{B}^0$	Comb tot
Signal Box	7.7±3.9	5095±101	5514±79	1942±36	4757±61	17316±169
R2 < 0.48	0±0	3341±81	4188±68	1904±36	4683±61	14116±144
$E_{hi} > 1.0$	0±0	531±35	534±26	141±10.	315±16	1519±54
$N_{\pi^0} = 0$	0±0	131±18	146±14	31±4.8	74.7±8.0	383±29
$N_{GTL} = 0$	0±0	21.7±4.7	21.1±3.5	4.7±1.2	12.2±2.2	59.8±7.8
$N_{CT} = 0$	0±0	1.8±1.3	3.2±1.5	1.20±0.67	0.92±0.58	7.2±2.6
$E_{neu} < 0.28$	0±0	2.4±1.9	2.5±1.5	1.19±0.83	0.41±0.44	6.5±3.3

Cut	Peaking $B^0\overline{B}^0$	Comb tot	Bkg tot	Data
Signal Box	8584±427	17316±169	25900±459	31340±177
R2 < 0.48	8263±407	14116±144	22379±432	27479±166
$E_{hi} > 1.0$	415±50.	1519±54	1934±74	2343±48
$N_{\pi^0} = 0$	80.±62	383±29	463±69	631±25
$N_{GTL} = 0$	36±28	59.8±7.8	96±29	119±11
$N_{CT} = 0$	7.6±9.2	7.2±2.6	14.7±9.6	15±3.9
$E_{neu} < 0.28$	4.0±4.8	6.5±3.3	10.4±5.9	7±2.7

$B^0 \rightarrow$ invisible $+ \gamma$ Photon Systematic

The uncertainty due to the modeling of the high energy photon in $B^0 \rightarrow$ invisible$+\gamma$ events is 1.8%, determined by data/MC agreement in $\mu\mu\gamma$ control samples [26]. This is applied as a systematic error on $B^0 \rightarrow$ invisible $+ \gamma$ signal efficiency.

Signal Efficiency Systematic from Doubly Tagged Events

To check the modelling of potential signal in data by signal MC, events with two independent hadronically tagged B^0s are used, with the assumption that the tracks and neutrals remaining after tagging two independent B^0s will correspond to the signal side of a singly tagged signal event. After all $B^0 \rightarrow$ invisible signal side cuts are applied to doubletag events, 48 ± 6.9 remain in data while 45.0 ± 3.7 remain in MC, for a ratio of 0.9365 ± 0.156. This is an error of 15.6%, which is taken as a systematic error on the signal efficiencies.

Total Systematic Error

All the systematic errors are gathered together in Table 3.16, Table 3.17, and Table 3.18. The total systematic error on the number of background events is 8.57 events for $B^0 \rightarrow$ invisible and 8.09 events for $B^0 \rightarrow$ invisible$+\gamma$. The error on the signal efficiency is 15.6% for $B^0 \rightarrow$ invisible and 15.% for $B^0 \rightarrow$ invisible $+ \gamma$. The systematic error on the tag B^0 yield is 3.4% for both $B^0 \rightarrow$ invisible and $B^0 \rightarrow$ invisible $+ \gamma$.

Table 3.16. Systematic errors on the background estimates, for $B^0 \rightarrow$ invisible and $B^0 \rightarrow$ invisible $+ \gamma$, in number of events.

	$B^0 \rightarrow$ invisible	$B^0 \rightarrow$ invisible $+ \gamma$
Combinatoric scaling	7.99	3.40
Control samples	3.11	7.34
Background tot.	8.57	8.09

Table 3.17. Systematic errors on signal efficiency, for $B^0 \rightarrow$ invisible and $B^0 \rightarrow$ invisible $+ \gamma$, in percent.

	$B^0 \rightarrow$ invisible	$B^0 \rightarrow$ invisible $+ \gamma$
Doubletags	15.6%	15.6%
photon efficiency	0	1.8%
Signal eff. tot.	15.6%	15.7%

Table 3.18. Systematic errors on the tag B^0 yield, for $B^0 \rightarrow$ invisible and $B^0 \rightarrow$ invisible $+ \gamma$, in percent.

	$B^0 \rightarrow$ invisible	$B^0 \rightarrow$ invisible $+ \gamma$
$B^0\overline{B}^0$ combinatoric shape	3.3%	3.3%
Yield method	1.0%	1.0%
Yield tot.	3.4%	3.4%

CHAPTER IV

CONCLUSIONS AND FURTHER RESEARCH

Branching Fractions

A branching fraction of a decay mode is the fraction of all decays of particles of the parent type that decay in the decay mode. The expected number of signal events in this experiment is the yield times the branching fraction of that signal mode, giving the number of correctly tagged events with the other neutral B meson decaying to the signal mode, times the efficiency of a signal event to pass the signal side cuts. As the total number of events that pass the signal cuts is the sum of the number of signal events and the number of background events, the branching fraction of $B^0 \rightarrow \nu\overline{\nu}(+\gamma)$ is given by:

$$\mathcal{B}(B^0 \rightarrow \nu\overline{\nu}(+\gamma)) = \frac{1}{S}(N_{evt} - N_{Bkgrnd}), \tag{IV.1}$$

$$S = N_{Yield} \times \varepsilon_{Sig}, \tag{IV.2}$$

where N_{evt} is the number of events seen in the signal box, N_{Bkgrnd} is the expected number of background events in the signal box, N_{Yield} is the number of tagged B^0s, ε_{Sig} is the efficiency of signal tagged signal events to pass all cuts and fall in the signal box, and the sensitivity S is the constant of proportionality between the

branching fraction and the number of signal events, and therefore is a branching fraction independent measure of the ability of an analysis to detect a signal.

From Table 3.5, the tagging efficiency for $B^0\rightarrow$ invisible is $(0.1767\pm0.0017)\%$ and for $B^0\rightarrow$ invisible $+\gamma$ is $(0.1793\pm0.0018)\%$. Combined with the total efficiencies of $(6.50\pm0.11)\times10^{-4}$ for $B^0\rightarrow$ invisible and $(4.846\pm0.091)\times10^{-4}$ for $B^0\rightarrow$ invisible $+\gamma$, the signal efficiencies are $\varepsilon_{Sig} = 0.368\pm0.007\pm0.057$ for $B^0\rightarrow$ invisible and $\varepsilon_{SigGam} = 0.270\pm0.006\pm0.042$ for $B^0\rightarrow$ invisible $+\gamma$. The yield is $(500.8\pm2.0\pm17.0)\times10^3$, which is combined with the signal efficiency yield corrections $C_{B^0\rightarrow\nu\bar{\nu}} = 1.344\pm0.013$ and $C_{B^0\rightarrow\nu\bar{\nu}\gamma} = 1.363\pm0.014$ to take into account the higher probability of $B^0\rightarrow$ invisible$(+\gamma)$ events to pass the tagging selection, and with the $B^0\rightarrow$ invisible$(+\gamma)$ signal efficiencies to give sensitivities of $S = 247.4\pm39.9\times10^3$ for $B^0\rightarrow$ invisible and $S = 184.5\pm30.0\times10^3$ for $B^0\rightarrow$ invisible $+\gamma$. The predicted background is $28.5\pm7.8\pm9.2$ in $B^0\rightarrow$ invisible and $14.1\pm5.5\pm8.1$ in $B^0\rightarrow$ invisible $+\gamma$. The number of events in data is 39 ± 6.2 in $B^0\rightarrow$ invisible and 8 ± 2.8 in $B^0\rightarrow$ invisible $+\gamma$. This gives a branching fraction of $\mathcal{B}(B^0\rightarrow$ invisible$) = (4.2\pm5.6)\times10^{-5}$ and $\mathcal{B}(B^0\rightarrow$ invisible $+\gamma) = (-3.2\pm5.4)\times10^{-5}$.

The upper limit of a decay at a given confidence for an experiment is the value that, if it were the true value of the branching fraction for the decay, would lead to a measured branching for the decay for repetitions of the experiment to be greater than the branching fraction actually measured at the experiment with a probability equal to the confidence. Therefore, the chance that an experiment would measure a branching

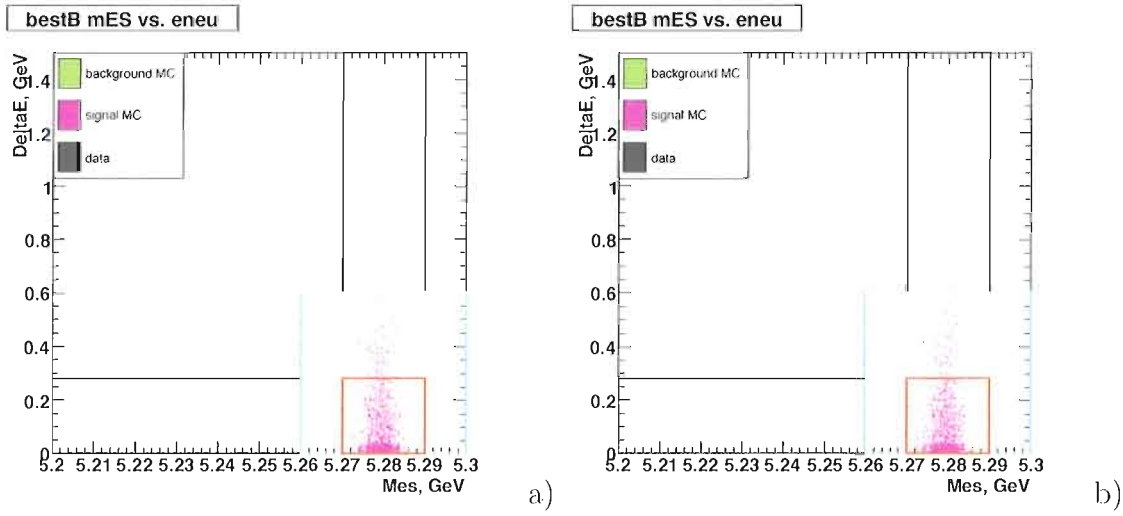

Figure 4.1. m_{ES} vs. E_{neu} plots for a) $B^0 \rightarrow$ invisible and b) $B^0 \rightarrow$ invisible $+ \gamma$, after all cuts.

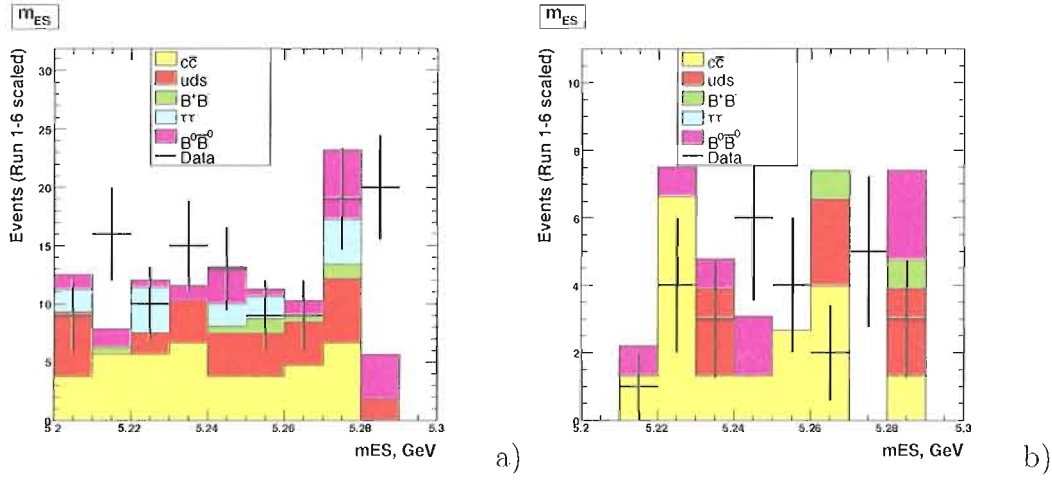

Figure 4.2. Data (points) and MC simulation, after all cuts, for a) m_{ES} in $B^0 \rightarrow$ invisible, b) m_{ES} in $B^0 \rightarrow$ invisible $+ \gamma$. Background scaled to the m_{ES} and E_{neu} sidebands.

fraction equal to that measured in the real experiment if the true branching fraction of the decay was greater than the upper limit is less than one minus the confidence.

To get an upper limit on the branching fractions, the repetition of experiments for an assumed true branching fraction is simulated as follows [27]. A value for the

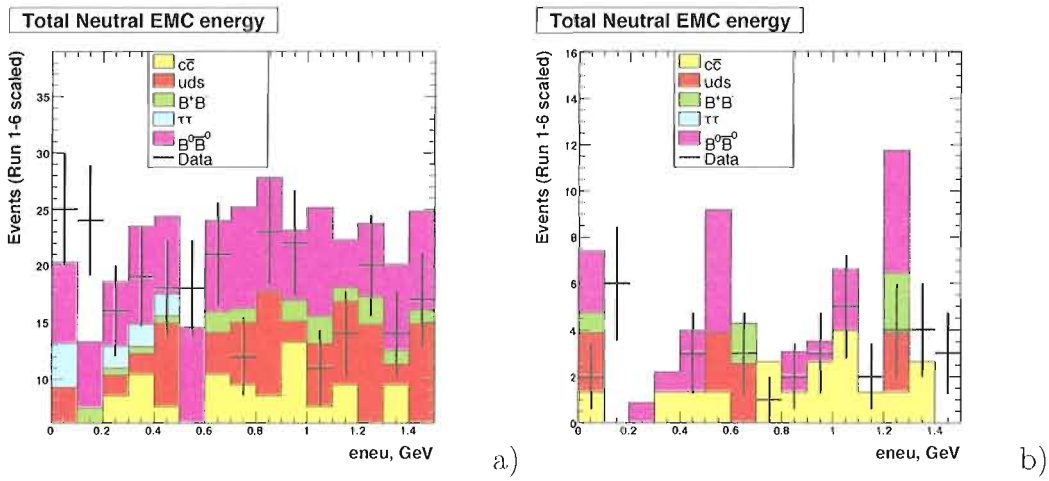

Figure 4.3. Data (points) and MC simulation, after all cuts, for a) E_{neu} in $B^0 \rightarrow$ invisible, b) E_{neu} in $B^0 \rightarrow$ invisible + γ. Background scaled to the m_{ES} and E_{neu} sidebands.

branching ratio is guessed, and 100000 toy MC experiments are produced using the values for N_{Bkgrnd} and S given above, assuming the errors are Gaussian. Each MC trial is performed as follows. For a number of background events $N_{Bkgrnd} \pm \epsilon_{Bkgrnd}$, a sensitivity $S \pm \epsilon_S$, an upper limit guess N_{UL}^{90}, and a number of data events N_{evt}, a number of trial background events N_{Bkg}^* is sampled from a Gaussian of mean N_{Bkgrnd} and width ϵ_{Bkgrnd}. A trial sensitivity of S^* is taken as $S^* = S \times (1 + x)$, where x is sampled from a Gaussian of mean 0 and width ϵ_S/S. A mean number of events seen N'_{evt} is determined by $N'_{evt} = N_{UL}^{90} \times S^* + N_{Bkg}^*$. The trial number of events seen N''_{evt} is sampled from a Poisson distribution of mean N'_{evt}. This is repeated for 10000 MC trials, and the confidence that the upper limit is less than N_{UL}^{90} is taken as the fraction of MC trials with $N''_{evt} > N_{evt}$. This is repeated for different values of N_{UL}^{90}

until a confidence of 0.9 is obtained. Using this method, the upper limits given in Table 4.1 were obtained.

Table 4.1. Upper limits for $B^0 \rightarrow$ invisible$(+\gamma)$ at the 90% confidence level.

Upper limit	Value
$N_{UL}^{90}(B^0 \rightarrow \text{invisible})$	11.7×10^{-5},
$N_{UL}^{90}(B^0 \rightarrow \text{invisible} + \gamma)$	4.3×10^{-5}

Conclusions

This analysis measured branching fractions of $\mathcal{B}(B^0 \rightarrow \text{invisible}) = (4.2 \pm 5.6) \times 10^{-5}$ and $\mathcal{B}(B^0 \rightarrow \text{invisible} + \gamma) = (-3.2 \pm 5.4) \times 10^{-5}$ leading to upper limits $\mathcal{B}(B^0 \rightarrow \text{invisible}) < 11.9 \times 10^{-5}$ and $\mathcal{B}(B^0 \rightarrow \text{invisible} + \gamma) < 4.3 \times 10^{-5}$ at the 90% confidence level. The branching fractions do not indicate significant signals and therefore are consistent with the SM. The upper limit on $B^0 \rightarrow$ invisible is still far above the 10^{-10} level needed to constrain the large extra dimension scenario. As shown in Figure 1.6, a limit on the branching fraction $\mathcal{B}(B^0 \rightarrow \tilde{\chi}_0^1 \bar{\nu})$ constrains possible values of the $\tilde{\chi}_0^1$ lifetime that result in the number of dimuon events seen at NuTeV. The upper limit of $\mathcal{B}(B^0 \rightarrow \text{invisible}) < 11.7 \times 10^{-5}$ does not reach the 10^{-5} level needed to significantly restrict the neutralino lifetimes.

In the previous search for $B^0 \rightarrow$ invisible$(+\gamma)$, an upper limit of $\mathcal{B}(B^0 \rightarrow \text{invisible}) = 22 \times 10^{-5}$ and $\mathcal{B}(B^0 \rightarrow \text{invisible} + \gamma) = 4.7 \times 10^{-5}$ were obtained [15]. It obtained these limits from a fitted signal of $N_{Sig}(B^0 \rightarrow \text{invisible}) = 17 \pm 9$ on top of a background of $N_{Bkgrnd}(B^0 \rightarrow \text{invisible}) = 19^{+10}_{-8}$, and a fitted signal of $N_{Sig}(B^0 \rightarrow \text{invisible} + \gamma) =$

$-1.1^{+2.4}_{-1.9}$ on top of a background of $N_{Bkgrnd}(B^0 \rightarrow \text{invisible} + \gamma) = 28^{+6}_{-5}$. The analysis detailed in this dissertation obtains an upper limit on $B^0 \rightarrow$ invisible almost a factor of two smaller than that obtained in the previous analysis. The upper limit on $B^0 \rightarrow$ invisible $+ \gamma$ is a slight improvement over the previous analysis.

Further Research

An experiment in its planning stages that should be promising for an improved measurement of $B^0 \rightarrow$ invisible$(+\gamma)$ is the Super$B$ experiment [28]. Its purpose would be to use precision measurements and rare decays of the B^0 meson to constrain new physics contributions, and in doing so help identify which theoretical models explain what new physics is found at the LHC and ILC. As with the *BABAR* and Belle experiments, Super$B$ would collide electrons and positrons with a center of mass energy at the $\Upsilon(4S)$ resonance, $E_{CMS} = 10.58\,\text{GeV}$. Super$B$ would have a design luminosity of $\mathcal{L} = 70 \times 10^{34}\,\text{cm}^{-2}s^{-1}$, leading to an integrated luminosity of $10\,\text{ab}^{-1}$/year. By its 3rd year of running, the Super$B$ would therefore collect a data sample of $30\,\text{ab}^{-1}$, approximately 60 times the data sample at *BABAR*. Assuming signal efficiencies and systematic errors equal to those in this analysis, a tag yield and predicted background 60 times larger than in this analysis, and a number of data events equal to the predicted background, upper limits of $\mathcal{B}(B^0 \rightarrow \text{invisible}) < 8.8 \times 10^{-5}$ and $\mathcal{B}(B^0 \rightarrow \text{invisible} + \gamma) < 5.2 \times 10^{-5}$ could be obtained. The systematic errors are largely dependent on MC statistics, however. The Super$B$ should optimally

have generic MC simulation that is at least as large as the total dataset. At *BABAR*, the generic MC sample is 3 times larger than data, so MC at Super$B$ should have at least 20 times the statistics as *BABAR*. If the systematics were completely dominated by MC statistics, this would lead to the relative systematic error being improved by greater than a factor of 4. This is probably not obtainable, but assuming a relative systematic error half that used in this analysis, upper limits at the Super B factory of $\mathcal{B}(B^0 \rightarrow \text{invisible}) < 2.4 \times 10^{-5}$ and $\mathcal{B}(B^0 \rightarrow \text{invisible} + \gamma) < 2.6 \times 10^{-5}$ could be obtained.

Also possible at Super$B$ would be the searches $B_s^0 \rightarrow$ invisible$(+\gamma)$, by running at the $\Upsilon(5s)$ resonance, which decays to $B_s^* \bar{B}_s^*$ with a branching fraction of 26%. $B_s^0 \rightarrow$ invisible$+\gamma$ would have a SM branching ratio of order 10^{-8} and be sensitive to new physics [29].

APPENDIX A

CUT OPTIMIZATION

$B^0 \rightarrow$ invisible

Figure A.1—Figure A.5 show FOM versus cut value for $B^0 \rightarrow$ invisible cuts for regular and high statistics samples. All cuts but the one on the variable plotted are applied, with the values of the other cuts chosen to maximize the FOM for the high statistics sample.

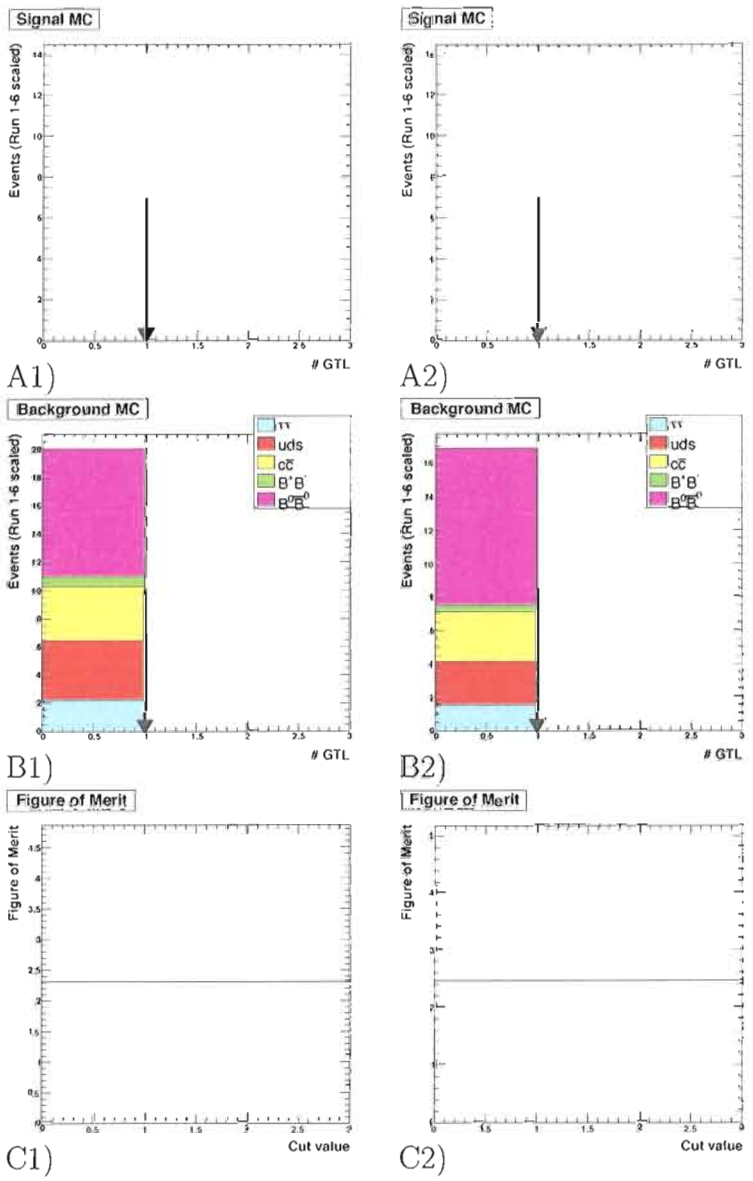

Figure A.1. N_{GTL} in A) B^0, B) background, and C) $N_{Sig}/(1.5+\sqrt{N_{Bkgrnd}})$ for 1) regular and 2) high statistics samples

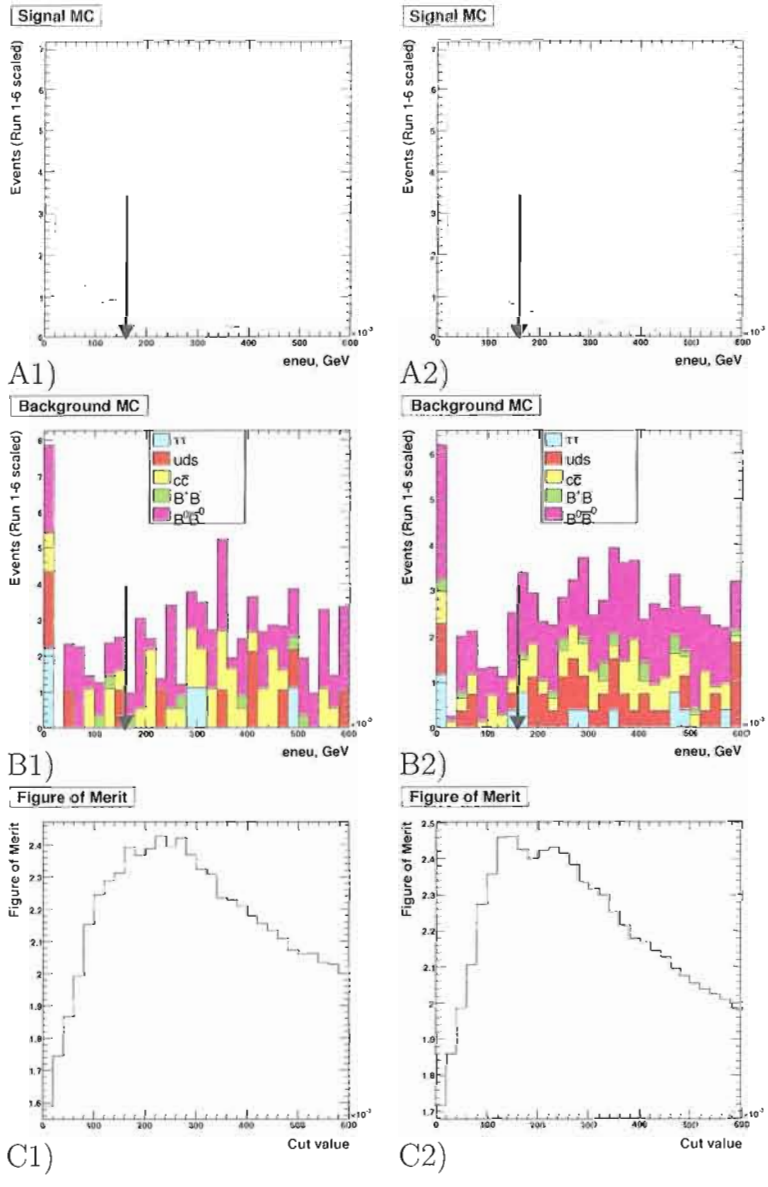

Figure A.2. E_{neu} in A) B^0, B) background, and C) $N_{Sig}/(1.5+\sqrt{N_{Bkgrnd}})$ for 1) regular and 2) high statistics samples

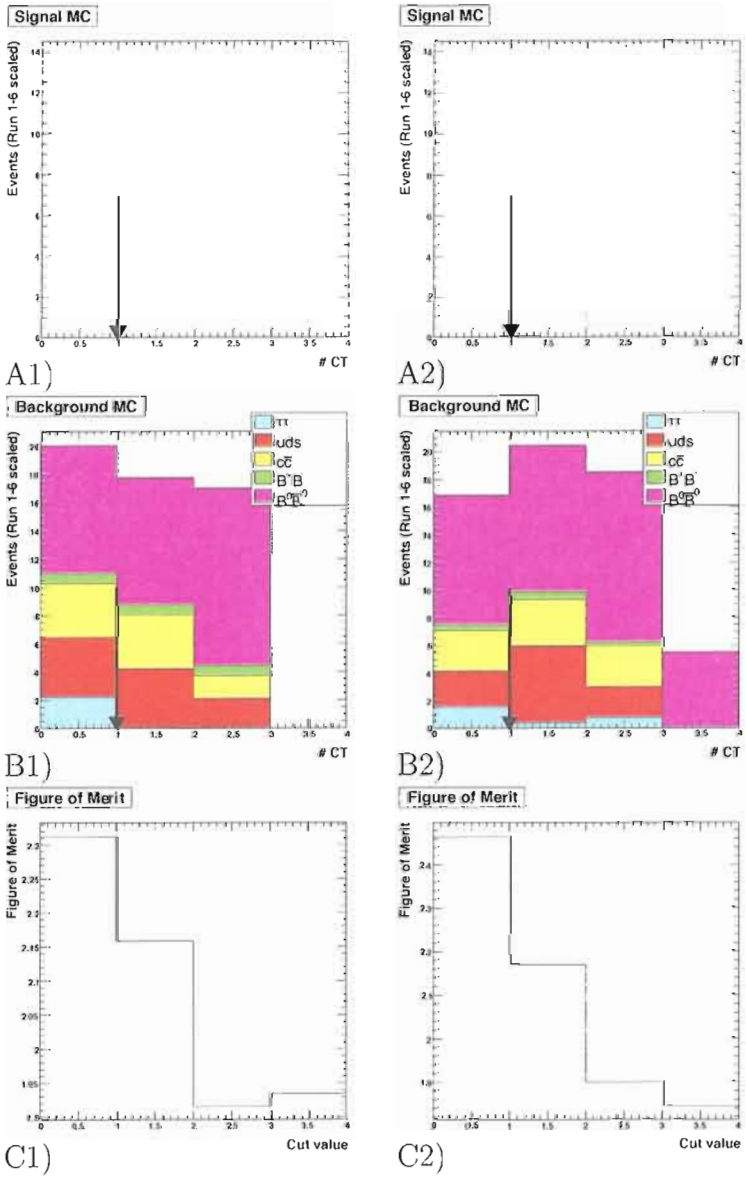

Figure A.3. N_{CT} in A) B^0, B) nBkg, and C) $N_{Sig}/(1.5+\sqrt{N_{Bkgrnd}})$ for 1) regular and 2) high statistics samples

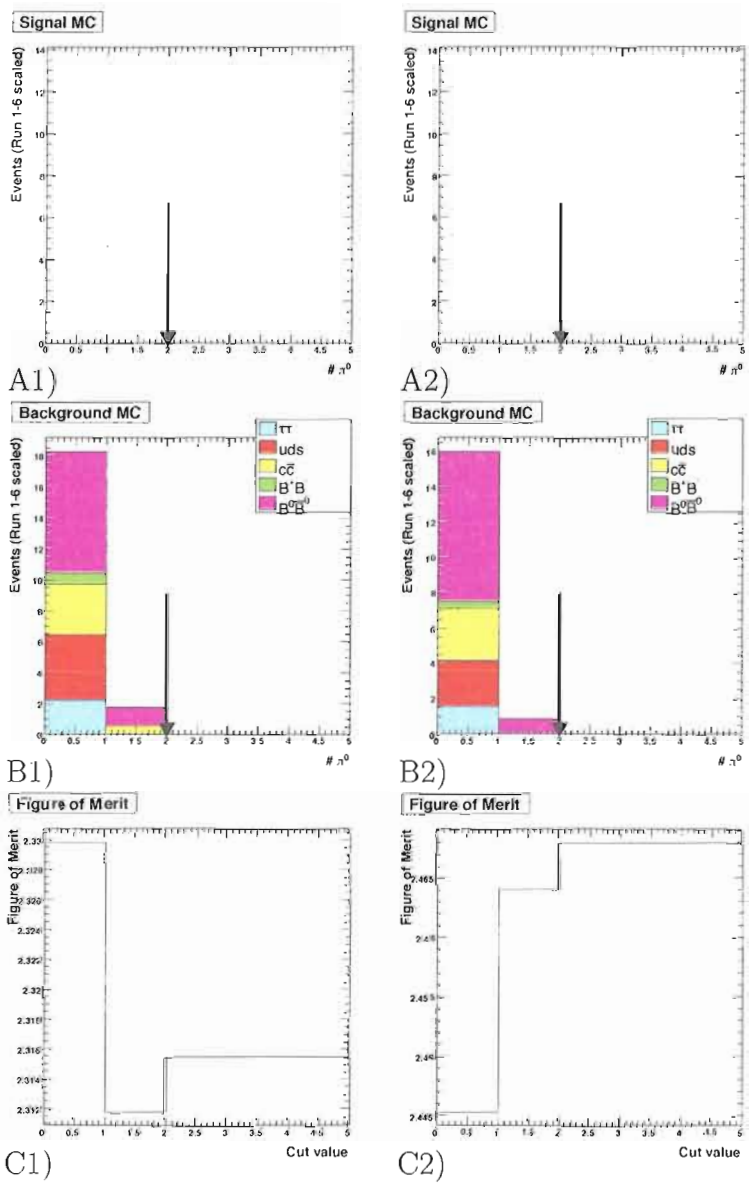

Figure A.4. N_{π^0} in A) B^0, B) background, and C) $N_{Sig}/(1.5+\sqrt{N_{Bkgrnd}})$ for 1) regular and 2) high statistics samples

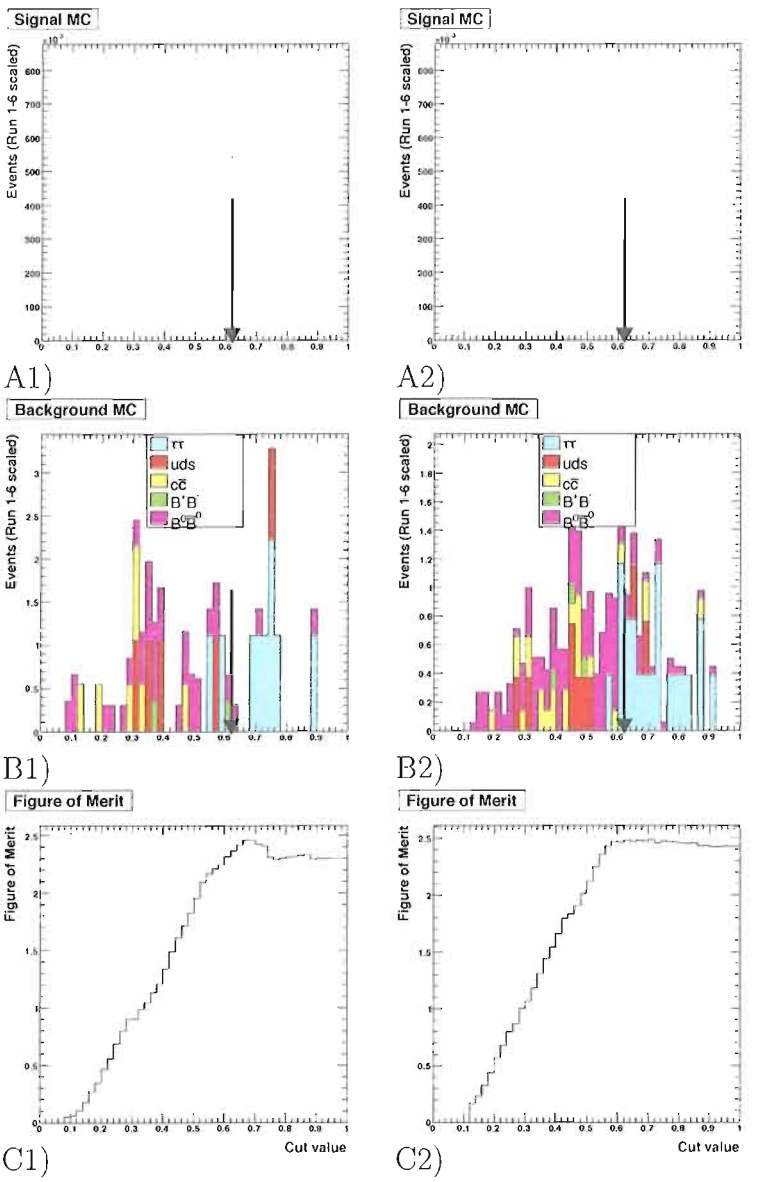

Figure A.5. R2 in A) B^0, B) background, and C) $N_{Sig}/(1.5+\sqrt{N_{Bkgrnd}})$ for 1) regular and 2) high statistics samples

$\underline{B^0 \rightarrow \text{ invisible} + \gamma}$

Figure A.6—Figure A.11 show FOM versus cut value for $B^0 \rightarrow$ invisible $+ \gamma$ cuts for regular and high statistics samples. All cuts but the one on the variable plotted are applied, with the values of the other cuts chosen to maximize the FOM for the high statistics sample.

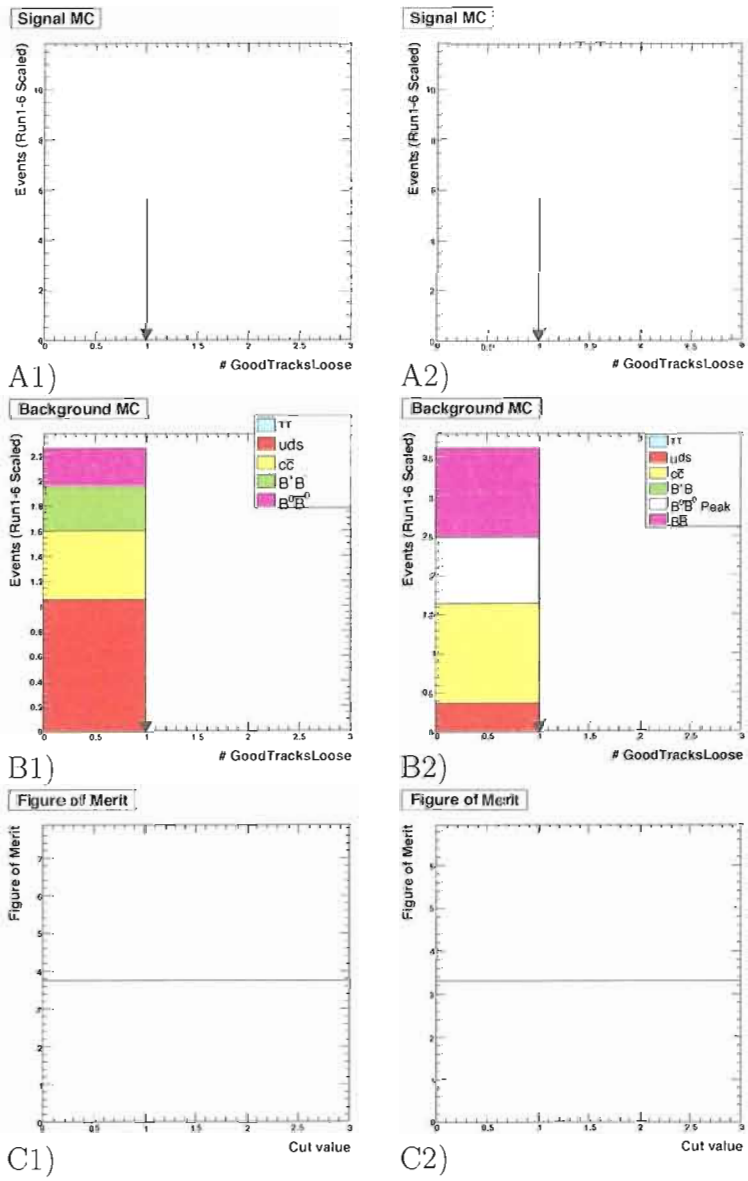

Figure A.6. N_{GTL} in A) B^0, B) background, and C) $N_{Sig}/(1.5+\sqrt{N_{Bkgrnd}})$ for 1) regular and 2) high statistics samples

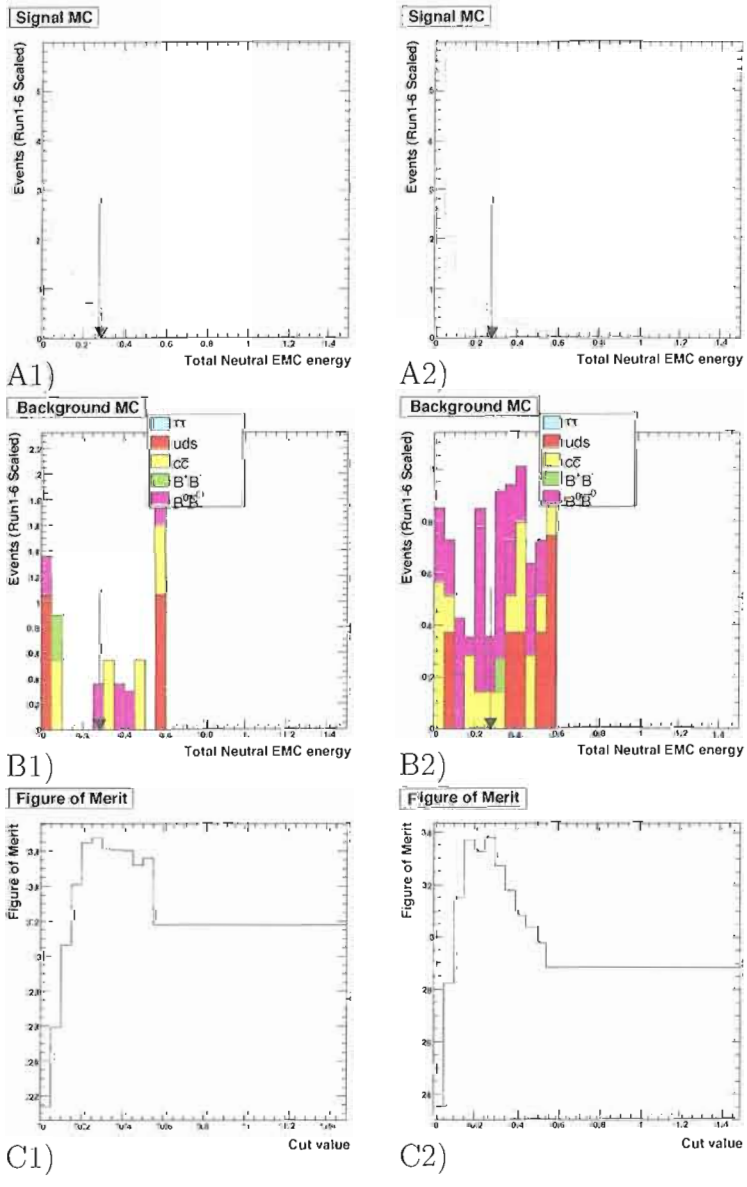

Figure A.7. E_{neu} in A) B^0, B) background, and C) $N_{Sig}/(1.5+\sqrt{N_{Bkgrnd}})$ for 1) regular and 2) high statistics samples

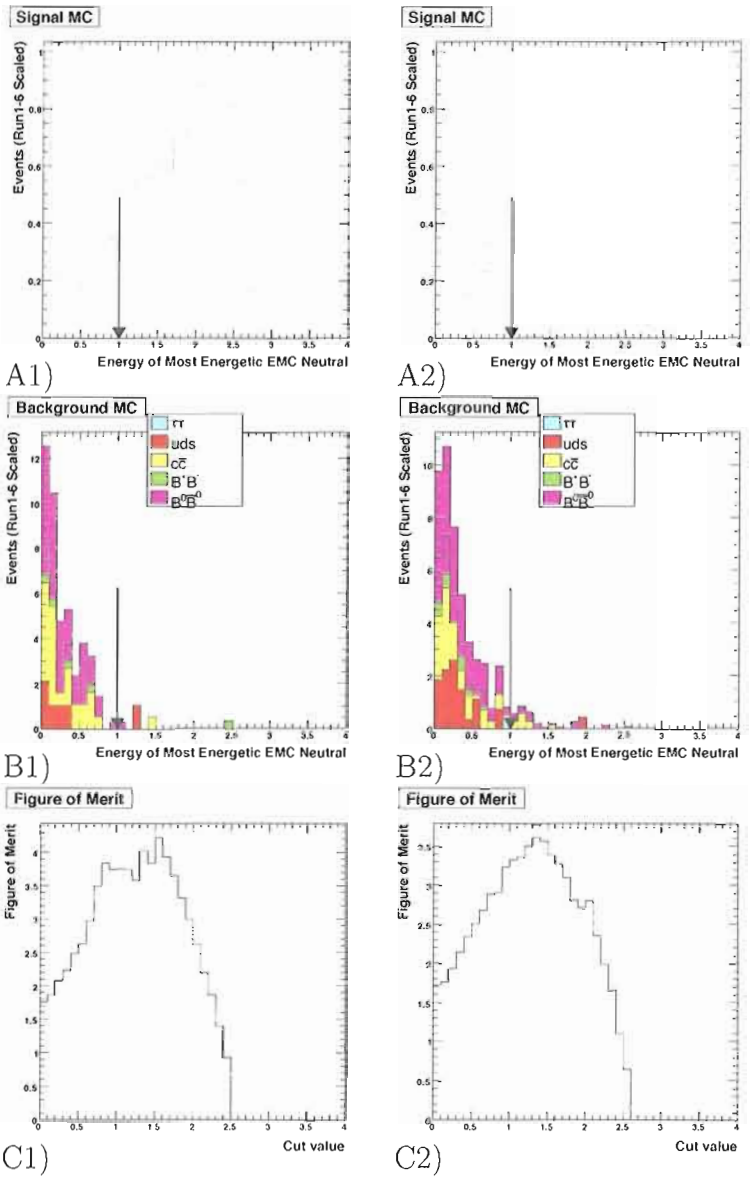

Figure A.8. E_{hi} in A) B^0, B) background, and C) $N_{Sig}/(1.5+\sqrt{N_{Bkgrnd}})$ for 1) regular and 2) high statistics samples

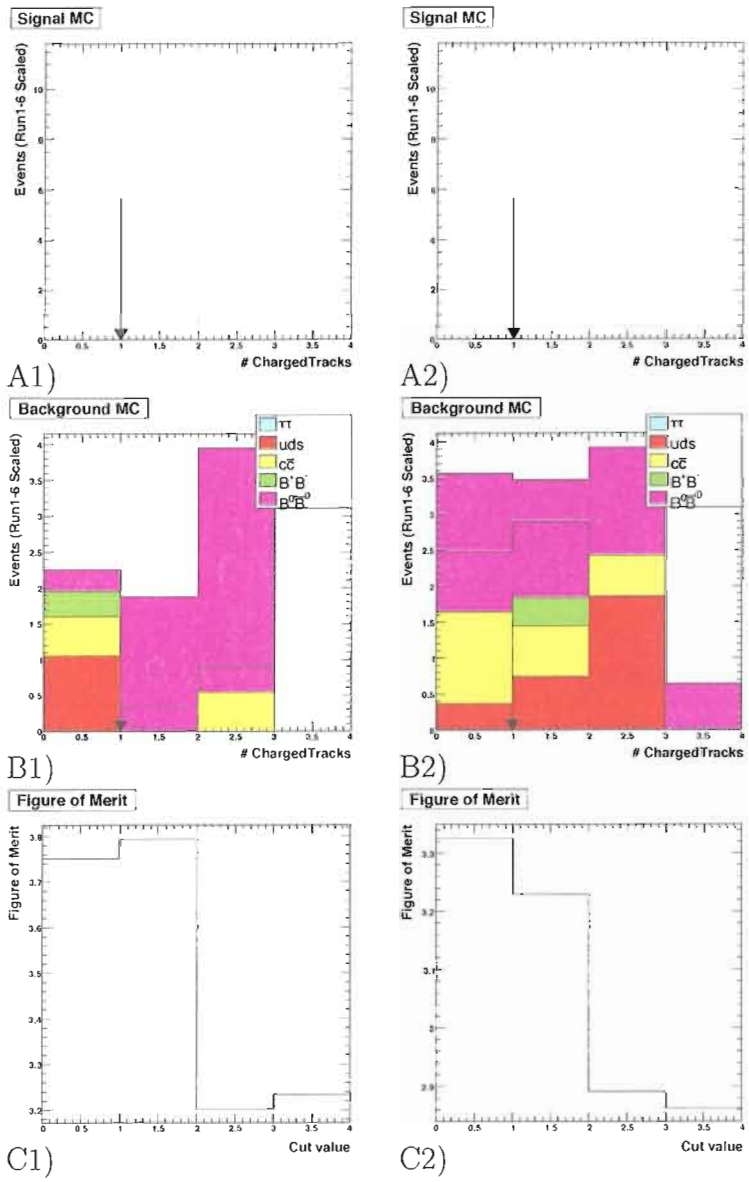

Figure A.9. N_{CT} in A) B^0, B) nBkg, and C) $N_{Sig}/(1.5+\sqrt{N_{Bkgrnd}})$ for 1) regular and 2) high statistics samples

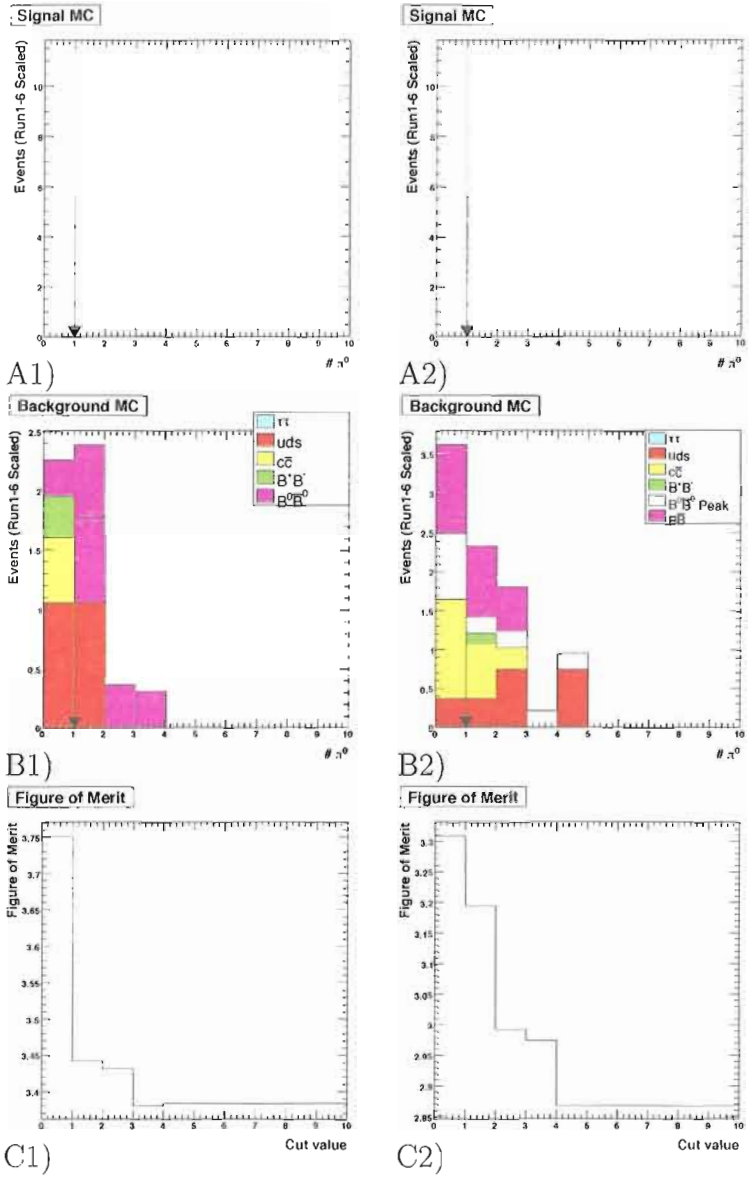

Figure A.10. N_{π^0} in A) B^0, B) background, and C) $N_{Sig}/(1.5+\sqrt{N_{Bkgrnd}})$ for 1) regular and 2) high statistics samples

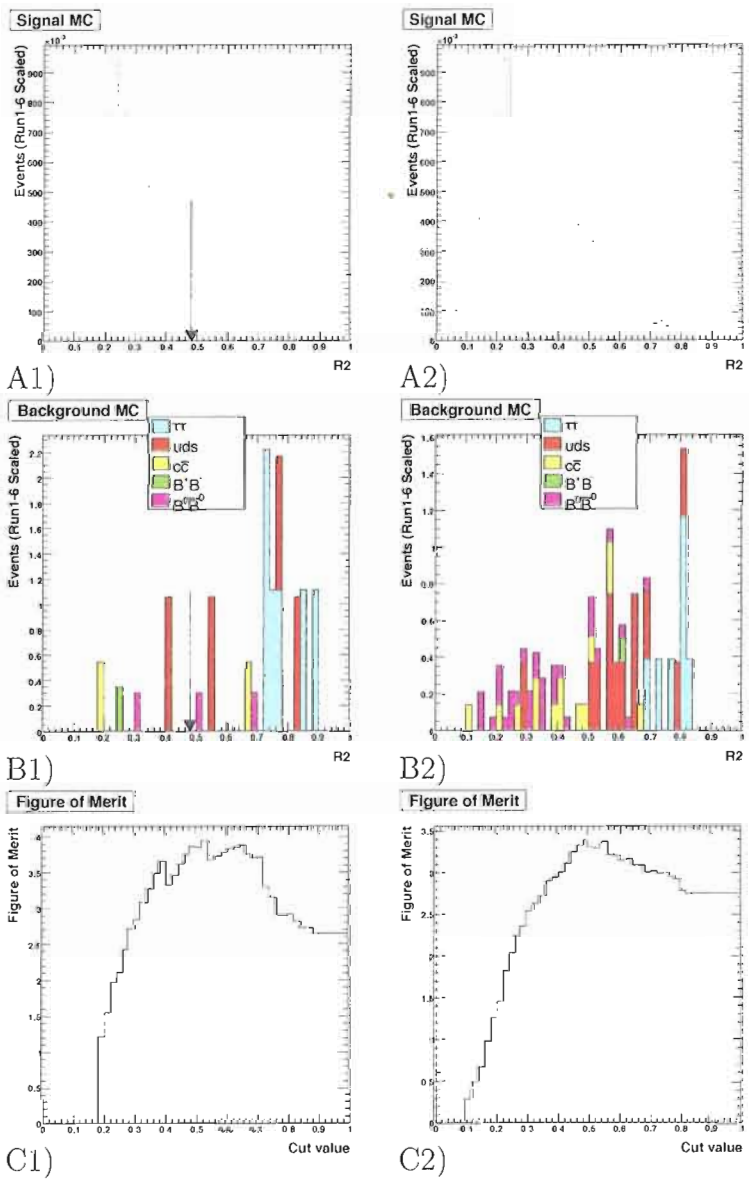

Figure A.11. R2 in A) B^0, B) background, and C) $N_{Sig}/(1.5+\sqrt{N_{Bkgrnd}})$ for 1) regular and 2) high statistics samples

APPENDIX B

BACKGROUND SCALING

Using luminosity scaling, there is significant disagreement between data and MC when some or all signal side cuts are applied, as shown in Table B.1 and Table B.2.

Table B.1. $B^0 \rightarrow$ invisible cutflow table. Peaking $B^0\overline{B}^0$ events are those that have $\theta^{P*} < .4$ and $N_{trk}^{diff} = 0$; combinatoric events do not. Signal is given as efficiency for tagged events, background and data as luminosity weighted number of events.

CUT	$B^0 \rightarrow \nu\overline{\nu}$ (10^{-4})	$\tau^+\tau^-$	uds	$c\overline{c}$	B^+B^-
SIGNAL BOX	14.8 ± 0.16	76.7±9.2	410.±21	412±15	166.8±7.7
R2 < 0.62	13.2 ± 0.15	18.9±4.6	355±19	387±15	163±7.6
$N_{\pi^0} < 3$	12.92 ± 0.15	14.5±4.0	294±18	311±13	115.1±6.4
$N_{GTL} = 0$	12.72 ± 0.15	7.8±2.9	63.5±8.2	72.0±6.3	12.3±2.1
$N_{CT} = 0$	10.03 ± 0.13	5.6±2.5	12.7±3.7	23.5±3.6	3.9±1.2
$E_{neu} < 0.16$	6.50 ± 0.11	2.2±1.6	4.2±2.1	3.8±1.4	0.70±0.50

Comb $B^0\overline{B}^0$	Peaking $B^0\overline{B}^0$	Comb tot	Bkg tot	Data
482±13	1671±23	1547±31	3219±39	3633±60.
474±13	1630±22	1399±29	3029±37	3393±58
376±12	1401±21	1111±26	2512±33	2803±53
40.3±3.8	120.3±6.1	196±12	316±13	376±19
11.5±2.0	34.1±3.2	57.1±6.2	91.2±6.9	BLINDED
1.44±0.72	7.6±1.5	12.4±3.1	20.0±3.5	BLINDED

Table B.2. $B^0 \rightarrow$ invisible + γ cutflow table. Peaking $B^0\overline{B}^0$ events are those that have $\theta^{P*} < .4$ and $N_{trk}^{diff} = 0$; combinatoric events do not. Signal is given as efficiency for tagged events, background and data as luminosity weighted number of events.

CUT	$B^0 \rightarrow \nu\overline{\nu}\gamma$ (10^{-4})	$\tau^+\tau^-$	uds	$c\overline{c}$	B^+B^-
SIGNAL BOX	14.99 ± 0.16	176±14	1559±40.	1573±29	591±14
R2 < 0.48	12.06 ± 0.14	8.9±3.1	933±31	1132±25	542±14
$E_{hi} > 1.0$	8.77 ± 0.12	0±0	109±11	93.3±7.1	38.0±3.7
$N_{\pi^0} = 0$	7.08 ± 0.11	0±0	30.7±5.7	24.5±3.7	7.4±1.6
$N_{GTL} = 0$	6.96 ± 0.11	0±0	3.2±1.8	4.4±1.5	1.06±0.61
$N_{CT} = 0$	5.561 ± 0.098	0±0	2.1±1.5	2.2±1.1	0.35±0.35
$E_{neu} < 0.3$	4.846 ± 0.091	0±0	1.1±1.1	0.55±0.55	0.35±0.35

Comb $B^0\overline{B}^0$	Peaking $B^0\overline{B}^0$	Comb tot	Bkg tot	Data
1415±23	4004±47	5314±58	9318±75	9975±100.
1335±22	3556±45	3951±48	7507±65	8097±90.
81.7±5.4	259±12	322±14	581±19	664±26
19.1±2.6	77.3±6.3	81.7±7.4	159±9.7	177±13
1.80±0.80	8.8±2.1	10.4±2.6	19.2±3.3	29±5.4
0.72±0.51	1.22±0.88	5.4±2.0	6.6±2.1	BLINDED
0±0	0.30±0.36	2.0±1.2	2.3±1.3	BLINDED

To remedy this, the combinatoric and peaking MC events are scaled using the $m_{\rm ES}$ and E_{neu} sidebands. To enhance the peaking MC statistics, the $B^0\overline{B}^0$ cocktail sample is used in place of generic peaking $B^0\overline{B}^0$ events. Table B.3 through Table B.14 show the yields and correction factors used in this scaling, and compare the peaking yields between cocktail and generic $B^0\overline{B}^0$ samples. For the E_{neu} sideband tables, E_{neu} low $m_{\rm ES}$ refers to the region $5.2 < m_{\rm ES} < 5.26$, $.6 < E_{neu} < 1.5$. The E_{neu} combinatoric correction is the ratio of MC to data in this region, and is used to scale the combinatoric background in the E_{neu} sideband. The peaking correction is obtained by dividing the cocktail MC yield in the E_{neu} sideband by the predicted peaking background, where predicted peaking background in the E_{neu} sideband is obtained by subtracting the scaled combinatoric background in the E_{neu} sideband from data.

In the $m_{\rm ES}$ sideband tables, the combinatoric correction is the ratio of MC to data in the $m_{\rm ES}$ sideband. The total scaled MC in the signal box is the sum of the cocktail MC events in the signal box scaled by the peaking correction and the combinatoric events in the signal box scaled by the combinatoric correction.

Table B.15 through Table B.20 give the number of events in the E_{neu} sideband and the signal box for generic and cocktail MC, as well as the ratio of signal box to E_{neu} sideband events for the two samples. The ratios are the same for the two samples, within statistics, and so, since the peaking MC in the E_{neu} sideband is used to scale the peaking MC in the signal box, the scaled peaking background using the

cocktail sample is in agreement with the scaled peaking background using peaking MC from the generic $B^0\overline{B}^0$ sample.

Table B.3. $B^0 \rightarrow$ invisible E_{neu} sideband.

Cut	Data E_{neu} low m_{ES}	MC E_{neu} low m_{ES}	SB Comb. Corr.	Cock MC E_{neu} SB	Comb MC E_{neu} SB	Data E_{neu} SB	Peaking Corr.
SignalBox	25135±159	25450±125	0.99±0.01	6309±21	8530±71	13215±115	0.76±0.02
R2 < .62	24055±155	24400±122	0.99±0.01	6247±21	8080±69	12755±113	0.77±0.02
$N_{\pi^0} < 2$	8330±91	9004±76	0.93±0.01	2758±14	2978±43	4970±70	0.80±0.03
$N_{GTL} = 0$	1643±41	1645±33	1.00±0.03	216.3±3.9	515±18	703±27	0.87±0.17
$N_{CT} = 0$	593±24	531±19	1.12±0.06	53.5±2.0	170±10	242±16	0.97±0.41
$E_{neu} < .16$	593±24	531±19	1.12±0.06	53.5±2.0	170±10	242±16	0.97±0.41

Table B.4. $B^0 \rightarrow$ invisible m_{ES} sideband.

Cut	Data m_{ES} SB	MC m_{ES} SB	Comb. Correction	Cock MC SignalBox	Comb MC SignalBox	Scaled MC SignalBox	Data SignalBox
SignalBox	4561±68	4246±53	1.07±0.02	2646±14	1547±31	3671±80	3633±60
R2 < .62	4124±64	3797±49	1.09±0.02	2573±14	1399±29	3492±76	3393±58
$N_{\pi^0} < 2$	3255±57	3060±45	1.06±0.02	2194±13	1111±26	2944±82	2298±48
$N_{GTL} = 0$	724±27	617±21	1.17±0.06	145.4±3.2	196±12	356±30	318±18
$N_{CT} = 0$	253±16	184±12	1.38±0.12	34.9±1.6	57.1±6.2	112±18	120±11
$E_{neu} < .16$	48.0±6.9	27.6±4.5	1.74±0.38	7.30±0.72	12.4±3.1	28.6±7.8	39.0±6.2

Table B.5. $B^0 \rightarrow$ invisible E_{neu} sideband e^- control.

Cut	Data E_{neu} low m_{ES}	MC E_{neu} low m_{ES}	SB Comb. Corr.	Cock MC E_{neu} SB	Comb MC E_{neu} SB	Data E_{neu} SB	Peaking Corr.
SignalBox	24664±157	24580±108	1.00±0.01	6801±22	8812±63	17729±133	1.31±0.02
R2 < .62	24205±156	24170±106	1.00±0.01	6759±22	8645±62	17525±132	1.31±0.02
$N_{\pi^0} < 2$	8163±90	8195±64	1.00±0.01	3330±15	3089±38	7459±86	1.32±0.03
$N_{GTL} = 0$	1516±39	1539±28	0.99±0.03	488.2±5.9	518±16	1285±36	1.59±0.09
$N_{CT} = 0$	402±20	385±13	1.04±0.06	181.6±3.6	139.4±7.6	441±21	1.63±0.14
$E_{neu} < .16$	402±20	385±13	1.04±0.06	181.6±3.6	139.4±7.6	441±21	1.63±0.14

Table B.6. $B^0 \rightarrow$ invisible m_{ES} sideband e^- control.

Cut	Data m_{ES} SB	MC m_{ES} SB	Comb. Correction	Cock MC SignalBox	Comb MC SignalBox	Scaled MC SignalBox	Data SignalBox
SignalBox	11899±109	4561±46	2.61±0.04	4035±17	2025±30	10555±146	7324±86
R2 < .62	11594±108	4412±45	2.63±0.04	3985±17	1964±29	10389±143	7219±85
$N_{\pi^0} < 2$	8905±94	3439±40	2.59±0.04	3470±16	1573±26	8639±145	5013±71
$N_{GTL} = 0$	608±25	586±17	1.04±0.05	428.6±5.5	230±10	919±42	658±26
$N_{CT} = 0$	159±13	143.0±7.9	1.11±0.11	140.1±3.2	51.1±4.5	285±21	209±14
$E_{neu} < .16$	25.0±5.0	19.1±3.0	1.31±0.33	31.0±1.5	8.6±2.0	61.7±6.2	69.0±8.3

Table B.7. $B^0 \rightarrow$ invisible E_{neu} sideband μ^- control.

Cut	Data E_{neu} low m_{ES}	MC E_{neu} low m_{ES}	SB Comb. Corr.	Cock MC E_{neu} SB	Comb MC E_{neu} SB	Data E_{neu} SB	Peaking Corr.
SignalBox	32236±180	38220±143	0.84±0.01	7450±23	12830±82	19766±141	1.20±0.02
R2 < .62	31564±178	37430±141	0.84±0.01	7409±23	12470±80	19406±139	1.20±0.02
$N_{\pi^0} < 2$	10923±105	13270±87	0.82±0.01	3567±16	4543±49	8019±90	1.20±0.03
$N_{GTL} = 0$	1949±44	2429±37	0.80±0.02	551.4±6.3	840±21	1423±38	1.36±0.08
$N_{CT} = 0$	481±22	571±18	0.84±0.05	203.9±3.8	205±10	447±21	1.34±0.12
$E_{neu} < .16$	481±22	571±18	0.84±0.05	203.9±3.8	205±10	447±21	1.34±0.12

Table B.8. $B^0 \rightarrow$ invisible m_{ES} sideband μ^- control.

Cut	Data m_{ES} SB	MC m_{ES} SB	Comb. Correction	Cock MC SignalBox	Comb MC SignalBox	Scaled MC SignalBox	Data SignalBox
SignalBox	16436±128	7269±63	2.26±0.03	4433±18	2859±38	11787±156	7935±89
R2 < .62	15867±126	6915±61	2.29±0.03	4374±18	2720±37	11490±153	7783±88
$N_{\pi^0} < 2$	12300±111	5455±54	2.25±0.03	3811±17	2182±33	9492±155	5463±74
$N_{GTL} = 0$	847±29	930±23	0.91±0.04	497.4±6.0	360±14	1004±46	771±28
$N_{CT} = 0$	200±14	200±10	1.00±0.09	157.7±3.4	73.5±5.9	285±22	229±15
$E_{neu} < .16$	29.0±5.4	28.5±3.8	1.02±0.23	38.6±1.7	12.8±2.6	64.8±6.6	62.0±7.9

Table B.9. $B^0 \rightarrow$ invisible $+ \gamma$ E_{neu} sideband.

Cut	Data E_{neu} low m_{ES}	MC E_{neu} low m_{ES}	SB Comb. Corr.	Cock MC E_{neu} SB	Comb MC E_{neu} SB	Data E_{neu} SB	Peaking Corr.
SignalBox	54350±233	56550±200	0.96±0.01	7822±24	17930±106	23329±153	0.78±0.03
R2 < .48	44930±212	46780±179	0.96±0.01	7438±23	14330±91	19553±140	0.78±0.02
$E_{hi} > 1.0$	7452±86	8395±78	0.89±0.01	1098.0±8.9	2550±41	3104±56	0.77±0.07
$N_{\pi^0} = 0$	382±20	456±19	0.84±0.05	61.0±2.1	130.1±9.3	182±13	1.20±0.28
$N_{GTL} = 0$	90.0±9.5	105.0±9.0	0.86±0.12	8.16±0.76	27.1±4.2	46.0±6.8	2.79±1.05
$N_{CT} = 0$	33.0±5.7	42.3±5.7	0.78±0.17	2.08±0.39	11.5±2.6	27.0±5.2	8.69±3.28
$E_{neu} < .28$	33.0±5.7	42.3±5.7	0.78±0.17	2.08±0.39	11.5±2.6	27.0±5.2	8.69±3.28

Table B.10. $B^0 \rightarrow$ invisible $+ \gamma$ m_{ES} sideband.

Cut	Data m_{ES} SB	MC m_{ES} SB	Comb. Correction	Cock MC SignalBox	Comb MC SignalBox	Scaled MC SignalBox	Data SignalBox
SignalBox	15150±123	15140±105	1.00±0.01	6133±21	5314±58	10098±183	9975±100
R2 < .48	11500±107	11510±89	1.00±0.01	5458±20	3951±48	8196±153	8097±90
$E_{hi} > 1.0$	1059±33	1172±30	0.90±0.04	387.5±5.3	322±14	587±32	664±26
$N_{\pi^0} = 0$	290±17	321±16	0.90±0.07	108.7±2.8	81.7±7.4	204±32	177±13
$N_{GTL} = 0$	65.0±8.1	57.4±6.6	1.13±0.19	8.73±0.79	10.4±2.6	36±10	29.0±5.4
$N_{CT} = 0$	34.0±5.8	19.4±3.8	1.75±0.45	2.36±0.41	5.4±2.0	29.9±9.5	11.0±3.3
$E_{neu} < .28$	18.0±4.2	7.4±2.2	2.43±0.92	1.07±0.28	2.0±1.2	14.1±5.5	8.0±2.8

Table B.11. $B^0 \rightarrow$ invisible $+ \gamma$ E_{neu} sideband e^- control.

Cut	Data E_{neu} low m_{ES}	MC E_{neu} low m_{ES}	SB Comb. Corr.	Cock MC E_{neu} SB	Comb MC E_{neu} SB	Data E_{neu} SB	Peaking Corr.
SignalBox	38416±196	39290±155	0.98±0.01	6124±21	13040±80	20460±143	1.26±0.03
R2 < .48	34949±187	35660±146	0.98±0.01	5879±21	11690±74	18851±137	1.26±0.03
$E_{hi} > 1.0$	3284±57	3395±47	0.97±0.02	618.3±6.7	1126±25	1815±43	1.17±0.09
$N_{\pi^0} = 0$	207±14	187±11	1.11±0.10	46.9±1.8	62.3±6.1	110±10	0.88±0.30
$N_{GTL} = 0$	47.0±6.9	41.1±5.2	1.14±0.22	8.73±0.79	16.7±3.1	19.0±4.4	-0.01±-0.77
$N_{CT} = 0$	10.0±3.2	10.2±2.4	0.98±0.38	3.58±0.51	5.9±2.0	11.0±3.3	1.45±1.26
$E_{neu} < .28$	10.0±3.2	10.2±2.4	0.98±0.38	3.58±0.51	5.6±2.0	11.0±3.3	1.53±1.25

Table B.12. $B^0 \rightarrow$ invisible $+ \gamma$ m_{ES} sideband e^- control.

Cut	Data m_{ES} SB	MC m_{ES} SB	Comb. Correction	Cock MC SignalBox	Comb MC SignalBox	Scaled MC SignalBox	Data SignalBox
SignalBox	22595±150	14230±94	1.59±0.01	8135±24	5764±51	19394±274	16389±128
R2 $<$ .48	19958±141	12450±87	1.60±0.02	7556±23	5061±47	17616±252	15163±123
$E_{hi} > 1.0$	1391±37	694±21	2.01±0.08	348.5±5.0	289±12	988±47	746±27
$N_{\pi^0} = 0$	374±19	162±10	2.30±0.19	100.6±2.7	72.3±6.5	255±36	225±15
$N_{GTL} = 0$	46.0±6.8	37.1±5.0	1.24±0.25	16.5±1.1	14.8±3.2	18±14	55.0±7.4
$N_{CT} = 0$	12.0±3.5	9.5±2.7	1.27±0.51	6.08±0.66	3.4±1.5	13.2±8.2	16.0±4.0
$E_{neu} <$ .28	8.0±2.8	4.8±2.0	1.67±0.90	3.08±0.47	2.0±1.2	8.0±4.8	11.0±3.3

Table B.13. $B^0 \rightarrow$ invisible $+ \gamma$ E_{neu} sideband μ^- control.

Cut	Data E_{neu} low m_{ES}	MC E_{neu} low m_{ES}	SB Comb. Corr.	Cock MC E_{neu} SB	Comb MC E_{neu} SB	Data E_{neu} SB	Peaking Corr.
SignalBox	52705±230	65050±207	0.81±0.00	7019±22	20750±108	24911±158	1.15±0.03
R2 < .48	46886±217	57570±192	0.81±0.00	6754±22	17800±96	22413±150	1.17±0.03
$E_{hi} > 1.0$	5110±71	6944±70	0.74±0.01	774.8±7.4	2130±36	2623±51	1.36±0.08
$N_{\pi^0} = 0$	285±17	373±17	0.76±0.06	48.5±1.9	98.3±7.9	140±12	1.34±0.30
$N_{GTL} = 0$	57.0±7.5	77.2±7.5	0.74±0.12	9.09±0.81	25.1±3.9	34.0±5.8	1.70±0.80
$N_{CT} = 0$	18.0±4.2	27.9±4.5	0.64±0.18	3.44±0.50	6.8±1.9	14.0±3.7	2.80±1.27
$E_{neu} < .28$	18.0±4.2	27.9±4.5	0.64±0.18	3.44±0.50	6.8±1.9	14.0±3.7	2.80±1.27

Table B.14. $B^0 \rightarrow$ invisible $+ \gamma$ m_{ES} sideband μ^- control.

Cut	Data m_{ES} SB	MC m_{ES} SB	Comb. Correction	Cock MC SignalBox	Comb MC SignalBox	Scaled MC SignalBox	Data SignalBox
SignalBox	31163±177	23000±124	1.35±0.01	8910±25	8444±67	21722±289	17901±134
R2 < .48	26511±163	19310±112	1.37±0.01	8274±24	7045±59	19370±261	16226±127
$E_{hi} > 1.0$	2227±47	1347±31	1.65±0.05	406.7±5.4	472±17	1334±50	850±29
$N_{\pi^0} = 0$	607±25	333±15	1.82±0.11	114.2±2.9	124.8±8.8	380±41	238±15
$N_{GTL} = 0$	59.0±7.7	73.3±7.3	0.80±0.13	20.7±1.2	26.8±4.2	57±17	47.0±6.9
$N_{CT} = 0$	18.0±4.2	19.7±3.8	0.91±0.28	7.87±0.75	4.8±1.7	26±10	11.0±3.3
$E_{neu} < .28$	9.0±3.0	10.2±2.9	0.88±0.39	5.01±0.60	2.1±1.2	15.9±6.7	8.0±2.8

Table B.15. $B^0 \rightarrow$ invisible Peaking Ratio

Cut	E_{neu} SB Peaking	SignalBox Peaking	Ratio	Eneu SB Cock	SigBox Cock	Cock Ratio
SignalBox	4113±35	1671±23	0.41±0.01	6309±21	2646±14	0.42±0.00
R2 < .62	4070±35	1630±22	0.40±0.01	6247±21	2573±14	0.41±0.00
$N_{\pi^0} < 2$	1894±24	1401±21	0.74±0.01	2758±14	2194±13	0.80±0.01
$N_{GTL} = 0$	180.8±7.4	120.3±6.1	0.67±0.04	216.3±3.9	145.4±3.2	0.67±0.02
$N_{CT} = 0$	66.4±4.5	34.1±3.2	0.51±0.06	53.5±2.0	34.9±1.6	0.65±0.04
$E_{neu} < .16$	66.4±4.5	7.6±1.5	0.11±0.02	53.5±2.0	7.30±0.72	0.14±0.01

Table B.16. $B^0 \rightarrow$ invisible Peaking Ratio e^- control

Cut	E_{neu} SB Peaking	SignalBox Peaking	Ratio	Eneu SB Cock	SigBox Cock	Cock Ratio
SignalBox	7754±49	4549±37	0.59±0.01	6801±22	4035±17	0.59±0.00
R2 < .62	7722±48	4504±37	0.58±0.01	6759±22	3985±17	0.59±0.00
$N_{\pi^0} < 2$	3792±34	3895±34	1.03±0.01	3330±15	3470±16	1.04±0.01
$N_{GTL} = 0$	594±13	503±12	0.85±0.03	488.2±5.9	428.6±5.5	0.88±0.02
$N_{CT} = 0$	221.3±8.2	162.9±7.0	0.74±0.04	181.6±3.6	140.1±3.2	0.77±0.02
$E_{neu} < .16$	221.3±8.2	37.1±3.4	0.17±0.02	181.6±3.6	31.0±1.5	0.17±0.01

Table B.17. $B^0 \rightarrow$ invisible Peaking Ratio μ^- control

Cut	E_{neu} SB Peaking	SignalBox Peaking	Ratio	Eneu SB Cock	SigBox Cock	Cock Ratio
SignalBox	8425±51	5146±40	0.61±0.01	7450±23	4433±18	0.60±0.00
R2 < .62	8384±51	5100±39	0.61±0.01	7409±23	4374±18	0.59±0.00
$N_{\pi^0} < 2$	4008±35	4409±37	1.10±0.01	3567±16	3811±17	1.07±0.01
$N_{GTL} = 0$	645±14	597±13	0.93±0.03	551.4±6.3	497.4±6.0	0.90±0.01
$N_{CT} = 0$	234.7±8.5	190.6±7.6	0.81±0.04	203.9±3.8	157.7±3.4	0.77±0.02
$E_{neu} < .16$	234.7±8.5	45.7±3.7	0.19±0.02	203.9±3.8	38.6±1.7	0.19±0.01

Table B.18. $B^0 \rightarrow$ invisible $+ \gamma$ Peaking Ratio

Cut	E_{neu} SB Peaking	SignalBox Peaking	Ratio	Eneu SB Cock	SigBox Cock	Cock Ratio
SignalBox	5153±60	4004±47	0.78±0.01	7822±24	6133±21	0.78±0.00
R2 < .48	4914±59	3556±45	0.72±0.01	7438±23	5458±20	0.73±0.00
$E_{hi} > 1.0$	790±23	259±12	0.33±0.02	1098.0±8.9	387.5±5.3	0.35±0.01
$N_{\pi^0} = 0$	46.9±5.3	77.3±6.3	1.65±0.23	61.0±2.1	108.7±2.8	1.78±0.08
$N_{GTL} = 0$	4.3±1.5	8.8±2.1	2.07±0.89	8.16±0.76	8.73±0.79	1.07±0.14
$N_{CT} = 0$	0.91±0.88	1.22±0.88	1.33±1.61	2.08±0.39	2.36±0.41	1.14±0.29
$E_{neu} < .28$	0.91±0.88	0.30±0.36	0.33±0.51	2.08±0.39	1.07±0.28	0.52±0.16

Table B.19. $B^0 \rightarrow$ invisible $+ \gamma$ Peaking Ratio e^- control

Cut	E_{neu} SB Peaking	SignalBox Peaking	Ratio	Eneu SB Cock	SigBox Cock	Cock Ratio
SignalBox	6902±68	9251±70	1.34±0.02	6124±21	8135±24	1.33±0.01
R2 < .48	6699±67	8771±69	1.31±0.02	5879±21	7556±23	1.29±0.01
$E_{hi} > 1.0$	685±20	400±15	0.58±0.03	618.3±6.7	348.5±5.0	0.56±0.01
$N_{\pi^0} = 0$	48.7±5.3	114.5±7.6	2.35±0.30	46.9±1.8	100.6±2.7	2.15±0.10
$N_{GTL} = 0$	8.8±2.5	19.2±3.1	2.17±0.70	8.73±0.79	16.5±1.1	1.89±0.21
$N_{CT} = 0$	3.7±1.5	5.2±1.5	1.42±0.71	3.58±0.51	6.08±0.66	1.70±0.30
$E_{neu} < .28$	4.3±1.2	3.3±1.2	0.78±0.36	3.58±0.51	3.08±0.47	0.86±0.18

Table B.20. $B^0 \rightarrow$ invisible $+ \gamma$ Peaking Ratio μ^- control

Cut	E_{neu} SB Peaking	SignalBox Peaking	Ratio	Eneu SB Cock	SigBox Cock	Cock Ratio
SignalBox	7944±74	10200±74	1.28±0.02	7019±22	8910±25	1.27±0.01
R2 < .48	7717±74	9660±73	1.25±0.02	6754±22	8274±24	1.23±0.01
$E_{hi} > 1.0$	921±24	468±16	0.51±0.02	774.8±7.4	406.7±5.4	0.52±0.01
$N_{\pi^0} = 0$	57.2±5.7	136.7±8.5	2.39±0.28	48.5±1.9	114.2±2.9	2.36±0.11
$N_{GTL} = 0$	10.7±2.8	23.1±3.4	2.17±0.66	9.09±0.81	20.7±1.2	2.28±0.24
$N_{CT} = 0$	3.7±1.6	7.6±1.9	2.08±1.04	3.44±0.50	7.87±0.75	2.29±0.40
$E_{neu} < .28$	3.7±1.6	3.7±1.3	1.00±0.56	3.44±0.50	5.01±0.60	1.46±0.27

APPENDIX C

PID LISTS

Track Lists

For the track list definitions the following variables are used:

- p_T— the transverse momentum of the track,
- DOCA_{xy}—the distance of closest approach of the track to the IP in the x-y plane,
- DOCA_z– the distance of closest approach of the track to the IP along the z-axis,
- N_{DCH}— the number of hits in the DCH associated with the track.

The definitions for the track lists used in this analysis are:

- ChargedTracks — candidates with non-zero charge, use a charged pion mass hypothesis
- GoodTracksLoose — ChargedTracks with $0.1 < p_T < 10\,\mathrm{GeV}$, $\mathrm{DOCA}_{xy} < 1.5cm$, $-10 < \mathrm{DOCA}_z < 10\,\mathrm{cm}$, and $N_{DCH} > 10$

Neutrals Lists

The following neutrals definitions use the following variables: E_{lab}— the energy of the cluster in the lab frame and L_γ— the lateral moment of the cluster. The definitions for the neutral lists used in this analysis are:

- CalorNeutral — Single unmatched EMC bumps
- GoodPhotonLoose — Calor Neutral with $E_{lab} > 0.30\,\mathrm{GeV}$ and $L_\gamma < 0$.
- GammaForPi0 — GoodPhotonLoose with $0.030 < E_{lab} < 10.0\,\mathrm{GeV}$

PID Lists

For the PID lists the following variables are used:

- E_{cand}— the energy deposited by the candidate in the EMC,
- $\mathrm{d}E/\mathrm{d}x$— the energy lost in the SVT and DCH,
- θ_c— the angle of the Cherenkov light cone in the DIRC,
- N_γ— the number of photons in the DIRC,
- N_γ^{exp}— the expected number of photons in the DIRC,
- E/p— the ratio of lab energy to momentum,

- N_{cry}— the number of crystals with clusters associated with the track,
- L_γ— the lateral moment in the EMC,
- A_{42}— the Zernike moment,
- $\Delta\phi$— the separation between the track and the nearest unassociated bump,
- N_L— the number of IFR layers with hits associated with the track,
- Λ_{meas}— the number of interaction lengths traversed by the track,
- $\Delta\Lambda$— the difference between the expected (for muons) and measured number of interaction lengths traversed,
- χ^2_{fit}— the chi squared per degree of freedom of a polynomial fit to the IFR hits,
- χ^2_{mat}— the chi squared per degree of freedom of the track extrapolation to the hits in the IFR,
- T_c— the track continuity,
- M– the average multiplicity of hit strips per IFR layer, and
- σ_M— the error on M.

The PID lists used in this analysis are:

- K^-— likelihood fit using $\mathrm{d}E/\mathrm{d}x$, θ_c, N_γ, and N_γ^{exp}
- e^-— likelihood fit using E/p, N_{cry}, L_γ, A_{42}, $\mathrm{d}E/\mathrm{d}x$, N_γ, N_γ^{exp}, and $\Delta\phi$

- μ^-— neural net using E_{cand}, N_L, Λ_{meas}, $\Delta\Lambda$, χ^2_{fit}, χ^2_{mat}, T_c, M, and σ_M

Composite Particles

For the composite particle definitions the following variables are used: m— the invariant mass of the sum of the 4-momenta of the daughter particles, m_{poca}— the invariant mass of the pion pair at their point of closest approach, E_{lab}— the energy of the composite particle in the lab frame, *Lat* is the photon lateral moment, m_P with P as the parent is the theoretical mass of the parent particle, m_X with X as the daughter particles is the invariant mass of the sum of the 4-vectors of the particles X, and p_X is the momentum in the lab frame of the sum of the 4-vectors of the particles X. The composite particle definitions are given in Table C.1, with the theoretical particle masses in Table C.2

Table C.1. Reconstructed composite particles used in the SemiExcl skim.

Parent	Daughters	Daughter requirements
D^{*+}	$D^0\pi^+$	$\lvert m_{D^{*+}} - m_{D^0\pi^+}\rvert < 2$ MeV, $p_{D^0} < 2.5$ GeV, $p_{D^{*+}} > 0.5$ GeV
D^0	$K^-\pi^+$	$\lvert m_{D^0} - m_{K^-\pi^+}\rvert < 15$ MeV
	$K^-\pi^+\pi^0$	$\lvert m_{D^0} - m_{K^-\pi^+\pi^0}\rvert < 25$ MeV
	$K^-\pi^+\pi^+\pi^-$	$\lvert m_{D^0} - m_{K^-\pi^+\pi^+\pi^-}\rvert < 15$ MeV
	$K^0_S\pi^+\pi^-$	$\lvert m_{D^0} - m_{K^0_S\pi^+\pi^-}\rvert < 20$ MeV
D^+	$K^-\pi^+\pi^+$	$\lvert m_{D^+} - m_{K^-\pi^+\pi^+}\rvert < 20$ MeV, $1.0 < p_{K^-\pi^+\pi^+} < 2.5$ GeV
	$K^-\pi^+\pi^+\pi^0$	$\lvert m_{D^+} - m_{K^-\pi^+\pi^+\pi^0}\rvert < 30$ MeV, $1.6 < p_{K^-\pi^+\pi^+\pi^0} < 2.5$ GeV
	$K^0_S\pi^+$	$\lvert m_{D^+} - m_{K^0_S\pi^+}\rvert < 20$ MeV, $1.0 < p_{K^0_S\pi^+} < 2.5$ GeV
	$K^0_S\pi^+\pi^-\pi^+$	$\lvert m_{D^+} - m_{K^0_S\pi^+\pi^-\pi^+}\rvert < 30$ MeV, $1.6 < p_{K^0_S\pi^+\pi^-\pi^+} < 2.5$ GeV
	$K^0_S\pi^+\pi^0$	$\lvert m_{D^+} - m_{K^0_S\pi^+\pi^0}\rvert < 30$ MeV, $1.0 < p_{K^0_S\pi^+\pi^0} < 2.5$ GeV
K^0_S	$\pi^+\pi^-$	$0.47267 < m_{\pi^+\pi^-} < 0.52267$ GeV, $0.45 < m_{poca} < 0.5$
π^0	$\gamma\gamma$	$0.115 < m_{\gamma\gamma} < 0.150$ GeV, $E_\gamma > 0.3$ GeV,$L_\gamma < 0.8$

Table C.2. Masses of particles used in making the seed in the SemiExcl skim.

mass	value (MeV)
m_D^{*0}	2007
m_D^0	1865
m_D^+	1869

BIBLIOGRAPHY

[1] R. Barate et al. (LEP Working Group for Higgs boson searches), Phys. Lett. **B565**, 61 (2003), hep-ex/0306033.

[2] Phys. Rept. **427**, 257 (2006), hep-ex/0509008.

[3] C. Amsler et al. (Particle Data Group), Phys. Lett. **B667**, 1 (2008).

[4] R. N. Mohapatra et al., Rept. Prog. Phys. **70**, 1757 (2007), hep-ph/0510213.

[5] S. Abe et al. (KamLAND), Phys. Rev. Lett. **100**, 221803 (2008), 0801.4589.

[6] H. Gallagher (for the MINOS) (2008), 0809.5240.

[7] A. Goobar, S. Hannestad, E. Mortsell, and H. Tu, Journal of Cosmology and Astroparticle Physics **2006**, 019 (2006), URL http://stacks.iop.org/1475-7516/2006/i=06/a=019.

[8] C.-D. Lu and D.-X. Zhang, Phys. Lett. **B381**, 348 (1996), hep-ph/9604378.

[9] G. Hinshaw et al. (WMAP) (2008), 0803.0732.

[10] K. Agashe, N. G. Deshpande, and G. H. Wu, Phys. Lett. **B489**, 367 (2000), hep-ph/0006122.

[11] N. G. Deshpande and D. K. Ghosh, Phys. Lett. **B567**, 235 (2003), hep-ph/0303160.

[12] A. Dedes, H. K. Dreiner, and P. Richardson, Phys. Rev. **D65**, 015001 (2002), hep-ph/0106199.

[13] A. C. Kraan (2005), hep-ex/0505002.

[14] T. Adams (CDF) (2008), 0808.0728.

[15] B. Aubert et al. (BABAR), Phys. Rev. Lett. **93**, 091802 (2004), hep-ex/0405071.

[16] SLAC-418.

[17] B. Aubert et al. (BABAR), Nucl. Instrum. Meth. **A479**, 1 (2002), hep-ex/0105044.

[18] J. Seeman, ePAC'08, 11th European Particle Accelerator Conference, 23- 27 June 2008, Genoa, Italy.

[19] e. Harrison, P. F. and e. Quinn, Helen R. (BABAR), papers from Workshop on Physics at an Asymmetric B Factory (BaBar Collaboration Meeting), Rome, Italy, 11-14 Nov 1996, Princeton, NJ, 17-20 Mar 1997, Orsay, France, 16-19 Jun 1997 and Pasadena, CA, 22-24 Sep 1997.

[20] W. Menges, IEEE Nucl. Sci. Symp. Conf. Rec. **5**, 1470 (2006), physics/0609039.

[21] I. Hrivnacova, J. Phys. Conf. Ser. **119**, 032025 (2008).

[22] H. Albrecht et al. (ARGUS), Phys. Lett. **B241**, 278 (1990).

[23] D. del Re, S. Grancagnolo, R. Faccini, A. Sarti, and G. Denardo, BABAR Analysis Document 271 (2001).

[24] G. Punzi (2003), physics/0308063.

[25] J. Gaiser, SLAC-0255.

[26] M. T. Allen, M. T. Naisbit, and A. Roodman, BABAR Analysis Document 525 (2004).

[27] R. Barlow, Comput. Phys. Commun. **149**, 97 (2002), hep-ex/0203002.

[28] M. Bona et al. (2007), 0709.0451.

[29] O. Cakir and B. Sirvanli, Acta Phys. Polon. **B34**, 2643 (2003), hep-ph/0210019.